Radical Block Copolymers of Linear Low Density Polyethylene Macromonomers

by

Connah Andrew Burnett

A thesis submitted in partial fulfilment of the requirements for the degree of Doctor of Philosophy in Chemistry

Department of Chemistry, University of Warwick

March 2018

Contents

List of Figures

List of Schemes

List of Tables

Acknowledgements

Firstly, I would like to give my sincere thanks to my supervisor Professor Peter Scott for proposing this project, getting it funded and giving me such a great opportunity as to be a part of it. I would also like to offer thanks for all the guidance, support and knowledge he has imparted over the last four years, from mechanistic insights to correct use of Latin abbreviations to what constitutes a proper pint of beer.

I would also like to extend my gratitude to the Infineum team members: Colin Morton, Ben Hornby, Giles Theaker (now at Celotex), Ken Lewtas, Mike Capaldi, Richard Hart and Kevin Smith who have supported the project with their hard work, knowledge and funding, as well as the occasional free lunch.

A great deal of thanks are also deserved to the Scott group members of the last 4 years for all their input and for helping to make life in the lab a happy one: Becky, Chris, Paul, Dan, Hualong, Shaun, Tom and Anish as well as the many multitudes of MChem students.

Thanks go also to the many colleagues within the department whose help with instrumentation and analysis was of key importance. Dan Lester, Sam Lawton and Rachel Hand for helping to maintain the GPC suite, (may I never have to look at Bertie again), to Ivan Prokes and Rob Perry for their vigilant supervision of the NMR suite, and for all their advice, Dave Hammond for DSC training, Phil Aston and Lijang Song for help with MALDI and mass spectrometry and thanks also to Rob Jenkins for his knowledge of all things safety and to Jason Noone for his help with IT issues.

I would like to offer my thanks to all of my friends from camps both at Warwick: Sam, Ross, Emma, Dan, Rachel, Jenny and Tom and those at home in Grimsby: Danny, Miller, Brad, Simone, Sam, Marsh, Leggett, and the Adams (Beckett, James and Tutte)

I would next like to thank my family, to my parents Kevin and Andrea, for their encouragement and support, for their insistence on the importance of education and for their endless supplies of help and kindness over these last year and all through my life. To my brothers Max and Luke as well.

And finally, I would like to thank my girlfriend Hannah for all her love and support, and for being patient with me through some of the more difficult times.

Funding

The work reported in this thesis was conducted with funding from the EPSRC and Infineum UK Ltd, a company based in Oxfordshire who produce additives for fuels and oils. Many of the materials discussed in this work were sent to Infineum for testing, as well as being tested in-house at University of Warwick using equipment provided by Infineum.

Declaration

The work performed in this thesis was carried out in the Department of Chemistry, University of Warwick between October 2013 and March 2018. Unless otherwise stated, it is the work of the author and has not been submitted in whole or in part for any degree at this or any other university.

Publications

The following paper has arisen from this thesis:

Chapters 2, 3 and 4

Interface active polyolefins from versatile new macromonomers, C. J. Kay, C. A. Burnett, P. D. Goring, Ben Hornby, Kenneth Lewtas, Shaun Morris, Colin Morton, Tony McNally, Giles W Theaker, Carl Waterson, Peter M Wright, and Peter Scott

- In preparation

Summary

Chapter 1 introduces the concept of wax crystal modification in middle distillate fuels and reviews the more common chemical additives used commercially, and by examination of the advantages and drawbacks of these additives discusses the possible benefits of polyolefin block copolymers. From this end functionalisation of polyethylene (PE) as a route to block copolymers is reviewed from different literature methods for their synthesis.

Chapter 2 introduces the catalytic hydride insertion polymerisation mechanism as a route to end functional polyolefins and goes on to focus on the production of end functional ethylene/hexene copolymers. Using a range of comonomer concentrations and a number of catalysts, end-functional copolymers with a range of comonomer incorporation are produced. The thermal properties of these polymers are investigated and matrix assisted laser desorption/ionisation (MALDI) mass spectra were acquired. Finally, the chapter discusses the synthesis of short chain analogues of end functional PE.

Chapter 3 describes the production of polyolefin-polar block copolymers *via* the free radical polymerisation of the functional polyolefins with a range of polar monomers. A reversible termination mechanism similar to nitroxide mediated polymerisation is proposed. The products are analysed by gel permeation chromatography (GPC) and by an in detail 2D NMR study to confirm block copolymer structure.

Chapter 4 examines the physical properties of the synthesised block copolymers. The tendency of the copolymers to aggregate in solution into particles of varying size is investigated by VT NMR and dynamic light scattering (DLS), these findings were supported by transmission electron microscopy (TEM). The thermal properties of these copolymers were studied by differential scanning calorimetry (DSC). Following this the efficacy of these polymers as wax crystal modifiers (WCM) for fuels was investigated by cold flow plugging point (CFPP), optical microscopy and DSC of the treated fuels. Finally, the behaviour of the polymers in solid polyethylene wax was

investigated by drop shape analysis (DSA) and x-ray photoelectron spectroscopy (XPS).

Chapter 5 details the various experimental procedures used to carry out the work in this thesis.

Appendix A gives an overview of polymerisations between ethylene and α-methylstyrene comonomers catalysed by hafnocene catalysts and goes on to detail the investigation of the materials acquired. Analysis was conducted using 2-D NMR, MALDI and diffusion-ordered spectroscopy (DOSY).

Appendix B contains the DLS correlograms for samples analysed in chapter 4.

Appendix C contains the schematic diagram for the gas burettes system used for metallocene polymerisations

Abbreviations

AIBN	2,2′-azobis(2-methylpropionitrile)
AMS	α-methylstyrene
ATRP	Atom Transfer Radical Polymerisation
BeCa	Behenyl Carbamate
BHT	2,6-di-tert-butyl-4-methylphenol
BP	Benzoyl peroxide
C_{14}MA	Myristyl Methacrylate
CCG	Catalytic Chain-Growth
CCTA	Catalytic Chain Transfer Agent
CCTP	Catalytic Chain Transfer Polymerisation
CFPP	Cold Filter Plugging Point
CHIP	Catalytic Hydride Insertion Polymerisation
COBF	Bis(boron difluorodimethylglyoximate)cobaltate(II)
COSY	Correlation Spectroscopy
Cp	Cyclopentadienyl
Cp*	Pentamethylcyclopentadienyl
$Cp^{\dagger}$	Tetramethylcyclopentadienyl
CTA	Chain Transfer Agent
d^2-TCE	1,1,2,2-tetrachloroethane-d^2
DD1	(4-[(2,2-dimethyl-4-(N-tert-Butyl-N(1-diethoxyphosphoryl-2,2-dimethylpropyl)aminoxy)-4-n-butoxycarbonyl)butanoyloxyl]- 2,2,6,6-tetramethylpiperidinyl-1-oxy
DD2	4-[(2,2-dimethyl-4-(N-tert-Butyl-N-(1- diethoxyphosphoryl-2,2-dimethylpropyl)aminoxy)-4-phenyl) butanoyloxyl]-2,2,6,6-tetramethylpiperidinyl-1-oxy
DIB	1,3-diisopropenylbenzene
DLS	Dynamic Light Scattering
DOSY	Diffusion Ordered Spectroscopy
DP	Degree of Polymerisation
DSA	Drop Shape Analysis
DSC	Differential Scanning Calorimetry
EBI	Ethylene bis(indenyl)

EGF	End Group Fidelity
EH	Ethylene/Hexene
EO	Ethylene Oxide
EVA	Ethylene-*co*-Vinyl acetate
FI	Phenoxy/imine
GA	Growth Arrestor
GPC	Gel Permeation Chromatography
HDPE	High Density Polyethylene
HMBC	Heteronuclear Multiple-Bond Correlation
HMQC	Heteronuclear Multiple-Quantum Correlation
IF	indenyl-fluorenyl
Ind	Indenyl
IR	Infra-red
LDPE	Low Density Polyethylene
LLDPE	Linear Low Density Polyethylene
MAC	Poly(Maleic anhydride amide co-α-olefin)
MALDI	Matrix Assisted Laser Desorption Ionisation
MAO	Methylaluminoxane
MMA	Methyl methacrylate
n-BA	*n*-butyl acrylate
NIPAM	*N*-isopropylacrylamide
NMP	Nitroxide Mediated Polymerisation
NMR	Nuclear Magnetic Resonance
NU	Nucleating agent
PD	Poly Dispersity
PDI	Poly Dispersity Index (in dynamic light scattering)
PE	Polyethylene
PEB	Poly(ethylene-butene)
PE-*i*-AMS	Polyethylene initiated with AMS
PE-*i*-DIB	Polyethylene initiated with DIB
PEO	Poly(ethylene oxide)
PE-PEP	Polyethylne-*b*-Poly(ethylene-propylene)
PE-*t*-PMS	PE terminated with PMS
PP	Polypropylene
PS	Polystyrene

RAFT	Reversible Addition−Fragmentation chain-Transfer
ROP	Ring Opening Polymerisation
STY	Styrene
TEM	Transmission Electron Microscopy
TEMPO	2,2,6,6-tetramethyl-1-piperidinyloxy
TMEDA	*N*,*N*,*N*′,*N*′-tetramethylethylenediamine
V2EH	Vinyl 2-ethylhexanoate
VA	Vinyl Alcohol
VAc	Vinyl Acetate
VT	Variable Temperature
WAT	Wax Appearance Temperature
WCM	Wax Crystal Modifier
XPS	X-Ray Photoelectron Spectroscopy
XRD	X-Ray Diffraction

Chapter 1

PE-b-PX copolymers as wax crystal modifiers

1.1 Introduction

Crude oil, and refined middle distillate fuel products such as diesel, contain between 10 and 30 wt% of paraffins.[1, 2] These paraffins constitute a high energy material and have a broad distribution of both linear and branched chains, ranging between 16 and 36 carbons in length.[3] The thickness of a single packing layer in a wax mixture is equal to the average length of the wax molecules which comprise it. For any wax molecules that are longer than the typical carbon number length will tend to bend itself within the layer of the wax crystal and associate itself with a shorter than average wax molecule. This causes a mismatch between the lengths of the molecules and therefore the thickness of the packing layers leads to the formation of conformational disorders

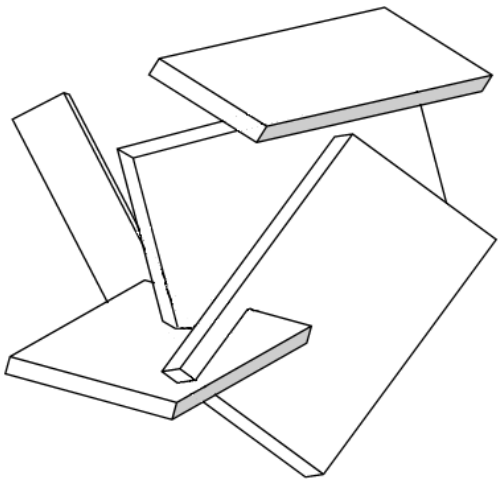

Figure 1.1: Wax crystals interlock into a 'House of cards' structure

in the inter-lamellar regions between the crystals, causing the wax like properties of the material.[4] Upon cooling of these fluids below ambient temperature the long chain paraffins begin to precipitate into plate-like wax crystals which range in size up to hundreds of micrometres. The precipitation of these waxes leads to a dramatic change in the viscosity and viscoelastic properties of the fluid. These individual platelets are then able to agglomerate and interlock to form an extended 'house of cards' style structure[5] shown here in Fig 1.1, the solid network traps large quantities of solvent.[5, 6]

The main technical problems associated with this precipitation are increased pump pressure and engine filter blocking in cold weather.[1, 6-8] Problems also arise in the related area of transport of extracted crudes that pass through pipelines at temperatures below 0°C, as this leads to sedimentation of the waxes and ultimately blocking of pipelines[9, 10] presenting with costs of upwards of $1 million per mile to clear.[11] Sedimentation of wax is also persistent in storage tanks and transportation vessels. The simple separation and removal of these waxy paraffin components is expensive and counterproductive as the high density paraffin is a valuable component of the fluid.[4]

The temperature at which crude or fuel forms a gel, is known as the pour point. This is usually reached at around 10°C in untreated crude oils and occurs over a range of temperatures below 0°C in untreated diesel. A similar parameter to this, which is used as a direct measure of the onset of low temperature operability problems caused by the wax is known as the cold filter plugging point (CFPP), as measured by a standard industry test. This value is relates to the temperature at which a 45 μm filter becomes blocked with wax under a set of standardized conditions[12] and will typically be several degrees higher than the pour point for untreated diesel fuels.

1.2 Mitigation of wax crystal growth

A multitude of methods exist to mitigate the technical problems presented by wax deposition; within pipelines and storage containers the most common methodology is wax removal, either by mechanical, thermal or chemical methods.[13] Meanwhile, in diesel fuels prevention is far more important and chemical additives are blended into the fuel to control and mitigate the precipitation of wax. These additives are known as middle distillate flow improvers or pour point depressants. The additives are typically polymeric species of random, graft or block nature with both amorphous and crystalline regions. The additives will tend to have similar chemical structures to precipitating wax and usually contain non-polar branches as well as polar segments.[14, 15]

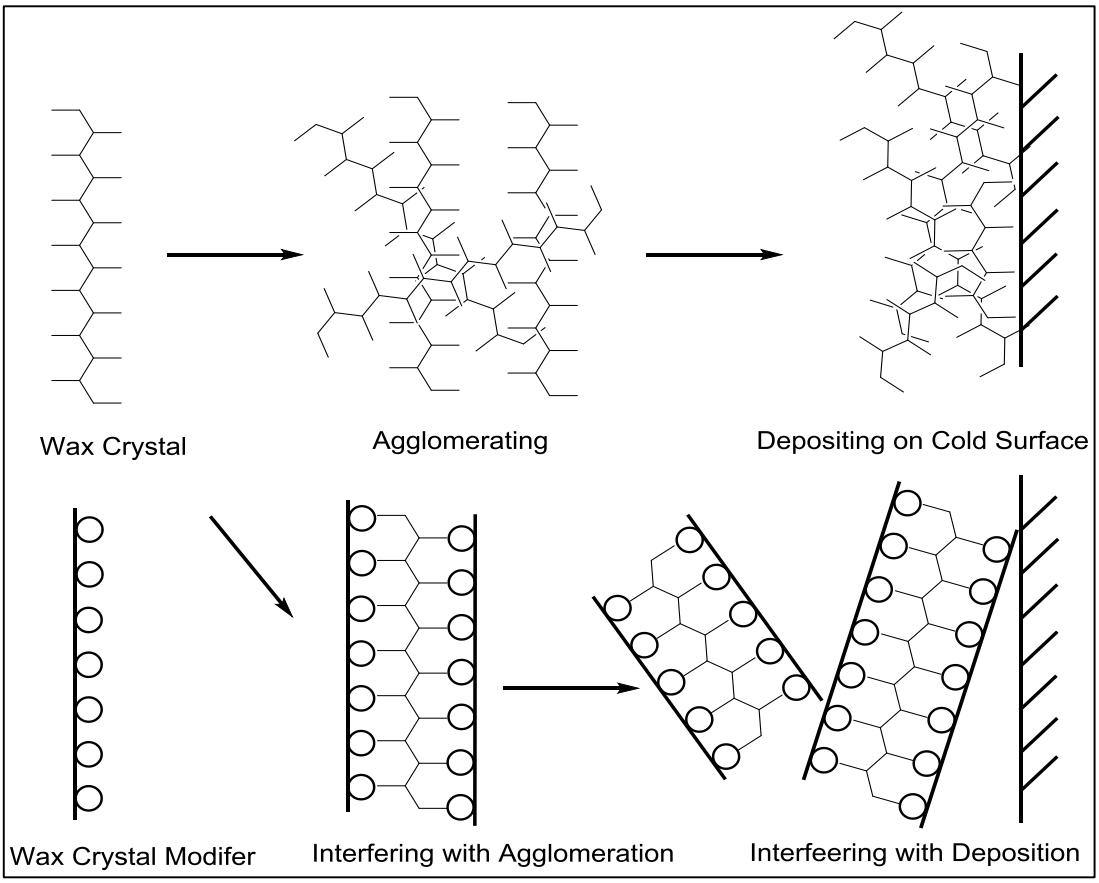

Figure 1.2: Schematic diagram of wax crystal modification by fuel additive.

The action of the additives to modify wax crystal formation is thought[16, 17] to occur in two ways: by providing nucleation sites for crystal growth or by co-precipitation with the wax by occupying a position on the crystal lattice. In the case of nucleation the polymer additives self-assemble in solution and produce micelles. Once formed the micelles are able to serve as templates for the formation of the wax crystals as they precipitate from solution.

In either case the purpose of the additives is to modify the size and shape of the precipitating wax crystals, as the fuel cools below the wax appearance temperature (WAT), and to prevent them from agglomerating into larger structures which could lead to blockages or sedimentation of the wax.[18] A general schematic diagram of this is shown in Figure 1.2. The primary feature of these additives is that they share a common structural characteristic with the wax, and bear both crystalline and amorphous segments present at room temperature. As the temperature of the system decreases these materials, in dilute solution, then undergo self-assembly of the crystalline segments and provides a 'nucleation site' to act as a site for wax formation. As these additive micelles 'take on' wax they are stabilised in solution by the amorphous fraction of the polymer.

1.3 Types of polymer additive

Much research has been conducted on the efficacy of different forms of wax inhibiting additives and the mechanisms by which this inhibition occurs. The overall effectiveness of any and all given additives is usually limited in one capacity or another and tends to vary between materials. For example, in some materials it has been found that additives inhibit the total amount of wax deposition but were unable to suppress the deposition of the higher molecular weight paraffins, (~C35 and

above)[19] which would lead to harder wax deposits. A selection of additives (Figure 1.3) and their limitations are discussed in the next sections.

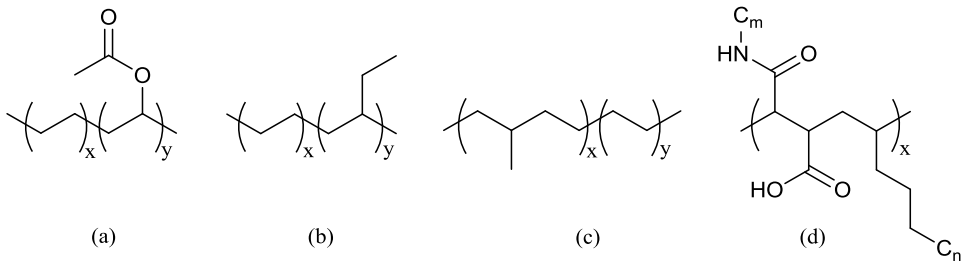

Figure 1.3: Chemical structure of (a)ethylene-vinyl acetate copolymer, (b) ethylene-propene copolymer, (c) Polyethylene-*b*-poly(ethylene propene) and (d) Poly(maleic anhydride amide co-*α*-olefin)

1.3.1 EVA copolymers

The copolymers of ethylene and vinyl acetate, known as EVAs, typically with a high ethylene content, have a long standing history of use as fuel additives and are by far the most extensively used. The copolymerisation of ethylene and vinyl acetate is identified as almost ideal as the reactivity ratios of the two monomers are similar, 0.8 and 1.2 respectively, and thus the monomer incorporation in the polymer will be random.[4]

EVA copolymers, as shown in Figure 1.3(a), have been shown to possess a varying ability to control the size and shape of precipitating wax crystals.[20] When EVA copolymers are used as wax crystal modifiers (WCM) then the wax crystals that precipitate are considerably smaller but there are a far greater number then appear in untreated fuel.[21] The copolymers of EVA can be made with a full range of vinyl acetate content and are shown to have different effects on fuel viscosity and pour point values based upon this value.[14] It has been shown that approximately a 30 mol% content of vinyl acetate gives the most significant change in pour point. The mechanism of wax crystal formation when modified with EVA copolymers depends upon the vinyl acetate content of the copolymer leading to the additive acting as either a nucleating

agent or growth inhibitor.[22] Molecular weight and dispersity of the copolymers also play an important part in the role of wax modification, with some researchers showing that molecular weights in the region of 1.2×10^4 Da gave the greatest effect.[23, 24] Additionally it has been shown that EVA copolymer additives show greater efficacy in suppressing fuels that contain high carbon number paraffins.[25] This assertion was supported in work by Ashbaugh,[26] where the dosage of the polymeric additive showed a lesser effect on the flow improvement in systems that contain lower carbon number paraffins.

Despite the long standing use of these materials they have certain limitations as flow improvers. For instance one such commercial EVA sacrifices ~55 wt% of the added polymer (the ethylene rich fraction) to premature phase separation i.e. precipitation.[6, 26]

1.3.2 PEB copolymers

It has been established that control of wax crystallisation can be achieved by nucleation of wax from the crystallisable segments of polymeric additives. Poly(ethylene-butene) (PEB), often synthesised through the anionic polymerisation and subsequent hydrogenation of 1,3-butadiene,[27] is a statistical copolymer with semi-crystalline and amorphous properties that has received a large amount of recent attention in research.[13] The structure of these polymers is shown in Figure 1.3(b). Like EVA, these copolymers consist of the crystalline ethylene segments with amorphous butene monomers interspersed throughout and the micro-crystallinity of the copolymers can be tuned by altering the ratio of ethylene to butene units.

The co-crystallisation process of PEB with high C_n chain waxes has been studied and was shown that the precipitated wax/polymer formed thin sheets with a single paraffin layer surrounded by the amorphous polymer hairs on each side of the

wax platelet, with polymer distributed homogenously throughout the wax.[27] It was also observed that the precipitating wax tends to form in relatively complex structures such as rods. The nature of the wax crystals serves to reduce the yield stress of the waxy oils as compared with the larger plate like structures that form in untreated samples.

1.3.3 MAC copolymers

Poly(maleic anhydride amide co-α-olefin) (MAC) copolymers are another class of additive which have been shown to reduce wax deposition. The chemical structure of these copolymers is shown in Figure 1.3(d). The performance of three classes of polymer additive, EVA, PEB and MAC, were tested by Tinsley *et al.* and showed that MAC polymers gave the greatest modification to the crystal structure.[28] MAC copolymers have been shown to either self-assemble into micelles, in much the same way as discussed previously, to provide nucleation sites for precipitating wax, or co-crystallise thereby inhibiting wax crystal growth. The length of the alkyl side chains within the copolymers is also of prime importance, with longer side chains seeming to give greater effect on crystal size and therefore greater impact on the flowability.[29] In paraffin crystallisation studies by x-ray diffraction (XRD) it was shown that scattering from the treated samples were greatly reduced or disappeared entirely. This suggests that the polymer additives anchor into the crystals by co-crystallisation and that the non-crystallisable components of the polymer prevent aggregation and platelet stacking by providing a steric barrier.[30]

1.3.4 PE-PEP block copolymers

Alternative wax crystal modifiers based upon low molecular weight crystalline-amorphous diblock copolymers have been developed and proven to show excellent

effects on CFPP even in typically problematic fuels.[31] Copolymers of polyethylene-poly(ethylene-propylene) (PE-PEP) are a diblock copolymer additive which have been shown to be able to act as nucleators for wax crystal size modification in middle distillate fuels.[32, 33] When in solution these polymers self-assemble to form plate like structures, which then function as nucleation templates, nucleating long chain paraffins by giving a large PE surface area for deposition. This gives wax structures with a PE core and amorphous PEP brushes protruding from the surface.

The brief summary of some of the most common WCM polymer additives shows a number of shortcomings and architectural variables that have yet to be explored. Random copolymers of EVA and PEB have been shown to generally act as nucleating agents in WCM, however EVA copolymers suffer from large additive loss (from precipitation) of the nucleation grade additive. While random crystalline-amorphous PEB copolymers maintain solubility via the use of side chain branching. Meanwhile, the crystalline-amorphous diblock copolymers of PE-PEB provide an alternative polymeric structure, and act instead as growth arrestors. However these additives contain no polar moieties and lack amphipathic character.

The creation of an additive which combines assets of the aforementioned additives is therefore attractive, as it may allow for additives which both nucleating and growth arresting ability. We thus envisaged polyolefin-polar diblock copolymers with tuneable block lengths, solubility and incorporation of side chain branches.

1.4 Production of end functional polyolefins

The most widely used commercial polymers are polyolefins, including polyethylene, polypropylene, poly(1-butene) and poly(1-octene). Polyethylene (PE) is the largest

volume synthetic polymer in the world with over 100 million tons of material produced each year.[34] PE comes in one of three major forms: high density polyethylene (HDPE), low density polyethylene (LDPE) and linear low density polyethylene (LLPDE). Control over the molecular weight and crystallinity of polyolefins gives access to a large array of mechanical and thermal properties which can be adjusted for individual applications. These materials appear in films, fibres, waxes and other viscous fluids and see application in every day consumer products to high temperature industrial applications to medical devices. The numerous advantages of PE as a material include its high mechanical strength, chemical stability and resistance to corrosion, not to mention its low production cost.

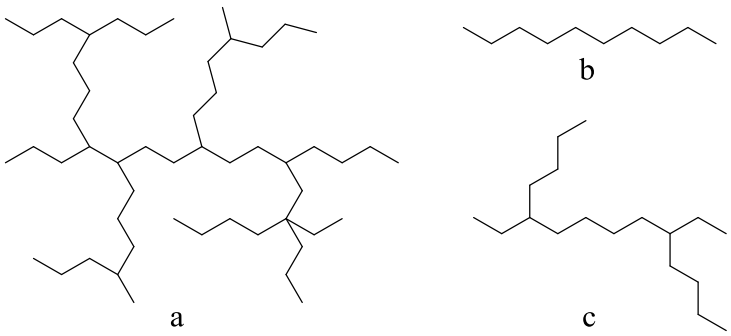

Figure 1.4: Different forms of PE (a) LDPE, (b) HDPE and (c) LLDPE

However PE suffers from its own lack of reactivity which imbues it with an incompatibility with other materials and limits its uses.[35] Therefore the functionalisation of these materials has received great attention, and polymers which bear functionalised polar groups are highly desirable materials, as introducing even a small amount of polar functionality into PE or LLDPE gives a tremendous effect on the properties of the polymer. When these materials are compared to the non-functionalised counterparts they exhibit beneficial properties with respect to adhesion,

toughness, print/paintability, miscibility and rheological properties. It is these outstanding material properties that make functional polymers based on polyolefins of particular interest. Polyolefins have been limited in their uses with materials like dyes, glass, fibres, clays, metals and other polymers due to incompatibility and low adhesive properties. Much time and effort has been dedicated to mitigating these limitations, however significant obstacles to effective compatibilisation still remain.

. It has long been known that block and graft copolymers are excellent for compatibilising mixtures of immiscible polymers, therefore if one wishes to blend polyolefins with other polar materials, polyolefin-polar block copolymers would represent the best choice. As noted by Chung: "Functional polyolefins with block and graft structures are the most desirable materials, with block copolymers being the most ideal, but also the most difficult to prepare." And so over the last 15 years, much work has been invested in finding effective and scalable synthetic routes to functional polyolefins. However despite this, an efficient and viable route to polyolefin-polar block copolymers remains elusive.

1.5 End-functionalisation of PE as a route to block copolymers

PE containing block copolymers are often synthesised from end-functional polyethylene intermediaries attained in one of three varieties (Figure 1.5), these include: (a) the use of a pre-existent vinyl end group in reaction with a functional species which allows synthesis of a polar block; (b) end-functionalisation imparted during ethylene polymerisation *via* metallic or non-metallic chain transfer agents (CTA) - the polar blocks may then be added by direct polymerisation of the end group; or (c) functionality imparted by using a 'reactive co-monomer' from which a second block can be produced *via* ionic polymerisation.

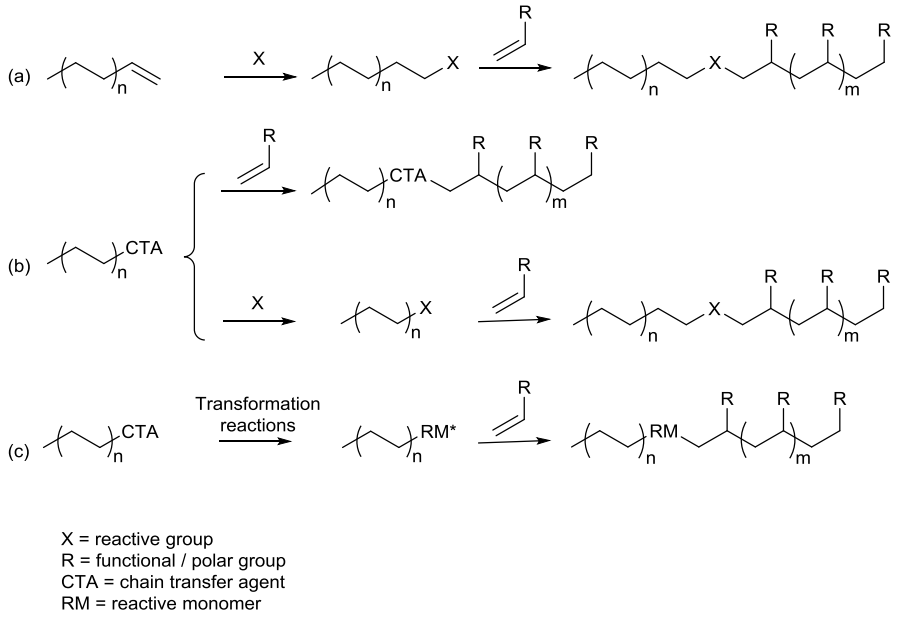

Figure 1.5: General synthesis routes for the production of end-functional PE as a route to block copolymers.

1.5.1 Vinyl end groups

Bis(phenoxy-imine) early transition metal complex catalysts, also known as FI catalysts were developed by Fujita and co-workers, and have been used as olefin polymerization catalysts. They have been shown to have extraordinarily high catalytic activity, even under mild conditions, and have been used to produce PE with low molecular weights, ranging from *ca* 2000-5000 g/mol. The produced polymers have a high vinyl end group fidelity with 78-90% of polymer chains bearing a vinyl group at one end.[36-40]

The vinyl terminated PE then may undergo Alder-ene style reaction with succinic anhydride in the melt phase. Hydrolysis yields succinate terminated PE (Scheme 1.1).[41] When dispersed in water this polymer self assembles to form particles and wormlike fibres.

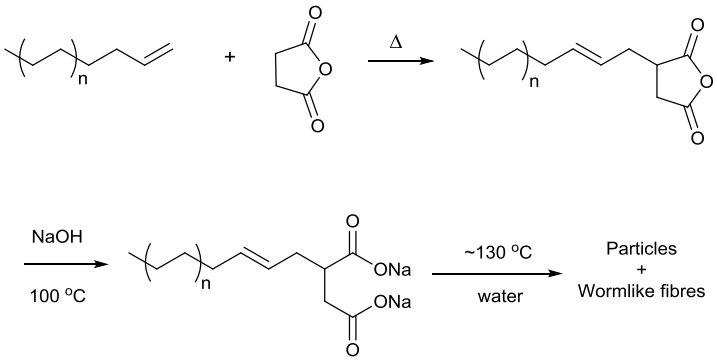

Scheme 1.1: Conversion vinyl terminated PE to succinate terminated PE.[41]

It was additionally reported that diol or triol terminated PE could be achieved *via* oxidation of the vinyl end group, which could be used to initiate ring opening polymerisation (ROP) of ethylene oxide (EO). This would yield PE with a number of pendant PEG chains (Scheme 1.2) [42] A review by Matoishi *et al.* describes each of these techniques as well as other routes to end-functional PE from vinyl terminated PE.[39]

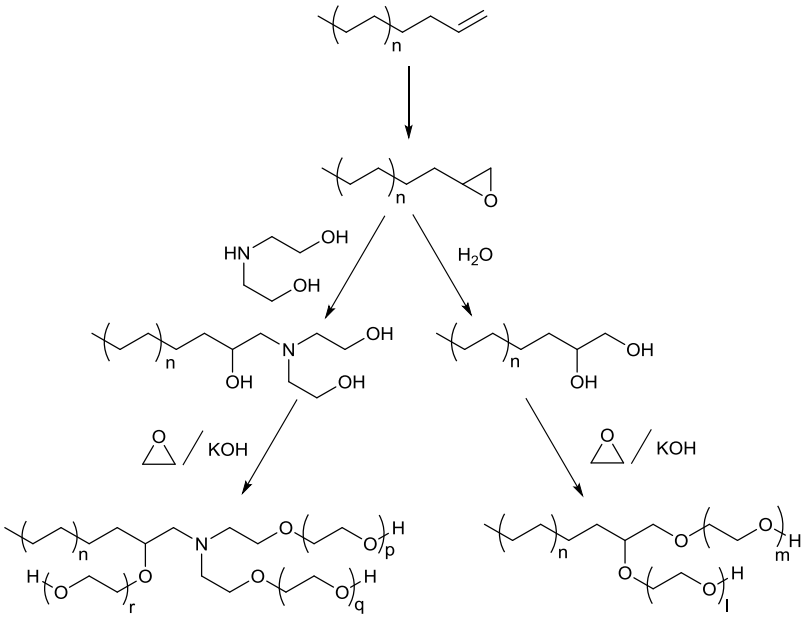

Scheme 1.2: Production of diol and triol-terminated PE from vinyl end groups, followed by ROP of EO.[42]

In 2006, Sengupta *et al.* reported the first example of addition of a thiol group to a vinyl terminated PE, yielding to a silane functionalised PE chain.[43] While such thiol-ene reactions are commonly seen in other branches of polymer chemistry,[44, 45] there have been few reported applications with polyolefins.

In more recent times Mazzolini *et al* have conducted reactions of vinyl terminated PE with a number of different thiols including: thioglycolic acid, methyl thioglycolate, 1-thioglycerol, chloropropanethiol and 2-mercaptoethanol (Scheme 1.3).[46] These studies used a PE with high vinyl end group fidelity (100%) and low molecular weight (M_n = 1440 g/mol) , made with a nickel phosphanylenolate catalyst.[47]

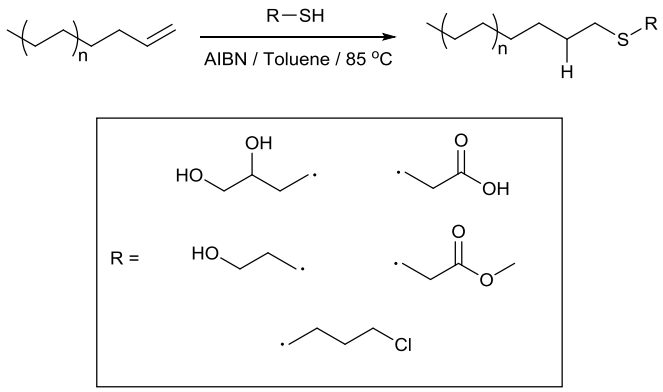

Scheme 1.3: Synthesis of thiol-ene end groups from vinyl-terminated PE.[46]

It has been shown that vinyl terminated PE may be converted into a macroinitiator for atom transfer radical polymerisation (ATRP), as a possible route to producing block or graft copolymers (Scheme 1.4). [48]

As before, a relatively low molecular weight PE (1800 g/mol) with a high vinyl end group fidelity (92%) was utilised, and upon reaction with 2-bromoisobutyric acid, catalysed by trifluoromethanesulfonic acid, was converted into a suitable ATRP macroinitiator. From this a range of block copolymers are accessible through

controlled radical polymerisation of a variety of monomers, including: *n*-butyl acrylate (*n*-BA), methyl methacrylate (MMA) or styrene, initiated by the functionalized PE. This three step process yielded block copolymers with good PE conversion (>75%) and control of molecular weight.

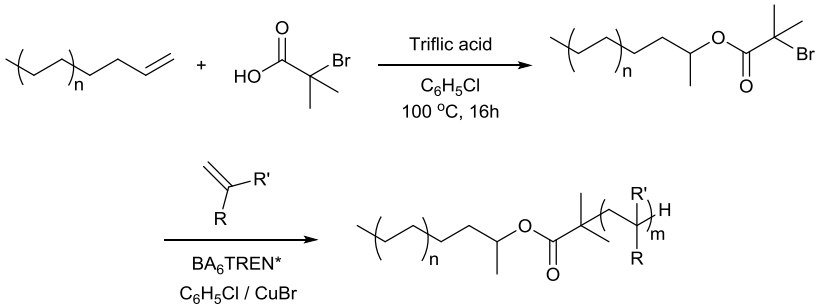

R = $COOC_4H_9$, R' = H
R = $COOCH_3$, R' = CH_3
R = Ph, R' = H
*tris(2-{di[2-(n-butoxycarbonyl)ethyl]amino}ethyl)amine

Scheme 1.4: Production of a PE based ATRP macroinitiator for subsequent polymerisation of *n*-BA, MMA or STY.

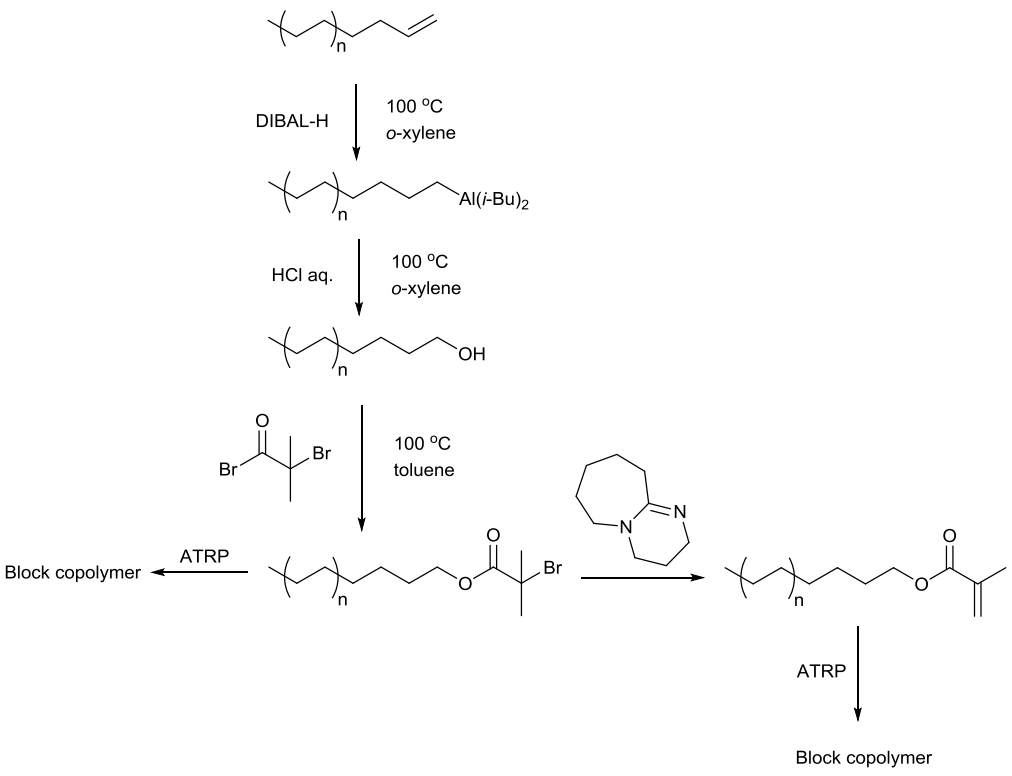

Scheme 1.5: Synthesis of a PE-based ATRP macroinitiator and conversion to a PE-based macromonomer leading to block and graft copolymers respectively.

Additionally Kaneyoshi reported the conversion of the vinyl end group to a hydroxyl group first by hydroalumination, then subsequent oxidation and hydrolysis (Scheme 1.5). Utilising this hydroxyl terminated PE in a reaction with 2-bromo-2-methylpropionyl bromide yielded PE with an α-bromoester terminal functionality. This species could then be used as a macroinitiator for ATRP in order to produce a block copolymer in a multi-step reaction. Alternatively the bromoester group can undergo dehydrobromination to give a methacrylate group, which can then be treated with e.g. styrene to produce graft copolymers.[49]

1.5.2 End-functionalisation *via* chain transfer

As a route to end functional polyolefins, chain transfer reactions benefit from high catalyst efficiency in that the active species produces multiple polymer chains.[50, 51] The result of this is that the polymers have a high end group fidelity and so a variation of the monomer to chain transfer agent ratio has a direct control of molecular weight. There are a number of types of chain transfer reaction including i) non-metallic chain transfer agents, ii) metallic chain transfer agents and iii) β-hydride elimination. In the final instance, β-hydride elimination, this is a process which often produces polymers of low molecular weight terminated with a vinyl group,[52] and as shown previously, modification of these end groups is possible through post polymerisation.

1.5.2.1 Non-metallic chain transfer agents

The addition of heteroatoms to the PE chain end *via* the use of chain transfer agents was reviewed by Marks and co-workers,[53] and a variety of end groups are accessible. Such end groups include amines and phosphines, incorporated through the use of

organolanthanide catalysts,[54, 55] and silane end groups added *via* metallocene and organolanthanide catalysts.[56-59]

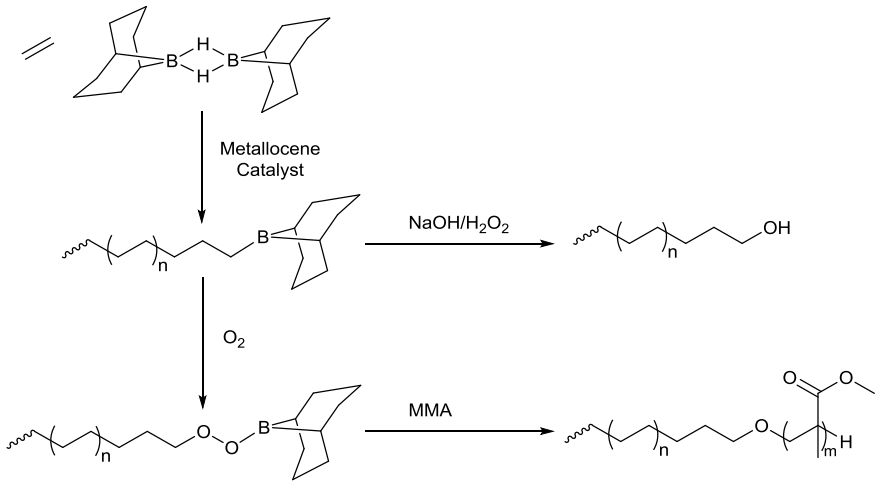

Scheme 1.6: Synthesis of borane-terminated PE.[60, 61]

Chung and co-workers have synthesised PE with a terminal borane group *via* chain transfer to the organoborane dimer 9-borabicyclo[3.3.1]nonane during metallocene catalysed polymerisation (Scheme1.6).[60] Additionally, it was reported that a terminal peroxide group (-BOOC-) could be formed from the borane group by reaction with gaseous oxygen. This terminal peroxide group was then utilised in a second step to initiate radical polymerisation of MMA and yield PE-*b*-PMMA block copolymers. Alternatively, Chung describes[62] the conversion of the borane terminated PE, into a terminal hydroxyl group *via* an oxidative process followed by metalation with potassium naphthalide. This produced a metallated polyolefin, which was suitable as an anionc macroinitiator for ROP of EO yielding a PE-*b*-P(EO) copolymer. Commercially available triethylborane was used by Dong and co-workers[63] as a chain transfer agent olefin polymerisation catalysed by metallocenes. Oxidation of these end groups formed hydroxyl terminated PE.

Conversely, vinyl chloride has been seldom seen as a chain transfer agent but was reported by Gaynor *et al.* in copolymerisation of ethylene to terminate *via* β-Cl elimination, yielding vinyl terminated PE.[64] The distinct advantage of this is the low cost of system as compare with other described above for silanes and boranes and produces vinyl terminate PE with a range of metallocene catalysts.

1.5.2.2 Metallic chain transfer agents

Coordinative chain transfer polymerisation (CCTP) and similar strategies were developed[65] to overcome the drawbacks of living olefin polymerisation[50, 51] such as catalytic activity, in that one molecule of catalyst is required per chain produced, while maintaining highly controlled polymerisation with $Đ < 1.1$. The process of CCTP typically makes use of transition metal catalysts and a main group metal alkyl chain transfer agent. This system produces many polymer chains per catalytic species and ensures that all chains are end capped with whichever chain transfer metal was used. A review of a variety of CCTP systems, yielding polyolefins terminated with a range of metals was produced by Valente *et al.*,[66] however the functionalisation of these metallated polymers was not discussed.

1.5.2.2.1 Zinc

Zn-alkyl terminate polyolefins that arise from chain transfer from transition metals to zinc are common in literature. Zn-C bond have a high reactivity and are used to produce vinyl,[67, 68] halogen,[69] hydroxyl,[70] carbonyl[69] and amine[71] end groups to polypropylene (PP).

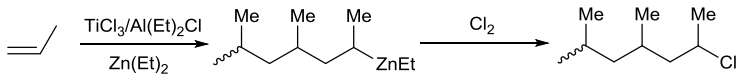

Scheme 1.7 – Halogen end-functionalisation of polypropylene *via* intermediate chain transfer to zinc.[69]

Gibson and co-workers[72-74] were the first to discover the conditions that give rise to catalytic chain-growth (CCG) utilizing zinc. Their work led to the synthesis of Zn terminated PE accessible from a range of catalytic systems, with high activity, using a variety of transition metals.

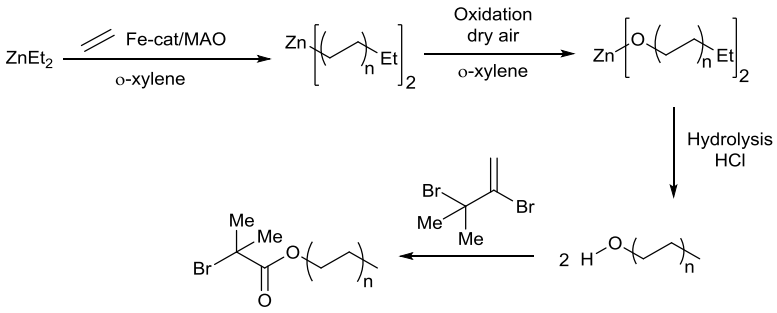

Scheme 1.8 - Synthesis hydroxyl terminated PE *via* the oxidation of a mid-chain zinc atom.[75]

The polymerisation of ethylene by iron catalysts in the presence of diethyl zinc has been reported to produce mid chain Zn-carbon bonds.[75] Through hydrolysis these mid chain metals could then be converted to hydroxyl end groups. (Scheme 1.8)

From this, a PE based ATRP macroinitiator could be synthesised *via* treatment of these hydroxyl end groups with 2-bromo-2-methylpropionyl bromide. A similar approach for producing ATRP macroinitiator was described by Zhu and co-workers.[76] Hydroxyl terminated PE macroinitiators of this type have also seen use in ROP of lactide, as was reported by Ring *et al.*.[77] Conversely, an end chain hydroxyl unit may be converted to a trithiocarbonate terminal group, through reaction with *S*-1-dodecyl-

S'-(α,α'-dimethyl-α"-acetic acid) trithiocarbonate. This PE based macroinitiator can then be used in RAFT polymerisation of NIPAM and 2-vinylpyridine.[78]

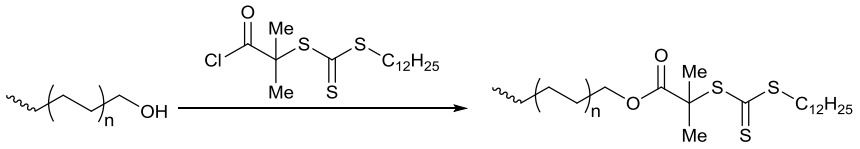

Scheme 1.9 - Synthesis of trithiocarbonate-terminated PE from PE-OH.[78]

1.5.2.2.2 Aluminium

Polymerisations conducted using transition metal catalysts in the presence of aluminium and zinc alkyls produce similar products, specifically hydroxyl terminated polyolefins. Polymerisations of ethylene and allylbenzene catalysed by metallocenes and methylaluminoxane (MAO) co-catalysts was shown to strongly favour a chain transfer to aluminium following insertion of allybenzene.[79, 80] Ligand structure of the catalyst was found to be of high importance to the mode of chain transfer, and a highly substituted species was likely to give chain transfer to aluminium. Oxidation of this species (Scheme 1.10) could then be done to produce PE-OH, which as shown previously could be used as a macroinitiator for ROP.[81]

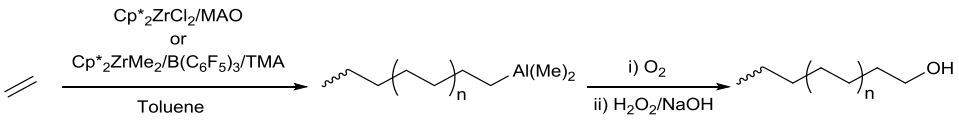

Scheme 1.10 - Synthesis of hydroxyl terminated PE *via* chain transfer to aluminium followed by oxidative workup.[81]

By varying reaction time and concentration of chain transfer agents Fujita and co-workers were able to produce a range of molecular weight PE-Al species through the use of Zr-FI catalysts and aluminium based chain transfer agents.[82] Hydroxyl

terminated PE *via* polymerisation with allyl alcohol comonomer and metallocene indenyl-fluorenyl (IF) catalysts in the presence of MAO co-catalyst was reported by Imuta *et al*.[83]

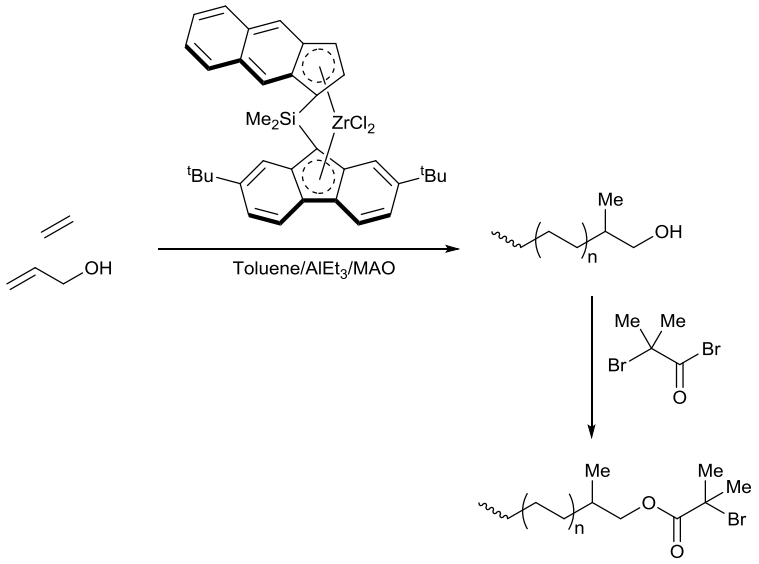

Scheme 1.11 - Copolymerisation of ethylene with allyl alcohol in presence of metallocene IF catalyst producing PE-OH followed by conversion to an ATRP macroinitiator.[83]

Chain transfer to aluminium occurs following the selective end chain incorporation of allyl alcohol monomer, then *via* oxidation, hydroxyl terminated PE is produced (Scheme 1.11). Imuta *et al.* further report, in a manner similar to Matyjaszewski, the conversion of the hydroxyl terminated PE into an ATRP macroinitiator. Other routes to the synthesis of PE-OH include the use of yttrium based catalysts in conjunction with aluminium transfer agents.[84]

1.5.2.2.3 Magnesium

Ziegler-Natta catalysts, using aluminium alkyl co-catalysts have been used to synthesise hydroxyl terminated polypropylene. $TiCl_3$ catalysts supported with $MgCl_2$, in the presence of $AlEt_3$[85] and Al(*i*-Bu)$_3$[86] co-catalysts were used to synthesise isotactic

and atactic polypropylene terminated with aluminium, which is then subsequently quenched with oxygen to produce a hydroxyl end group.

N-butyloctylmagnesium and other such magnesium based compounds were used as metallic chain transfer agents in combination with neodymium catalyst $(Cp^*)_2NdCl_2Li(OEt_2)_2$ in work described by Mortreux and co-workers (Scheme 1.12).[87] This produces a PE-Mg-PE polymeric species with a narrow dispersity and low molecular weight. Post-polymerisation of this PE-Mg-PE species would later be used by Boisson and co-workers to produce a range of end-functionalised PE.[88]

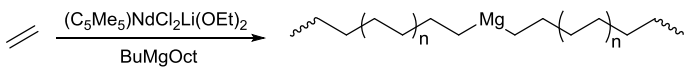

Scheme 1.12 - Synthesis of PE-Mg-PE[87]

PE bearing a terminal alkoxyamine group has been reported by the same authors *via* the reaction of the in-chain magnesium-carbon bonds with 2,2,6,6-tetramethy-1-piperidinyloxy (TEMPO), yielding a polymer end group fidelity of *ca* 63% (Scheme 1.13).[89] Further to this Boisson *et al*. demonstrated the synthesis of two additional nitroxides (DD1 & DD2) and their following addition to the PE chain end.[90] A far lower temperature (60°C) was needed in reactions utilising the second of these nitroxides (DD2), than was necessary for TEMPO to initiate the nitroxide mediated polymerisation *via* cleaving of the C-ON bond, however despite this end group fidelity of the polymer remained low *ca* 40%.

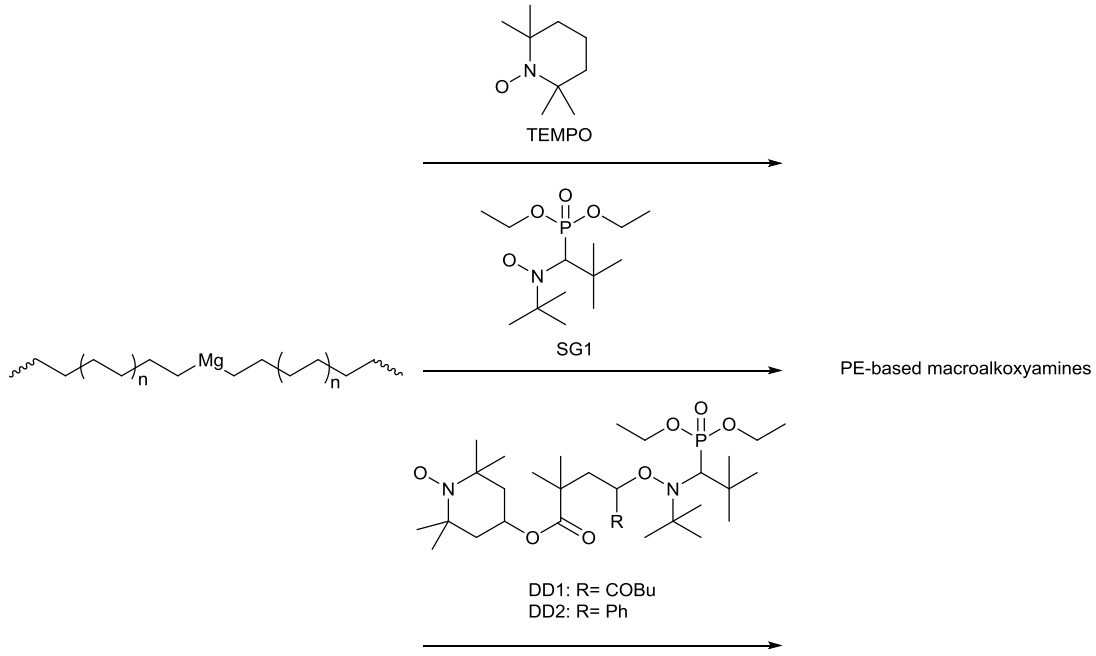

Scheme 1.13 - Synthesis of PE-based macroalkoxyamines for NMP. [89-91]

The conversion of PE-Mg-PE to a thiocarbonylate terminated PE (Scheme 1.14) was also investigated for its use as in RAFT polymerisations by the same group. This synthesis however suffered from side-reactions and low conversion of end groups. [92, 93]

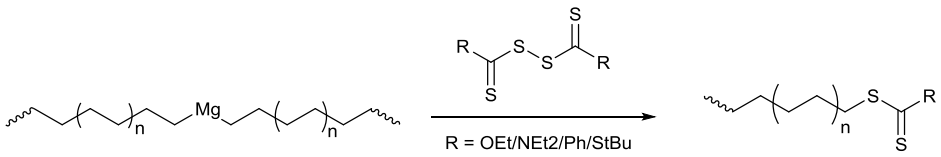

Scheme 1.14 - Synthesis of PE-based RAFT agents.[92, 93]

Iodine terminated PE was also synthesised from these PE-Mg-PE species and was achieved with high efficiency from such species the synthesis of azide terminated PE was achieved.[94] This azide group can then be reduced to give a terminal amine. (Scheme 1.15).

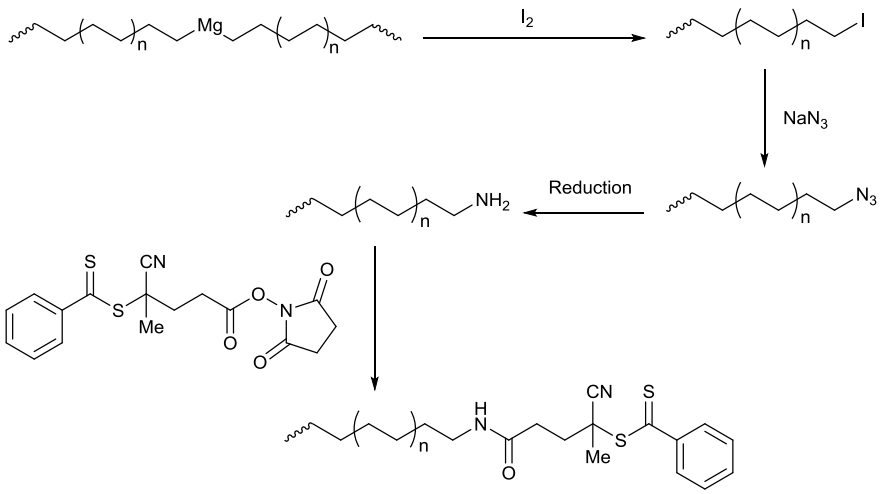

Scheme 1.15 – Functionalisation of PE from the PE-Mg-PE species, including synthesis of a macroRAFT agent.[94]

Thiol terminated PE is accessible from PE-Mg-PE through a number of methods, as investigated by Boisson and co-workers. Most notably was through the use of $LiAlH_4$ to reduce dithiocarbonylate terminated PE (Scheme 1.16)[95] The ROP of lactide could then be initiated from the resultant thiol-PE.[96] Additionally a coupling reaction between PE-SH and an acrylate-terminated PEO was found to be possible, giving rise to PE-*b*-PEO block copolymers.[97]

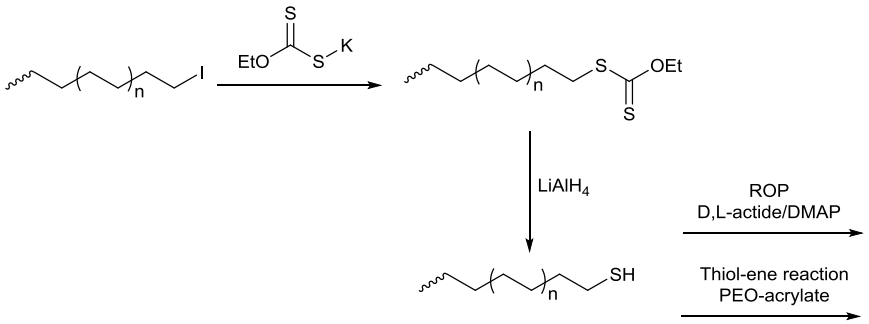

Scheme 1.16 - Synthesis of PE-SH from PE-I.[95-97]

1.5.3 Reactive comonomer approach

Chung describes[98] the concept of using reactive comonomers in the functionalisation of polyolefins. The critical requirements of such a reactive comonomer must include: (a) no catalytic deactivation; (b) effective comonomer incorporation; (c) versatile transformation reactions, and (d) "living" graft from polymerisation reactions. Within his investigation, Chung describes two types of reactive comonomers which led to the termination of PE; borane monomers and *para*-methylstyrene (PMS).

1.5.3.1 PMS-terminated PE

The synthesis of PE terminated with PMS (PE-*t*-PMS) which was catalysed by group IV metal catalysts (including Cp_2ZrCl_2) is shown (Scheme 1.22).[99]

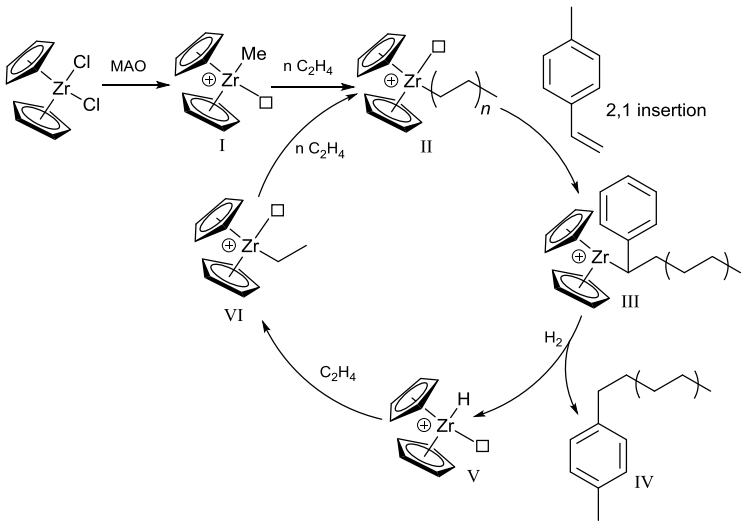

Scheme 1.17: Chain transfer to PMS and hydrogenolysis exemplified in the Chung system[99, 100]

Following pre-catalyst activation by methylaluminoxane (MAO) gives catalyst species **I** multiple ethylene units are inserted to yield species **II**, a growing PE chain. This growing chain will eventually insert, *via* 2,1-insertion, a molecule of PMS

leading to species **III**. In the presence of hydrogen, species **III** will undergo hydrogenolysis to give PE-*t*-PMS (this was termed as a consecutive chain transfer reaction by the authors) and species **VI** a cationic zirconium-hydride catalytic species. The hydride species **VI** is then able to insert ethylene once more and the catalytic cycle continues.

The formation of PE-t-PMS via the mechanism outlined above is dependent upon the formation of a dormant state that arise after the selective 2,1-insertion of PMS monomer into the Zr-C bond of species **II**, as well as a very low rate or 1,2-insetion that would yield in chain incorporations of PMS.

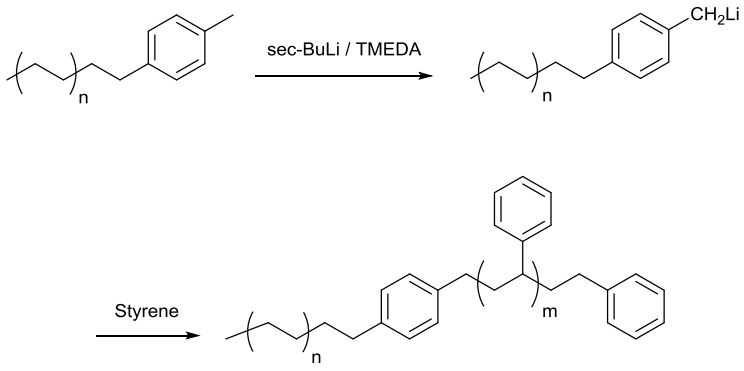

Scheme 1.18: Synthesis of PE-*b*-PS from PE-*t*-PMS.[99]

The PE-t-PMS macromonomer was then used as an anionic macroinitiator in the synthesis of block copolymers, namely PE-b-PS, in a multi-step reaction (Scheme 1.23), based upon work with polypropylene. An anion on the PE-t-PMS was generated by deprotonation of the tolyl group. This was achieved by treatment with *sec*-BuLi and *N*,*N*,*N*′,*N*′-tetramethylethylenediamine (TMEDA) in the absence of water and oxygen. Following this styrene monomer was added to the polymer suspension, producing PE-b-PS.

1.6 Conclusions

The sheer volume of interest in the development of functional polyolefin materials that has been shown in recent years is indicative of the importance of the field. Despite this, while the many examples and successes that have been reported provide routes for the production of end functionalisation of polyolefins, they are all hindered in at least one of a number of ways. Synthetic strategies may make use of less accessible and expensive catalysts, require the use of expensive reagents or suffer from low productivities, making the process un-scalable. These process often require multiple steps or rely on ionic polymerisation.

The next chapter of this thesis will begin with the development of a modification of the Chung mechanism (*vide supra*), and how this may be used to produce end functional LLDPE materials. Other chapters will discuss the use of these end functional materials to produce block copolymers, and the testing of the efficacy of these materials as WCM.

1.7 References

1. P. Claudy, J.-M. Létoffé, B. Bonardi, D. Vassilakis and B. Damin, *Fuel*, 1993, 72, 821-827.
2. J. A. P. Coutinho, C. Dauphin and J. L. Daridon, *Fuel*, 2000, 79, 607-616.
3. A. P. Radlinski, L. Barré and D. Espinat, *J . Mol Cryst*, 1996, 383, 51-56.
4. A. Radulescu, L. J. Fetters and D. Richter, in *Wax Crystal Control · Nanocomposites · Stimuli-Responsive Polymers*, Springer Berlin Heidelberg, 2008, vol. 210, ch. 124, pp. 1-100.
5. D. J. Abdallah and R. G. Weiss, *Langmuir*, 2000, 16, 352-355.
6. H. S. Ashbaugh, A. Radulescu, R. K. Prud'homme, D. Schwahn, D. Richter and L. J. Fetters, *Macromolecules*, 2002, 35, 7044-7053.
7. I. M. El-Gamal and A. M. Al-Sabbagh, *Fuel*, 1996, 75, 743-750.
8. A. A. Gupta, K. K. Swami, D. T. Wakade, A. K. Misra and A. K. Bhatnagar, *6th LAWPSP Symposium*, Indian Institute of Technology, Bombay, 1989.
9. R. Venkatesan, J.-A. Östlund, H. Chawla, P. Wattana, M. Nydén and H. S. Fogler, *Energy Fuels*, 2003, 17, 1630-1640.

10. R. Venkatesan, N. R. Nagarajan, K. Paso, Y. B. Yi, A. M. Sastry and H. S. Fogler, *Chem. Eng. Sci.*, 2005, 60, 3587-3598.
11. M. Senra, E. Panacharoensawad, K. Kraiwattanawong, P. Singh and H. S. Fogler, *Energy Fuels*, 2008, 22, 545-555.
12. in *ASTM Standard D6371* ASTM International, West Conshohocken, PA, 2016.
13. B. Wei, *J. Pet Expl Prod Technol*, 2015, 5, 391-401.
14. A. L. C. Machado, E. F. Lucas and G. González, *J. Pet. Sci. Eng.*, 2001, 32, 159-165.
15. K. G. Paso and H. S. Fogler, *Energy Fuels*, 2004, 18, 1005-1013.
16. A. M. Atta, H. I. Al-Shafy and E. A. Ismail, *J. Dispersion Sci. Technol.*, 2011, 32, 1296-1305.
17. L. Fang, X. Zhang, J. Ma and B. Zhang, *Ind. Eng. Chem. Res.*, 2012, 51, 11605-11612.
18. F. Yang, Y. Zhao, J. Sjöblom, C. Li and K. G. Paso, *J. Dispersion Sci. Technol.*, 2014, 36, 213-225.
19. K.-S. Wang, C.-H. Wu, J. L. Creek, P. J. Shuler and Y. Tang, *Pet. Sci. Technol.*, 2003, 21, 369-379.
20. L. C. Vieira, M. B. Buchuid and E. F. Lucas, *J Appl Polym Sci*, 2012, 126, 143-149.
21. J. C. Petinelli, *Rev. Inst. Fr. Pet.*, 1979, 34, 791-811.
22. E. Marie, Y. Chevalier, F. Eydoux, L. Germanaud and P. Flores, *J Colloid Interface Sci*, 2005, 290, 406-418.
23. F. Yang, C. Li and M. Lin, *Zhongguo Shiyou Daxue Xuebao, Ziran Kexueban*, 2009, 33, 108-113.
24. Q.-z. Jiang, G. Yue and Z.-z. Song, *Xinan Shiyou Xueyuan Xuebao*, 2006, 28, 71-74.
25. A. L. C. Machado and E. F. Lucas, *J. Appl. Polym. Sci.*, 2002, 85, 1337-1348.
26. H. S. Ashbaugh, X. Guo, D. Schwahn, R. K. Prud'homme, D. Richter and L. J. Fetters, *Energy Fuels*, 2005, 19, 138-144.
27. D. Schwahn, D. Richter, M. Lin and L. J. Fetters, *Macromolecules*, 2002, 35, 3762-3768.
28. J. F. Tinsley, R. K. Prud'homme, X. Guo, D. H. Adamson, S. Callahan, D. Amin, S. Shao, R. M. Kriegel and R. Saini, *Energy Fuels*, 2007, 21, 1301-1308.
29. J. Xu, X. Zhang, J. Sun, L. Li and X. Guo, *Asia-Pac. J. Chem. Eng.*, 2009, 4, 551-556.
30. L. Li, X. Guo, D. H. Adamson, B. A. Pethica, J. S. Huang and R. K. Prud'homme, *Ind. Eng. Chem. Res.*, 2011, 50, 316-321.
31. D. G. Goberdhan, R. D. Tack, K. Lewtas, A. M. Mcaleer, L. J. Fetters and J. Huang, Google Patents, 2006.
32. W. Leube, M. Monkenbusch, D. Schneiders, D. Richter, D. Adamson, L. Fetters, P. Dounis and R. Lovegrove, *Energy Fuels*, 2000, 14, 419-430.

33. M. Monkenbusch, D. Schneiders, D. Richter, L. Willner, W. Leube, L. J. Fetters, J. S. Huang and M. Lin, *Physica B (Amsterdam, Neth.)*, 2000, 276, 941-943.
34. W. Kaminsky, *Macromol. Chem. Phys.*, 2008, 209, 459-466.
35. T. Matsugi, S.-I. Kojoh, N. Kawahara, S. Matsuo, H. Kaneko and N. Kashiwa, *J. Polym. Sci., Part A: Polym. Chem.*, 2003, 41, 3965-3973.
36. I. Sei-ichi, M. Makoto, S. Junji, M. Sadahiko, K. Shin-ichi, K. Norio and F. Terunori, *Chem. Lett.*, 2002, 31, 740-741.
37. H. Terao, S.-i. Ishii, J. Saito, S. Matsuura, M. Mitani, N. Nagai, H. Tanaka and T. Fujita, *Macromolecules*, 2006, 39, 8584-8593.
38. S.-i. Kojoh, S. Matsuo, T. Matsugi, S.-i. Ishii, S. Matsuura, T. Fujita and N. Kashiwa, in *Stud. Surf. Sci. Catal.*, eds. M. O. Masakazu Anpo and Y. Hiromi, Elsevier, 2003, vol. Volume 145, pp. 519-520.
39. K. Matoishi, K. Nakai, N. Nagai, H. Terao and T. Fujita, *Catal. Today*, 2011, 164, 2-8.
40. H. Makio, H. Terao, A. Iwashita and T. Fujita, *Chem. Rev.*, 2011, 111, 2363-2449.
41. A. V. Sesha Sainath, M. Isokawa, M. Suzuki, S. Ishii, S. Matsuura, N. Nagai and T. Fujita, *Macromolecules*, 2009, 42, 4356-4358.
42. K. Matoishi, S. Nakatsuka, K. Nakai, M. Isokawa, N. Nagai and T. Fujita, *Chem. Lett.*, 2010, 39, 1028-1029.
43. S. S. Sengupta and J. S. Parent, *Polym. Eng. Sci.*, 2006, 46, 480-485.
44. C. E. Hoyle and C. N. Bowman, *Angew. Chem. Int. Ed.*, 2010, 49, 1540-1573.
45. M. J. Kade, D. J. Burke and C. J. Hawker, *J. Polym. Sci., Part A: Polym. Chem.*, 2010, 48, 743-750.
46. J. Mazzolini, O. Boyron, V. Monteil, D. Gigmes, D. Bertin, F. D'Agosto and C. Boisson, *Macromolecules*, 2011, 44, 3381-3387.
47. P. Kuhn, D. Sémeril, C. Jeunesse, D. Matt, M. Neuburger and A. Mota, *Chem. Eur. J.*, 2006, 12, 5210-5219.
48. Y. Inoue and K. Matyjaszewski, *J. Polym. Sci., Part A: Polym. Chem.*, 2004, 42, 496-504.
49. H. Kaneyoshi and K. Matyjaszewski, *J. Appl. Polym. Sci.*, 2007, 105, 3-13.
50. G. J. Domski, J. M. Rose, G. W. Coates, A. D. Bolig and M. Brookhart, *Prog. Polym. Sci.*, 2007, 32, 30-92.
51. G. W. Coates, P. D. Hustad and S. Reinartz, *Angew. Chem. Int. Ed.*, 2002, 41, 2236-2257.
52. N. M. G. Franssen, J. N. H. Reek and B. de Bruin, *Chem. Soc. Rev.*, 2013, 42, 5809-5832.
53. S. B. Amin and T. J. Marks, *Angew. Chem. Int. Ed.*, 2008, 47, 2006-2025.
54. S. B. Amin, S. Seo and T. J. Marks, *Organometallics*, 2008, 27, 2411-2420.
55. A. M. Kawaoka and T. J. Marks, *J. Am. Chem. Soc.*, 2005, 127, 6311-6324.
56. K. Koo and T. J. Marks, *J. Am. Chem. Soc.*, 1999, 121, 8791-8802.
57. K. Koo, P.-F. Fu and T. J. Marks, *Macromolecules*, 1999, 32, 981-988.

58. K. Koo and T. J. Marks, *J. Am. Chem. Soc.*, 1998, 120, 4019-4020.
59. P.-F. Fu and T. J. Marks, *J. Am. Chem. Soc.*, 1995, 117, 10747-10748.
60. G. Xu and T. C. Chung, *J. Am. Chem. Soc.*, 1999, 121, 6763-6764.
61. T. C. Chung, G. Xu, Y. Lu and Y. Hu, *Macromolecules*, 2001, 34, 8040-8050.
62. Y. Lu, Y. Hu, Z. M. Wang, E. Manias and T. C. Chung, *J. Polym. Sci., Part A: Polym. Chem.*, 2002, 40, 3416-3425.
63. W. Lin, H. Niu, T. C. M. Chung and J.-Y. Dong, *J. Polym. Sci., Part A: Polym. Chem.*, 2010, 48, 3534-3541.
64. S. G. Gaynor, *Macromolecules*, 2003, 36, 4692-4698.
65. R. Kempe, *Chem. Eur. J.*, 2007, 13, 2764-2773.
66. A. Valente, A. Mortreux, M. Visseaux and P. Zinck, *Chem. Rev.*, 2013, 113, 3836-3857.
67. T. Shiono, H. Kurosawa and K. Soga, *Macromolecules*, 1995, 28, 437-443.
68. H. Kurosawa, T. Shiono and K. Soga, *Macromol. Chem. Phys.*, 1994, 195, 1381-1388.
69. T. Shiono, H. Kurosawa and K. Soga, *Makromol. Chem.*, 1992, 193, 2751-2761.
70. D. R. Burfield, *Polymer*, 1984, 25, 1817-1822.
71. T. Shiono, H. Kurosawa and K. Soga, *Macromolecules*, 1994, 27, 2635-2637.
72. G. J. P. Britovsek, S. A. Cohen, V. C. Gibson, P. J. Maddox and M. van Meurs, *Angew. Chem. ,* 2002, 114, 507-509.
73. G. J. P. Britovsek, S. A. Cohen, V. C. Gibson and M. van Meurs, *J. Am. Chem. Soc.*, 2004, 126, 10701-10712.
74. M. van Meurs, G. J. P. Britovsek, V. C. Gibson and S. A. Cohen, *J. Am. Chem. Soc.*, 2005, 127, 9913-9923.
75. H. Kaneyoshi, Y. Inoue and K. Matyjaszewski, *Macromolecules*, 2005, 38, 5425-5435.
76. W. Wang, R. Liu, Z. Li, C. Meng, Q. Wu and F. Zhu, *Macromol. Chem. Phys.*, 2010, 211, 1452-1459.
77. J. O. Ring, R. Thomann, R. Mülhaupt, J.-M. Raquez, P. Degée and P. Dubois, *Macromol. Chem. Phys.*, 2007, 208, 896-902.
78. Y. Zhao, X. Shi, H. Gao, L. Zhang, F. Zhu and Q. Wu, *J. Mater. Chem.*, 2012, 22, 5737-5745.
79. D.-J. Byun, D.-K. Shin and S. Y. Kim, *Macromol. Rapid Commun.*, 1999, 20, 419-422.
80. D.-J. Byun and S. Y. Kim, *Macromolecules*, 2000, 33, 1921-1923.
81. C. J. Han, M. S. Lee, D.-J. Byun and S. Y. Kim, *Macromolecules*, 2002, 35, 8923-8925.
82. J. Saito, Y. Tohi, N. Matsukawa, M. Mitani and T. Fujita, *Macromolecules*, 2005, 38, 4955-4957.
83. J.-i. Imuta, N. Kashiwa and Y. Toda, *J. Am. Chem. Soc.*, 2002, 124, 1176-1177.

84. W. P. Kretschmer, T. Bauer, B. Hessen and R. Kempe, *Dalton Trans.*, 2010, 39, 6847-6852.
85. T. Shiono, K. K. Kang, H. Hagihara and T. Ikeda, *Macromolecules*, 1997, 30, 5997-6000.
86. K. K. Kang, T. Shiono and T. Ikeda, *Macromolecules*, 1997, 30, 1231-1233.
87. J.-F. Pelletier, A. Mortreux, X. Olonde and K. Bujadoux, *Angew. Chem. Int. Ed.*, 1996, 35, 1854-1856.
88. J. Mazzolini, E. Espinosa, F. D'Agosto and C. Boisson, *Polym. Chem.*, 2010, 1, 793-800.
89. R. G. Lopez, C. Boisson, F. D'Agosto, R. Spitz, F. Boisson, D. Bertin and P. Tordo, *Macromolecules*, 2004, 37, 3540-3542.
90. R. Godoy Lopez, C. Boisson, F. D'Agosto, R. Spitz, F. Boisson, D. Gigmes and D. Bertin, *J. Polym. Sci., Part A: Polym. Chem.*, 2007, 45, 2705-2718.
91. D. Benoit, V. Chaplinski, R. Braslau and C. J. Hawker, *J. Am. Chem. Soc.*, 1999, 121, 3904-3920.
92. R. Godoy Lopez, C. Boisson, F. D'Agosto, R. Spitz, F. Boisson, D. Gigmes and D. Bertin, *Macromol. Rapid Commun.*, 2006, 27, 173-181.
93. F. D'Agosto and C. Boisson, *Australian Journal of Chemistry*, 2010, 63, 1155-1158.
94. R. Briquel, J. Mazzolini, T. Le Bris, O. Boyron, F. Boisson, F. Delolme, F. D'Agosto, C. Boisson and R. Spitz, *Angew. Chem. Int. Ed.*, 2008, 47, 9311-9313.
95. J. Mazzolini, I. Mokthari, R. Briquel, O. Boyron, F. Delolme, V. Monteil, D. Bertin, D. Gigmes, F. D'Agosto and C. Boisson, *Macromolecules*, 2010, 43, 7495-7503.
96. C. Lefay, D. Glé, M. Rollet, J. Mazzolini, D. Bertin, S. Viel, C. Schmid, C. Boisson, F. D'Agosto, D. Gigmes and C. Barner-Kowollik, *J. Polym. Sci., Part A: Polym. Chem.*, 2011, 49, 803-813.
97. J. Mazzolini, O. Boyron, V. Monteil, F. D'Agosto, C. Boisson, G. C. Sanders, J. P. A. Heuts, R. Duchateau, D. Gigmes and D. Bertin, *Polym. Chem.*, 2012, 3, 2383-2392.
98. T. C. M. Chung, *Functionalization of Polyolefins*, Academic Press, London, 2002.
99. J. Y. Dong and T. C. Chung, *Macromolecules*, 2002, 35, 1622-1631.
100. T. C. Chung and J. Y. Dong, *J. Am. Chem. Soc.*, 2001, 123, 4871-4876.

Chapter 2

Production of End-functionalized LLDPE via the Catalytic Hydride Insertion Polymerization mechanism

2.1 Introduction

Linear low density polyethylenes (LLDPE), commonly made by copolymerisation of ethylene and α-olefins such as hexene, are very important commercial products. The presence of short side chain branches has the effect of lowering melting point, crystallinity and density compared to polyethylene (PE), yielding polymers which are more flexible and better suited for processing. These copolymers have found a wide range of applications in film coatings, packing materials, adhesives, medical implants as well as in the production of other plastic products.[1-4]

A major production method for LLDPE uses metallocene catalysts combined with methylaluminoxane (MAO) co-catalysts. These systems typically demonstrate high activity, the single site nature of the catalyst giving rise to the production of polymers with uniform distributions and comonomer incorporations.[5, 6] In the search to produce and develop end-functionalised polyolefins, as described in the previous chapter, another important goal is to develop functionalised ethylene, α-olefin copolymers. This would produce functionalised linear low density polyethylene (LLDPE) with tuneable properties, applicable to a broad range of applications.

2.1.1 Introduction to Catalytic Hydride Initiation Polymerisation (CHIP)

α-Methylstyrenes are not typically used as comonomers in metallocene catalysed polymerisations as they do not insert into the M-C bond at the active site of the catalyst, as demonstrated by Schwecke and Kaminsky.[7] Despite this, the Scott group has developed methods for the synthesis PE chains bearing α-methylstyrenyl head groups using a range of related monomers (Figure 2.1) *via* a metallocene-based Catalytic Hydride Insertion Polymerization (CHIP) mechanism.[8]

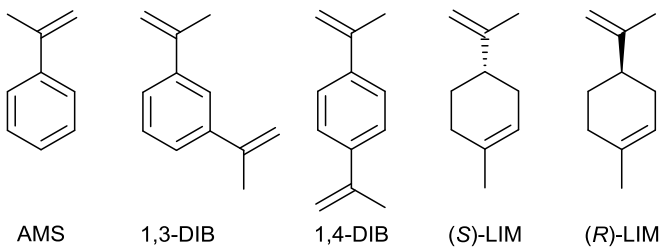

Figure 2.1: α-Methylstyrene and derivatives

In the proposed CHIP mechanism (Scheme 2.1, shown for the prototypical comonomner AMS) the alkyl cation species **I**, formed by MAO activation of the precatalyst, will either undergo hydrogenolysis to form the hydride **III** or, more likely insert ethylene to give polymeryl **II**. Species **II** is presumed to be responsible for the production of a small amount of unfunctionalised PE formed in the reaction, *via* hydrogenation to **III**.

The formation of the Zr-H bond in species **III** is of vital importance to the production of end functionalised PE. While α-methylstyrenyl comonomers are unable to insert into Zr-C bonds, they will readily insert at Zr-H centres, even in neutral

systems, as demonstrated by Chirik and Bercaw.[9] For a combination of steric and electronic reasons, the 1,2-regiochemistry is exclusively observed, with the α-methyl group being further away from the relatively bulky reaction centre, and the build-up of positive charge at the benzylic position being stabilised.[9] This latter stabilisation is particularly important in the CHIP mechanism given the cationic catalytic centre, and this is proposed to enhance the rate constant for the α-methylstyrenyl monomer *vs* ethylene.

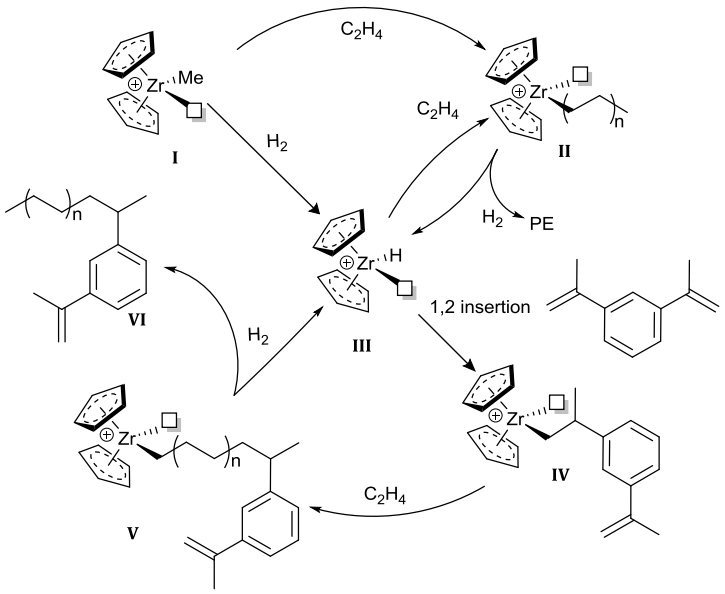

Scheme 2.1: CHIP mechanism describing the formation of PE-i-DIB

Overall, with typical monomer concentrations in the reaction mixture (*ca* 2 mol/L for comonomer as compared with 0.2 mol/L for ethylene), hydride **III** is expected to undergo highly selective 1,2-insertion of the comonomer to yield alkyl cation **IV**[†]. Further AMS insertion is not expected (*vide supra*), as **IV** is primary and not benzylic. Insertion of ethylene units occurs to produce the growing polymer species **V**. This polymer continues to grow until it interacts with a molecule of

[†] If 2,1-insertion of the 1,3-DIB take place, in spite of the steric crowding, then the dormant species produced will eventually by hydrogenated and regenerate **III**

dihydrogen and undergoes subsequent hydrogenolysis to reform **III** and the end functional polyethylene with a single AMS unit at the head of the chain (PE-*i*-AMS) **VI**.

Metallocene/MAO catalyst systems have been used extensively in the production of ethylene/α-olefin copolymers and so comprise a route for exploitation in this research. The rate of insertion of the α-olefin comonomer into the Zr-H bond must be much slower than that of the α-methylstyrenyl commonomer in order for the latter to remain the first inserted monomer. It is expected that the insertion of the α-olefin would have a lower rate constant than that of the α-methylstyrenyl commonomer, and therefore it would be possible to operate under a high concentration of both monomers, allowing the α-olefin to compete with ethylene in the main chain while maintaining the end-group fidelity of the AMS derivative.

It was found that the molecular weight of the end functional polymer could be controlled through the manipulation of hydrogen partial pressures used in the reaction. However this also has a strong effect on the productivity; a higher H_2 concentration causes higher productivity. By utilising these effects, it is possible to produce end functional polyethylene with tuneable M_w, high end group fidelity and in large yields. These factors combined give materials with excellent potential application in fuel, where the control of solubility is essential.

Solubility of the polyolefin component in any fuel additive is particularly important as large fractions of additive can be lost to premature precipitation.[10] This method could produce functional polyethylene to give functional LLDPE, which would decrease crystallinity through the incorporation of short side chain branches. Therefore, monomer 1,3-DIB (Figure 2.1) is of particular interest in this research, due

to the presence of two isopropenyl groups. One group can incorporate into the macromonomer, leaving the second group in the 3-position available for use in subsequent radical polymerisation.

2.2 Synthesis of functionalised LLDPE materials

A variety of zirconocene catalysts **1,** were used in the polymerisations (Figure 2.2). These were selected due to their commercial availability, common use in both homogeneous and, in the case of **1a-c** at least, supported heterogeneous polymerisations, and to provide a range of sizes of active site. The latter parameter in particular would affect the relative rates of monomer insertion and indeed hydrogenation.

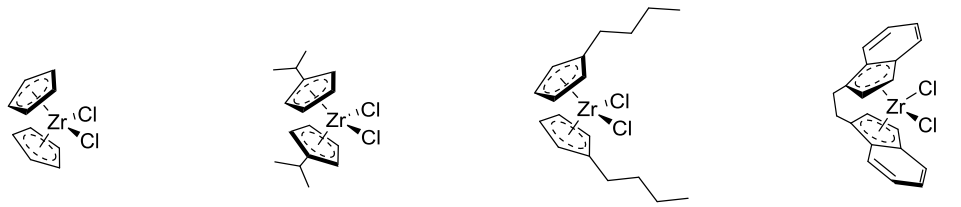

1a **1b** **1c** **1d**

Figure 2.2: Structures of catalysts: $ZrCp_2Cl_2$ 1a, (^iPr -Cp)$_2ZrCl_2$ 1b, (n-BuCp)$_2$ $ZrCl_2$ 1c and rac-EBI$ZrCl_2$ 1d

The reactions A-D (Table 2.1) are homopolymerisations of ethylene with 1,3-DIB in the presence of dihydrogen. Molecular weight, dispersity, productivity, and end group fidelity (>95%) of the PE-i-DIB polymers produced by catalysts **1a-c** were found to be similar. However, polymers produced by catalyst **1d** had higher molecular weights but lower productivities. The former is likely due to the more open active site

Table 2.1 Copolymerisations of ethylene and hexene with 1,3-DIB in presence of hydrogen

RUN [a]	Comonomer 1	Comonomer 2	[Comon.1] (mol/L)	[Comon.2] (mol/L)	Catalyst	M_p (g/mol) [b]	M_w (g/mol)	M_n (g/mol)	Đ	Yield (g)	Productivity [c]	Comonomer Incorp. (mol%) [d]
A	DIB	-	2.07	0.00	$ZrCp_2Cl_2$	6500	6400	3300	2.0	12.4	15000	n/a
B	DIB	-	2.07	0.00	$(^{i}Pr\text{-}Cp)_2ZrCl_2$	3700	7400	3500	2.1	13.7	16000	n/a
C	DIB	-	2.07	0.00	$(n\text{-}BuCp)_2\,ZrCl_2$	3700	6200	3100	2.0	11.3	13000	n/a
D	DIB	-	2.07	0.00	rac-EBIZrCl$_2$	9500	12600	5400	2.32	7.01	8400	n/a
1	DIB	HEX	2.07	0.43	$ZrCp_2Cl_2$	6700	9660	4200	2.3	8.2	9800	2.9
2	DIB	HEX	2.07	0.87	$ZrCp_2Cl_2$	6100	8600	3900	2.2	12.4	14000	6.2
3	DIB	HEX	2.07	1.3	$ZrCp_2Cl_2$	4800	5800	2200	2.5	10.5	13000	12.1
4	DIB	HEX	2.07	1.73	$ZrCp_2Cl_2$	4300	5000	2000	2.4	17.7	21000	13.1
5	DIB	HEX	2.07	0.43	$(^{i}Pr\text{-}Cp)_2ZrCl_2$	4400	6800	3100	2.2	11.2	13300	4.7
6	DIB	HEX	2.07	0.87	$(^{i}Pr\text{-}Cp)_2ZrCl_2$	5500	7600	3900	1.9	11.4	13500	6.1
7	DIB	HEX	2.07	1.3	$(^{i}Pr\text{-}Cp)_2ZrCl_2$	5300	6600	2800	2.3	12.0	14200	9.4
8	DIB	HEX	2.07	1.73	$(^{i}Pr\text{-}Cp)_2ZrCl_2$	3100	4600	2200	2.1	21.1	25000	17.2
9	DIB	HEX	2.07	0.43	$(n\text{-}BuCp)_2\,ZrCl_2$	7300	7700	3400	2.3	7.3	8700	3.1
10	DIB	HEX	2.07	0.87	$(n\text{-}BuCp)_2\,ZrCl_2$	5300	9000	3900	2.3	7.9	9400	5.8
11	DIB	HEX	2.07	1.3	$(n\text{-}BuCp)_2\,ZrCl_2$	4500	37900	3600	2.2	10.4	12400	7.5
12	DIB	HEX	2.07	1.73	$(n\text{-}BuCp)_2\,ZrCl_2$	4200	8400	3400	2.5	18.6	22000	16.6
13	DIB	HEX	2.07	0.43	rac-EBIZrCl$_2$	8400	8900	3700	2.4	7.6	9033	9.1
14	DIB	HEX	2.07	0.87	rac-EBIZrCl$_2$	13000	18000	7900	2.3	5.5	6500	9.7
15	DIB	HEX	2.07	1.3	rac-EBIZrCl$_2$	19000	20000	8300	2.4	5.1	6100	
16	DIB	HEX	2.07	1.73	rac-EBIZrCl$_2$	15000	20000	9100	2.2	4.5	5300	21.5

[a] Reaction Conditions: $Cp_2ZrCl_2 = 2.5\times10^{-6}$ mol; MAO = 1800 equivalents; C_2H_4 partial pressure = 32 psi except where indicated; solvent = toluene; reaction volume = 90 ml; reaction time = 20 min; reaction temperature = 60°C.
[b] GPC data were based on universal calibration from PS standards
[c] (kg polymer/(mol[Zr].h))
[d] Comonomer incorporation determined via ^{1}H method

presented by the ansa-bridged catalyst, which would increase the rate of insertion of ethylene versus di-hydrogen, the latter may be a consequence of faster formation of inactive dimers.

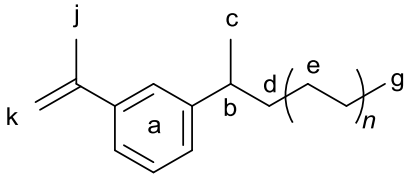

Figure 2.3: Labelled structure of PE-i-DIB

The polymers produced in reactions A-D were polyethylene initiated with 1,3-DIB (PE-*i*-DIB, Figure 2.3). The high temperature ^{1}H NMR spectrum of a typical example of the PE-*i*-DIB produced in run A is shown below in Figure 2.4. The percentage of the product initiated with DIB, and therefore the percentage of product

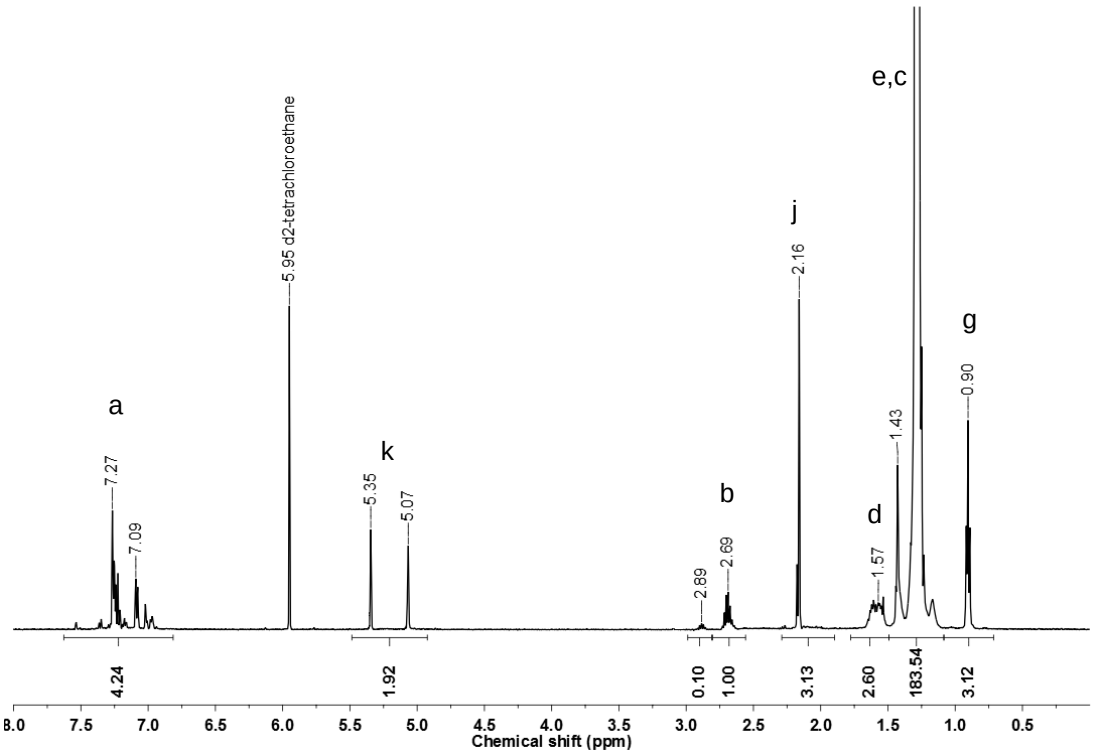

Figure 2.4: ^{1}H NMR spectrum of run A in *d*2-TCE. The top of the peak at 1.30 ppm corresponding to the PE main chain has been omitted for clarity.

bearing an end chain functionality, can be determined by regarding the ratio of the integrals of proton environments of the end chain methyl **g**, appearing at 0.91 ppm and the benzylic proton **b** appearing at 2.69 ppm.

The end group fidelity of the polymers is calculated using Equation 2.1. For the example of the ^{1}H NMR spectrum of Figure 4, equation 2.1, gives an end group fidelity of 98%.

$$\frac{b}{b + (g/3)} \times 200 \qquad \textbf{(2.1)}$$

It is possible to observe a small number of chains bearing a second type of aryl end group caused by the presence of 3-isopropylphenyl end group in the ^{1}H NMR spectrum. The isopropyl groups do not appear in the ^{1}H NMR of the 1,3-DIB monomer, therefore are thought to be produced during synthesis. Attempts to artificially produce this end group by hydrogenating the DIB monomer under similar conditions to the polyethylene reaction did not give a higher concentration of isopropyl groups. It was concluded that this process is a selective hydrogenation which occurs during polymerisation.

A series of runs (1-16 in Table 2.1) were conducted with each catalyst for the copolymerisations of ethylene and hexene at varying concentrations of the 1-hexene comonomer. Runs 1-4 show the polymerisations catalysed by zirconocene dichloride **1a**, which demonstrate the expected incorporation of hexene increasing with concentration of the comonomer. The observed increases in comonomer incorporation are not reflected in increases in the molecular weight of the copolymer, and in fact the observed molecular weight appears to decrease across the concentration range within this catalyst group. An increase in the mass productivity of the reaction with increasing comonomer content is observed. These trends are all expected from a sterically

congested catalyst system for which hexene insertion is not rapidly followed by ethylene, but which remains susceptible to hydrogenation. The increase in mass productivity seen (*ca* two-fold) cannot be completely accounted for by the higher average molecular weight of the monomer (*ca* 20% at 13% hexene incorporation; run 4) and is ascribed by a number of authors[11-13] to be the result of an activation of dormant polymerisation sites as well as a possible enhancement of the rate of insertion of ethylene in the presence of comonomer, and an increase in the solubility of the copolymer produced leading to a reduction in the diffusion limitations.[14] The trends for comonomer incorporation and reaction productivity are reflected in runs 5-12, which are conducted with an isopropyl substituted zirconocene catalyst **1b** and n-butyl substituted zirconocene catalyst 1**c**, indicating that the substituted nature of the catalyst has not significantly affected the nature of the products formed.

For runs 13-16, which use the ansa-bridged catalyst **1d**, rac-ethylenebis(indenyl)zirconocene dichloride, comonomer incorporation was also observed to increase with comonomer concentration. The incorporation of comonomer at equivalent concentration levels was significantly higher than that achieved with unbridged catalysts (**1a-c**). Molecular weights of the copolymers were significantly higher than those observed under the same conditions with **1a-c**. This is likely an effect of the larger active site which allows a higher rate of hexene insertion relative to the ethylene. Similarly, termination by hydrogenation is also less likely, increasing the molecular weight of polymers produced. Additionally the mass productivity of the reaction decreased as comonomer concentration increased.

The end group fidelities of the copolymers could not be calculated in the manner described for PE-*i*-DIB due to an overlap of the peaks corresponding to the methyl end group and methyl side chains in the ^{1}H NMR spectrum. A new method was required, which is described in section 2.3, that showed that end group fidelities were maintained at levels >95%.

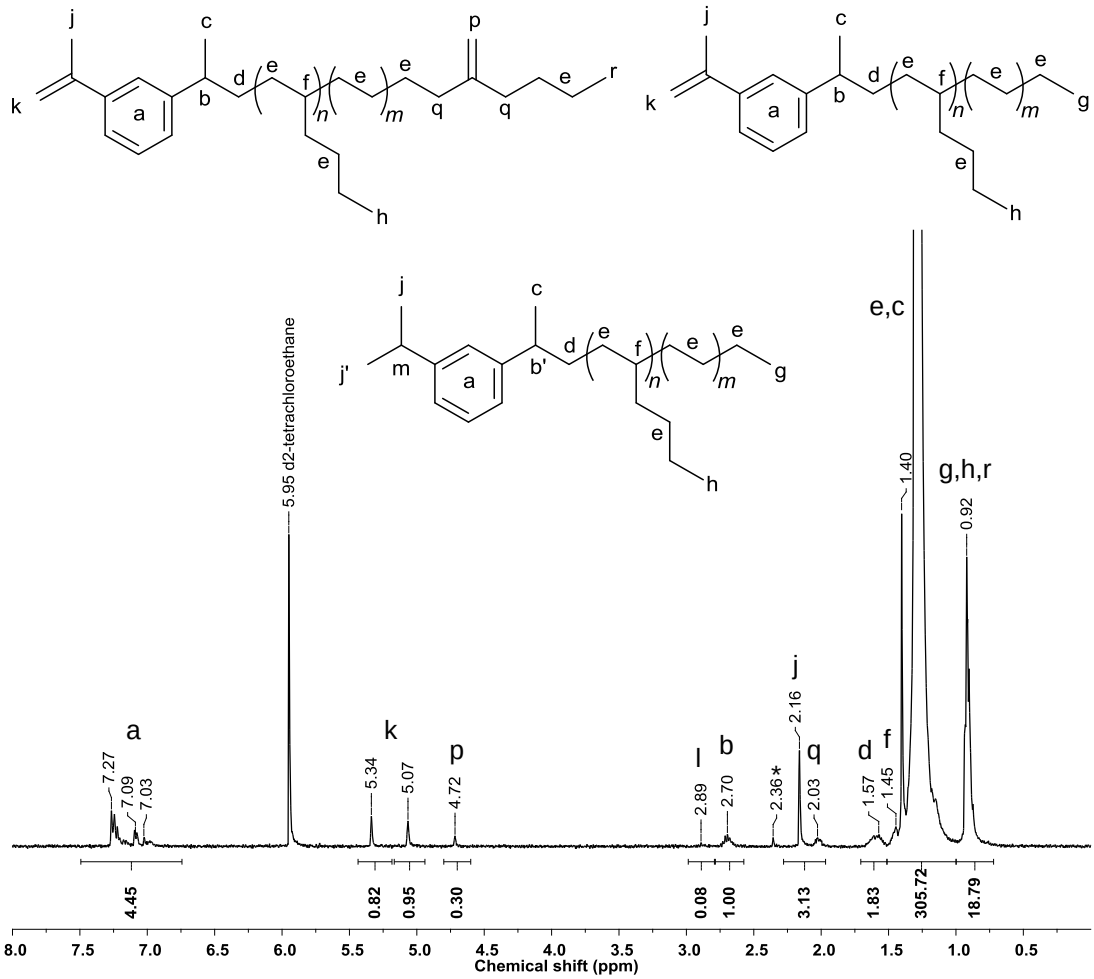

Figure 2.5: ^{1}H NMR spectrum of run 2 in *d*2-TCE. The top of the peak at 1.30 ppm corresponding to the PE main chain has been omitted for clarity.

The high temperature ^{1}H NMR spectrum of EH-*i*-DIB (Figure 2.5), has several features in common with that of PE-*i*-DIB. Isopropenyl end groups are observed at 5.34 and 5.07 ppm, a benzylic proton peak at 2.70 ppm and the polyethylene main

chain peak at 1.30 ppm. The presence of incorporated hexene monomers leads to a large increase in the methyl integral at 0.92 ppm. A peak at 4.72 ppm results from vinylidene termination when hexene is the last inserted monomer (*vide infra*). Full assignments are given in Figure 2.5.

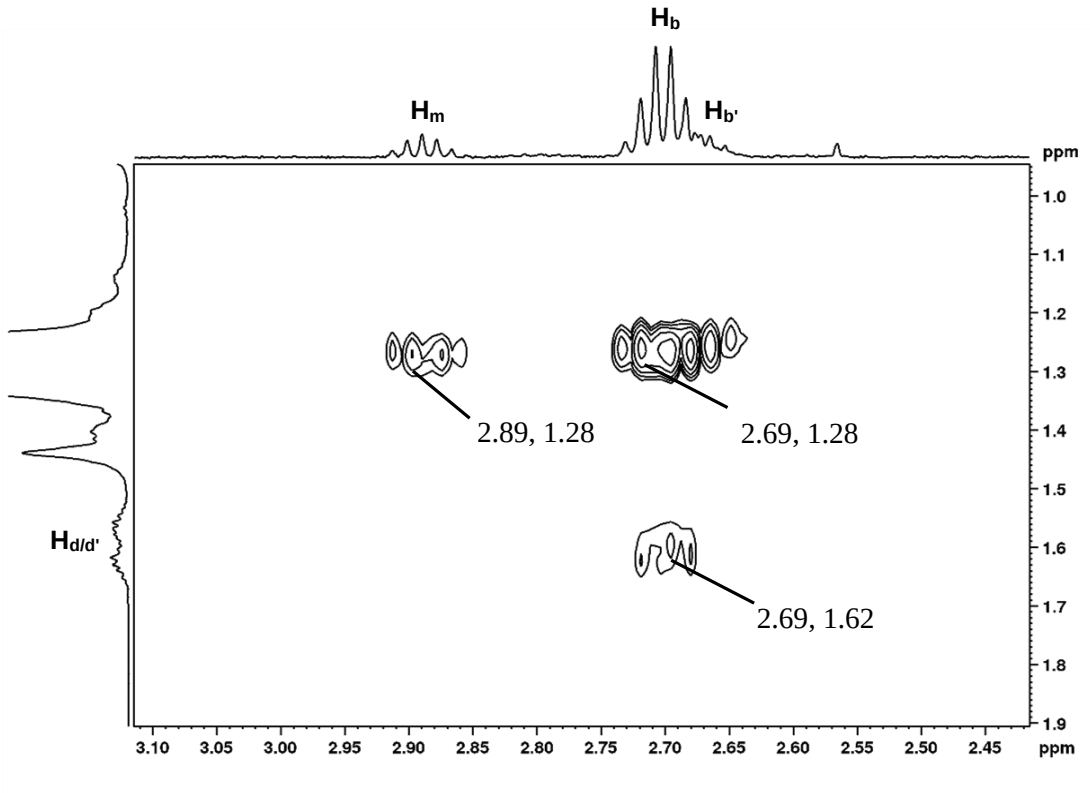

Figure 2.6: Detail of ^{1}H-^{1}H COSY correlation spectrum (run 2, Table 2.1)

In Figure 2.6 a segment of the ^{1}H-^{1}H COSY spectrum, under the same conditions, shows the multiplet resonance for benzylic proton **H_b** has a correlation with the methyl protons of **H_c**[‡] and the diastereotopic methylene protons of **H_d**[§]. Additionally, for the 3-isopropylphenyl impurity, it is possible to see a correlation between the septet peak for **H_m** at 2.89 ppm[**] with the methyl protons **H_j** on the same

[‡] Expected chemical shifts for **Me_c** and **Me_j** calculated by ACD/I-LAB to be 1.17 ± 0.22 and 2.06 ± 0.9 ppm respectively.
[§] Expected chemical shift for **Me_d** calculated by ACD/I-LAB to be 1.52/1.76 ± 0.54
[**] Expected chemical shifts for isopropyl methyl groups calculated by ACD/I-LAB to be 1.23 ± 0.07

hydrogenated end group. It is also possible to observe centred around 2.66 ppm which is the benzylic proton $\mathbf{H_{b'}}$ which arises from the equivalent benzylic proton in the 3-isopropylphenyl species, this is further highlighted in the correlation as what appears to be two overlapping diastereotopic correlations.

Another section of the ^{1}H-^{1}H COSY spectrum is shown below in Figure 2.7 where correlations between the vinylidene protons $\mathbf{H_k}$ in the DIB end group of the polymer and the adjacent methyl group $\mathbf{H_j}$ are observed. The correlation between vinylidene protons $\mathbf{H_p}$ at 4.72 ppm, and the α-position methylene proton environments $\mathbf{H_q}$ at 2.03 ppm[††] can also be seen.

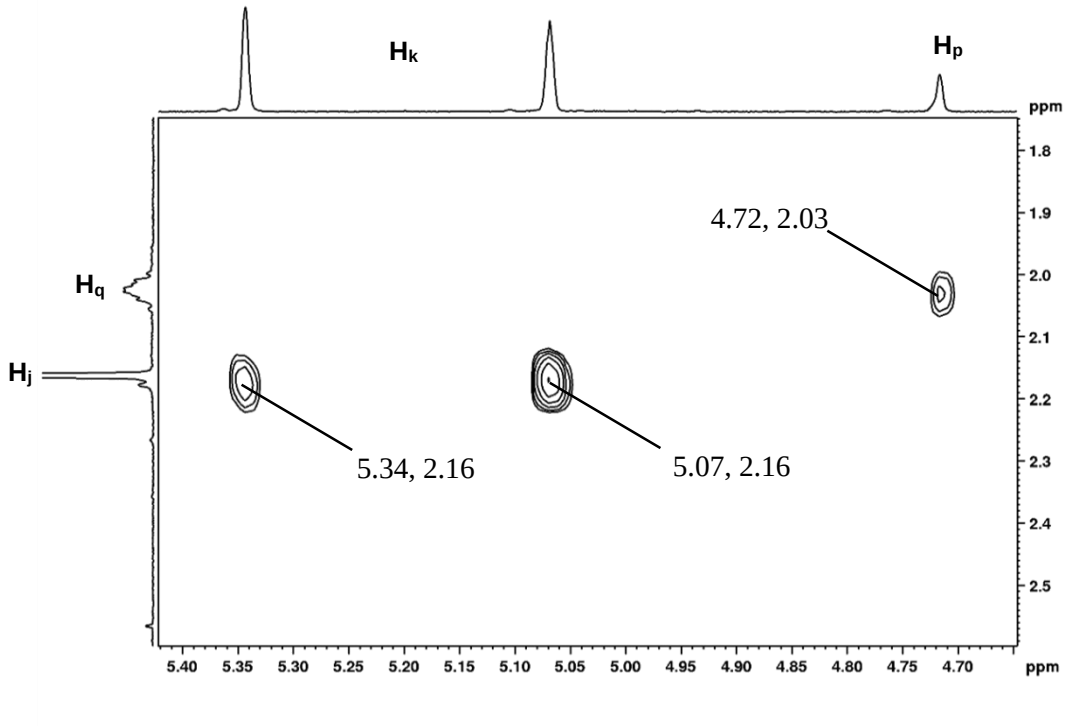

Figure 2.7: Detail of ^{1}H-^{1}H COSY correlation spectrum (run 2, Table 2.1)

[††] Expected chemical shift for $\mathbf{H_q}$ calculated by ACD/I-LAB to be 1.98/2.02 ± 0.32

2.2.1 Termination pathways for ethylene/hexene copolymers

The copolymers of ethylene and hexene may have a number of end groups depending upon the final inserted monomer unit and the termination process. When ethylene is the final inserted monomer there are three possible end groups: vinyl, *trans*-vinylene and saturated ends (Figure 2.8). The vinyl end groups are formed by either intramolecular β-hydride elimination or by β-hydrogen transfer to the monomer. *Trans*-vinylene groups form following an isomerization reaction and subsequent termination steps. Finally the saturated chain ends are formed principally by hydrogenolysis of the polymer chain by interaction with a molecule of dihydrogen.

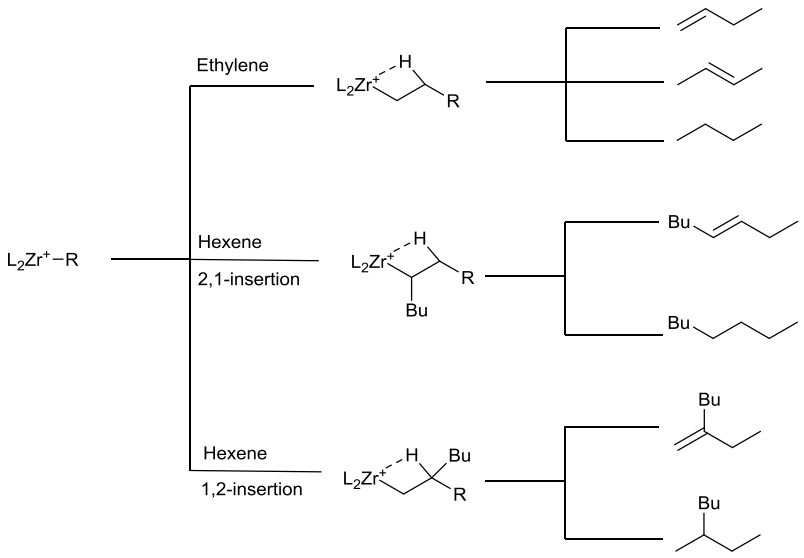

Figure 2.8: Termination reactions occurring during ethylene/1-hexene copolymerisations

There is also the possibility of a minor termination process, noted by Bruaseth *et al.,* furnishing trisubstituted end groups.[14] These end groups occur after chain transfer to minor amounts of trimethylaluminium (TMA), present in commercially

available MAO. Following the chain transfer to TMA and subsequent hydrolysis, polymeryl-dimethyl aluminium chains are formed.

When 1-hexene is the final inserted monomer, termination will depend upon the manner of the insertion mechanism. If 1-hexene undergoes 2,1-insertion then either saturated chain ends or vinylene unsaturations are observed (Figure 2.8). However, the occurrence of these two end groups is not expected as it has been shown in literature that 2,1-insertion of 1-hexene is of minor occurrence for this catalyst system for steric reasons.[15, 16]

The two final possible end groups follow a 1,2-insertion of 1-hexene as the last monomer unit. Either a saturated end can form in a similar hydrogenolysis process to ethylene, or a vinylidene end group appears by one of two possible processes: β-hydrogen transfer to the catalytic metal center or β-hydrogen transfer to a coordinating ethylene unit or an incoming 1,3-DIB.

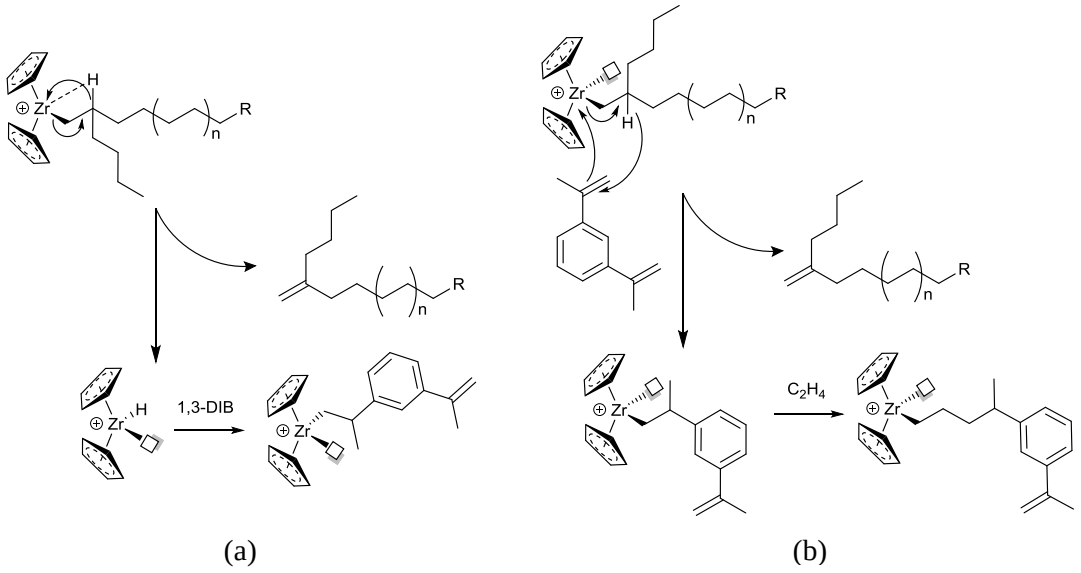

Scheme 2.2: Mechanisms of the hexene termination by (a) β-hydride elimination and (b) β-hydride transfer to monomer

These two possible pathways are shown in Scheme 2.2. In work by Bruaseth *et al* it was shown that as ethylene concentration increased, there was no increase in the percentage of vinylidene unsaturations produced.[14] From this it can be concluded that β-hydrogen elimination (Scheme 2.2 (a)), i.e. transfer to the catalytic metal center, is of more importance than that of β-hydrogen transfer to monomer (Scheme 2.2 (b)) after 1,2-insertion of hexene.

Of all the possible end group terminations, other than the usual saturated chain ends following hydrogenolysis, the occurrence of vinylidene end groups was observed within ^{1}H NMR spectra. These end groups occur on up to 50% of polymer chains and the observed percentage of vinylidene end groups was seen to increase with increasing comonomer incorporation.

2.3 Determination of comonomer content

2.3.1 Calculation by ^{13}C NMR:

The method to calculate the mol% incorporation of the hexene comonomers described by Pooter *et al*.[17] involves detailed assignment and integration of the ^{13}C NMR spectrum. The acquisition parameters for the ^{13}C NMR spectra were highly specific. Spectra were acquired at 130°C with a pulse width of 90° and a relaxation delay of 10 s with a high number of scans (*ca* ~ 5000).

Hexene incorporation was calculated by integrating the precise regions detailed in Table 2.2 and applying the calculations shown below. A detailed analysis of the peaks contained within each region is also detailed in Table 2.3. The integration limits set take into account both the isolated side chain branches, those branches that

are separated by a single ethylene unit and branches occurring next to each other, where the latter two occurrences are infrequent.

Table 2.2: Integral regions of ^{13}C NMR spectra of EH-*i*-DIB polymers.

Region	Range (ppm)
A	40.8-39.8
B	39.8-38.8
C	38.8-36.3
D	Peak at 35.1
D+E	36.1-32.5
F+G	32.5-24.8
G	27.8-25.8
H	24.2-23.4

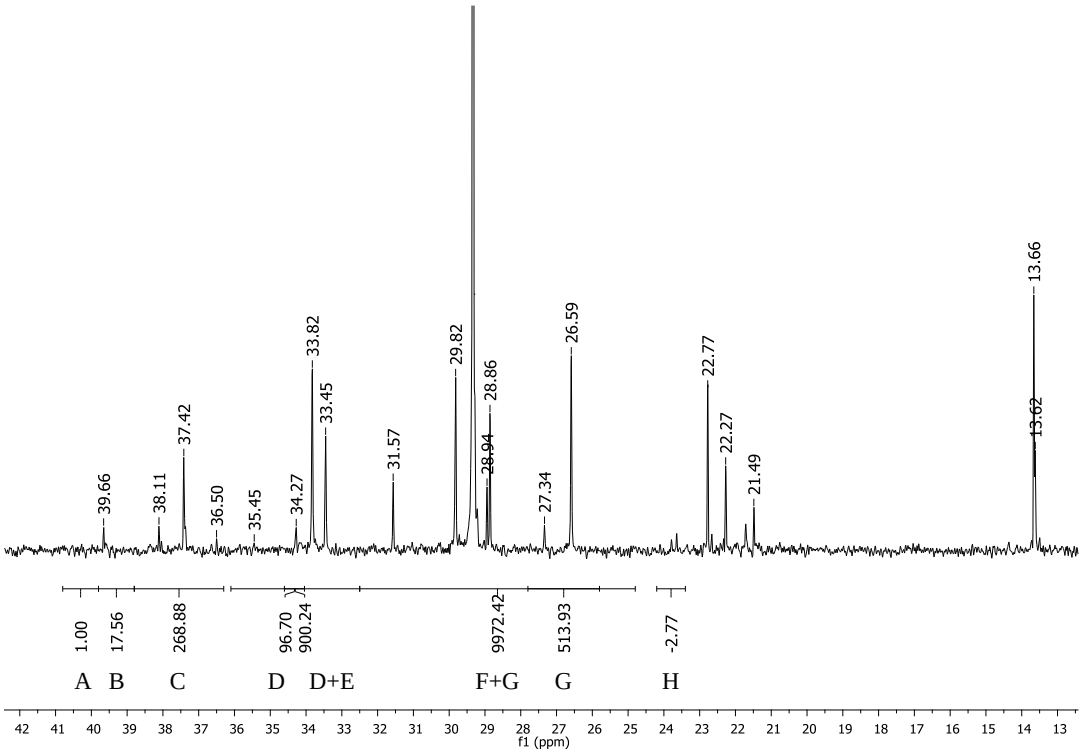

Figure 2.9: Excerpt of the 13C NMR spectra of EH-*i*-DIB showing the integration regions for hexene incorporation calculations

Figure 2.9 shows the ^{13}C NMR spectrum of EH-*i*-DIB (run 2, Table 2.1) and details the integration regions defined in Table 2.2. The calculations preformed based upon these relative integrations are described below.

Using Equation 2.4 the proportion of branch point (br) carbons (H_1) within the polymer is calculated. There will be a branch point tertiary carbon for every unit of hexene incorporated within the polymer.

$$H_1 = \frac{A + 2C + 2D}{2} \quad \textbf{(2.2)}$$

Using Equation 2.5, the proportion of α carbons (H_2) – the methylene units either side of the branch point – is determined. For each hexene unit incorporated there will be two α carbon environments.

$$H_2 = \frac{1.5A + 2B + (D + E) - D}{3} \quad \textbf{(2.3)}$$

The average amount of hexene (H'), present within the copolymer is derived from Equation 2.6, calculating a ratio of the branch point (H_1) and α carbon (H_2) environments.

$$H' = \frac{H_1 + H_2}{2} \quad \textbf{(2.4)}$$

Next the amount of ethylene (E') within the copolymer is calculated in Equation 2.7. This establishes the ratio of monomer units.

$$E' = \frac{(F + G) - 3A - 3B - G - H}{2} \quad \textbf{(2.5)}$$

Finally, the mol% of hexene present within the polymer is calculated using Equation 2.8, which establishes the ratio of the moles of hexene (H') and of ethylene (E').

$$mol\%\ hexene = 100\ \times \frac{H'}{H' + E'} \quad \textbf{(2.6)}$$

By using Equations 2.4 – 2.8 to the NMR spectrum shown in Figure 2.9 (run 2, Table 2.1) the incorporation of hexene was calculated to be 6.04 mol%. This analysis method is time-consuming and tedious however gives excellent precision. Analysis was repeated multiple times on a range of samples. The relative standard deviation at the 95% confidence limit was calculated to be between 4.4 and 10.3%

Table 2.3: ^{13}C NMR integration regions

Region	Chemical Shift (ppm)	EE**X**EE		EE**X**E**X**EE		EE**XX**EE		EE**XXX**EE	
		Type	#	Type	#	Type	#	Type	#
A	~40.1							αα**γ**	2
B	~39.5					αα	1		
C	37.4	CH	1	CH	2				
D	~35.1					CHβ	2		
E	33.8-34.3	α	2	α,αγ	4	B1,αγ	4	B1,αγ	5
	33.5	B1	1	B1	2				
	32.8							CHββ	1
F	29.8	γ	2	γ	2	γ	2	γ	2
	29.4	δ, δ*	3	δ, δ*	3	δ, δ*	3	δ, δ*	3
	28.8	B2	1	B2	2	B2	2	B2	3
G	26.6	β	2	β	2	β	2	β	2
H	23.8			ββ	1				

2.3.2 Calculation from ^{1}H NMR.

The NMR experimental parameters required to acquire ^{13}C NMR spectra of sufficient quality for integration necessitate long relaxation delays and high numbers of scans at high temperature. As such, this is a time-consuming and resource-intensive method of calculating mol% incorporation for every sample of EH-*i*-DIB produced. Instead it would be preferential if incorporation could be calculated from ^{1}H NMR. This is a

viable method due to the end functional nature of the polymer giving a peak of known integration that can then be used as reference for calculation.

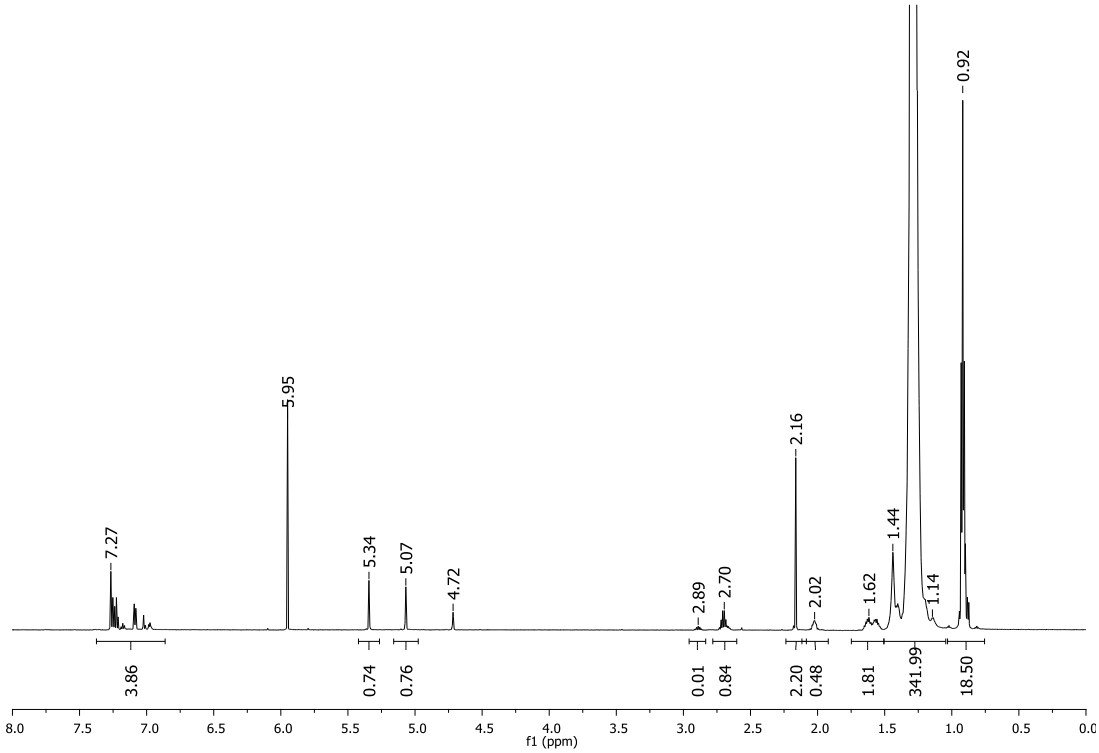

Figure 2.10: ^{1}H NMR spectrum of EH-i-DIB (run 2, Table 2.1) in TCE at 100°C, showing the integrals of relevant peaks

This calculation requires a known percentage end group fidelity (EGF), which in this case cannot be calculated using Equation 2.1 as the methyl integral encompasses the not only the terminal methyl group, but also the side chain branch methyls. In previous work, EGF was typically observed to be 95-97%.[8] Therefore for the following case, EGF was assumed to be 95%. Using this assumption the expected integral of the end chain methyl group (3.15) was calculated by considering the relative ratios of chain ends. Assuming 95% EGF means that 95% of chains have a single methyl group (3H) and 5% have two (6H). This ratio is shown below in equation 2.9.

$$\frac{(95 \times 3) + \big((100 - 95) \times 6\big)}{100} \quad \textbf{(2.7)}$$

This gives a value of 3.15. Subtracting this value from the methyl integral observed in EH-*i*-DIB materials, gives a value that is representative of the side chain branch methyls given by the comonomer. This value is then divided by three – the number of protons in each methyl group – to determine the number of branches in the product. The degree of polymerisation (DP) of the polymer is calculated by dividing the integral of the PE main chain by four. Finally the mol% incorporation is determined using the Equation 2.10, below. For the example of Run 2 (Table 2.1) incorporation is estimated to be 6.2 mol% *cf*. 6.04 mol% from the ^{13}C method.

$$mol\%\ incorporation = \frac{Hex\ units}{Ethylene\ units + Hex\ units} \times 100 \quad \textbf{(2.8)}$$

The validity of assuming an EGF of 95% can be tested by applying the above reasoning in reverse. Using the ^{13}C calculated value of 6.04 mol% comonomer incorporation, the expected integral of the side chain methyls from this the end group methyls gives a calculated EGF of 93%.

This dual methodology was applied to copolymers at low, medium and high levels of incorporation and the results were found to be comparable. Given the good agreement between the techniques, the more convenient ^{1}H NMR method was then used routinely.

Table 2.4: Summary of hexene contents calculated by ^{1}H and ^{13}C NMR for low medium and high incorporation levels

Method	Comonomer incorporation (mol%) at different comonomer concentration levels		
	Low (0.43 mol/L)	Medium (0.87 mol/L)	High (1.73 mol/L)
^{13}C Calculation	2.90	6.04	22.30
^{1}H Calculation	2.80	6.20	21.50

2.4 Thermal analysis of EH-*i*-DIB materials

Differential Scanning Calorimetry (DSC)[18] is an important tool in polymer analysis, allowing for investigation of phase transitions and related phenomena such as melting, glass transition and phase separation. The temperature of a sample is changed at a controlled rate, and the amount of heat required to maintain that rate is compared with that required for a reference material. Data from the subsequent thermogram plot of heat flow *vs* temperature is characteristic of the material under study and allows *e.g.* estimation of the heat and entropy of fusion and thereby comparative crystallinity.[19]

PE-*i*-DIB and five samples of solid copolymers of EH-*i*-DIB, with varying hexene content, was investigated by DSC. The samples were heated to 160°C and then cooled to -160°C at a rate of 10°C/min, this cycle being repeated three times to remove the thermal history of the samples.[20] These limits were selected to completely encompass the physical transitions the materials experience *i.e.* T_g and T_m. A comparison of the third heating curves[‡‡] of these materials is shown in Figure 2.11.

The glass transition (at temperature T_g) is the reversible endothermic process in an amorphous material (or amorphous regions in a semi-crystalline material) associated with conversion from a lower temperature glassy state into a higher

[‡‡] The second heating curves of these materials are indistinguishable from those shown.

temperature viscous or rubbery state. In HDPE this is usually observed between -80 and -110°C.[21] The sample of PE-*i*-DIB used (M_n = 2700 g/mol) underwent glass transition (T_g) at the lower temperature of -148°C. In the five samples of hexene incorporated EH-*i*-DIB, T_g was found not to be significantly affected by increasing mol% of hexene in the polymer. However, the size of the step (in units mW/g) increased significantly in some cases. This is interpreted as being the result of the increasing proportion of amorphous material in the sample. The T_g step observed in the case of the highest hexene content sample (21.5 %) was significantly lower than that of the 17.2% sample. This is potentially due to this is as a result of the much higher molecular weight of the former.

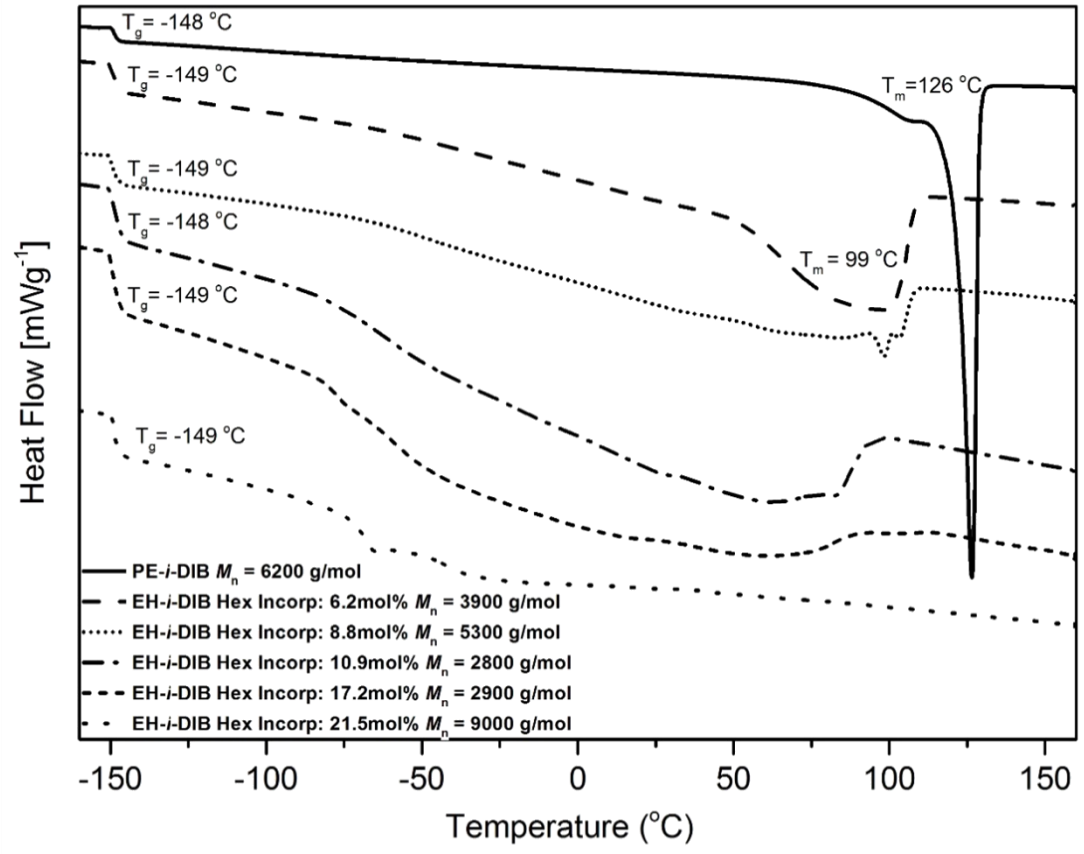

Figure 2.11: Thermal data for a range of functionalised EH materials

A sharp melting point (T_m) was observed for the PE-*i*-DIB sample at 126°C. This was preceded by a pre-melting region, associated with the crystalline domains bordered by amorphous material, such as crystal defects.[22] For the 6.2 mol% hexene comonomer sample, a broad melting region was observed with a peak temperature of approximately 99°C. Further broadening of the melting curves of the four additional hexene comonomer samples was observed, which makes the exact T_m hard to define in each case. The shift in 'peak' position indicates a progressive decrease in the melting point of the copolymers upon increasing amounts of side chain branches, and a decrease in the amount of crystalline material to undergo fusion.[19] The percentage crystallinity of PE is determined via DSC by comparing the enthalpy of melting of the sample with the enthalpy of 100% crystalline PE (294 J/g).[23-25] In Equation (2.11) the enthalpies of fusion of the test sample, $\Delta H_f (T_m)$, and totally crystalline polymer (PE) $\Delta H_f^0(T_m^0)$, measured in J/g at the equilibrium melting point T_m^0.

$$\% \, crystalinity = \frac{\Delta H_f \, (T_m)}{\Delta H_f^0 \, (T_m^0)} \times 100 \qquad \textbf{(2.9)}$$

The calculated crystallinity falls sharply as hexene content increases; 78.3% in PE-*i*-DIB to *ca* 40.7% in EH-*i*-DIB (6.2 mol% hexene). The crystallinity value for the EH-*i*-DIB with the highest hexene content (21.5%) was is calculated as 0.5%, although the lack of a well-defined crystallisation peak in the thermogram places a large error bar on this value.

Figure 2.12 shows the third DSC cooling curves of the PE-*i*-DIB and five samples of solid copolymers of EH-*i*-DIB, with varying hexene content. The crystallization temperature (T_c) was found to decrease significantly with increasing

hexene content, similar to the observations of melting temperature. The discrepancy between the T_m and T_c is known as supercooling or undercooling.[26] The undercooling in the samples was found to not be strongly affected by hexene content, falling from 12°C in PE-*i*-DIB to *ca* 8-10°C in the hexene copolymers. This indicates that nucleation of crystalline PE domains is not substantially inhibited by the increasing hexene content.

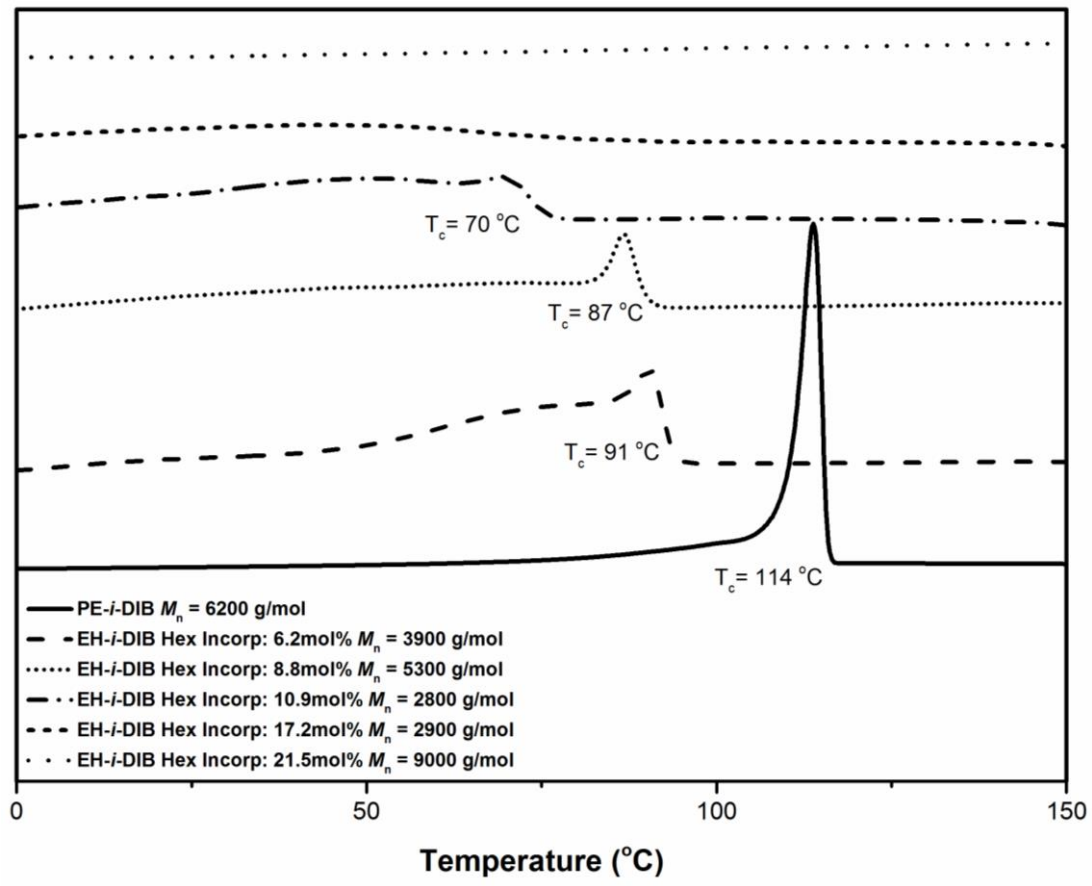

Figure 2.12: Thermal data for a range of functionalised LLDPE materials

2.5 MALDI Mass spec analysis

Matrix assisted laser desorption/ionisation (MALDI) analysis of polyethylene materials is not commonly conducted, indeed only a handful of examples of this were found in literature.[27-29] This is due to the inert nature of polyethylene which lacks the

presence of any heteroatom or double bond for potential proton to metal ion attachment, which inhibits ionization. However, there has been some success reported using silver salts to promote ionization.[29]

In the case of PE-*i*-DIB, it was hypothesised that the presence of the arene group at the end of the polyolefin would be able to promote ionisation and give a useful MALDI spectrum. MALDI analysis was conducted on two functional polyethylene materials, PE-*i*-AMS (M_n- 1700 g/mol) (Fig 2.13) and PE-*i*-DIB (M_n- 2700 g/mol) (Fig, 2.14).

While several sample preparation methods were attempted which did not produce reliable data, a modification of a method found in literature[27] was ultimately used and significant results were obtained. The samples were dissolved in chlorobenzene (5 mg/mL), with gentle heating where necessary. Following the preparation of a 0.1 M solution of the matrix 9-nitroanthracene in THF and a saturated solution of silver nitrate methanol, the solutions were deposited on a stainless steel sample target plate in a layered dropwise fashion in the order of (i) matrix, (ii) silver nitrate then (iii) sample solution.

Figures 2.13 and 2.14 show single polymer distributions, spanning 400-2000 m/z with a peak separation between two adjacent peaks of 28 Da, indicative of a single ethylene repeat unit. Each peak in Figure 2.13 is equivalent to a single silver ion plus an AMS unit and the attached polyethylene chain. This indicates that the polyethylene produced via the CHIP mechanism contains only a single AMS unit. The dispersity of the polymer (*ca* ~ 2.0) would indicate that the entire distribution of the polymers is not represented in the acquired spectra and are not completely representative of the molecular mass distributions. When polymers with broad distributions are analysed by MALDI, the charge distribution leads to an upper mass limit above which

individual oligomers cannot be distinguished. It is therefore common for MALDI data to underestimate the higher mass polymer distribution hence resulting in noticeably lower average molecular weight.[30, 31] The mass discrimination effect is thought to be due mass discrimination in the ion detection and sample preparation.

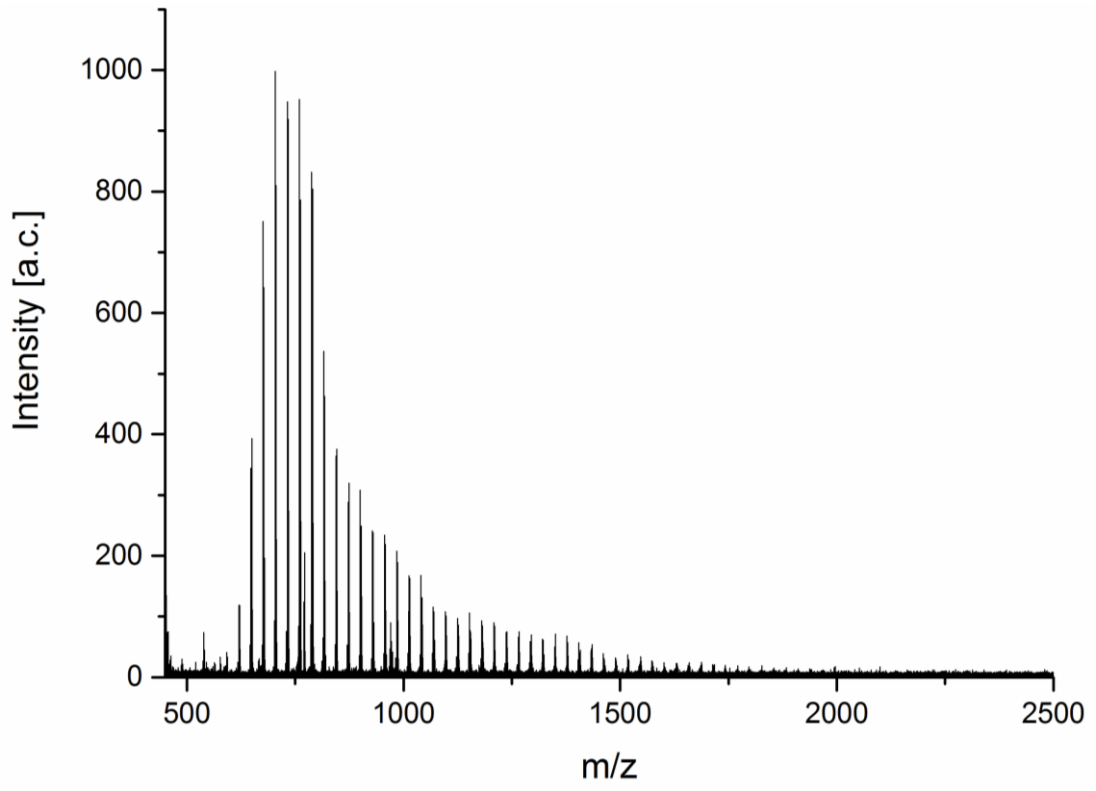

Figure 2.13: MALDI spectrum of PE-i-AMS

The enlarged section of Figure 2.14 shows the isotope distribution pattern of a PE oligomer attached to a silver ion; this pattern matches with theory. All major mass peaks correspond with individual [PE-*i*-DIB + Ag] $^{+}$. Also visible are a set of minor peaks, separated from the larger peaks by 2 Da (denoted by the X). These minor peaks are the result of an isotope of [PE-*i*-DIB + Ag]$^{+}$ which has lost an additional 2H, resulting in a single alkene bond within the polymer. This is likely a result of dehydrogenation of [PE-*i*-DIB + Ag] $^{+}$. Similar peaks were observed by Chen *et al* [27]

who argued that these peaks were not truly representative of the amount of the mono-alkene material present within the sample. An alkene product is more easily ionized by silver ion attachment due to d-π interactions, whereas only weak static interaction is exhibited between the saturated alkane product and silver ions.

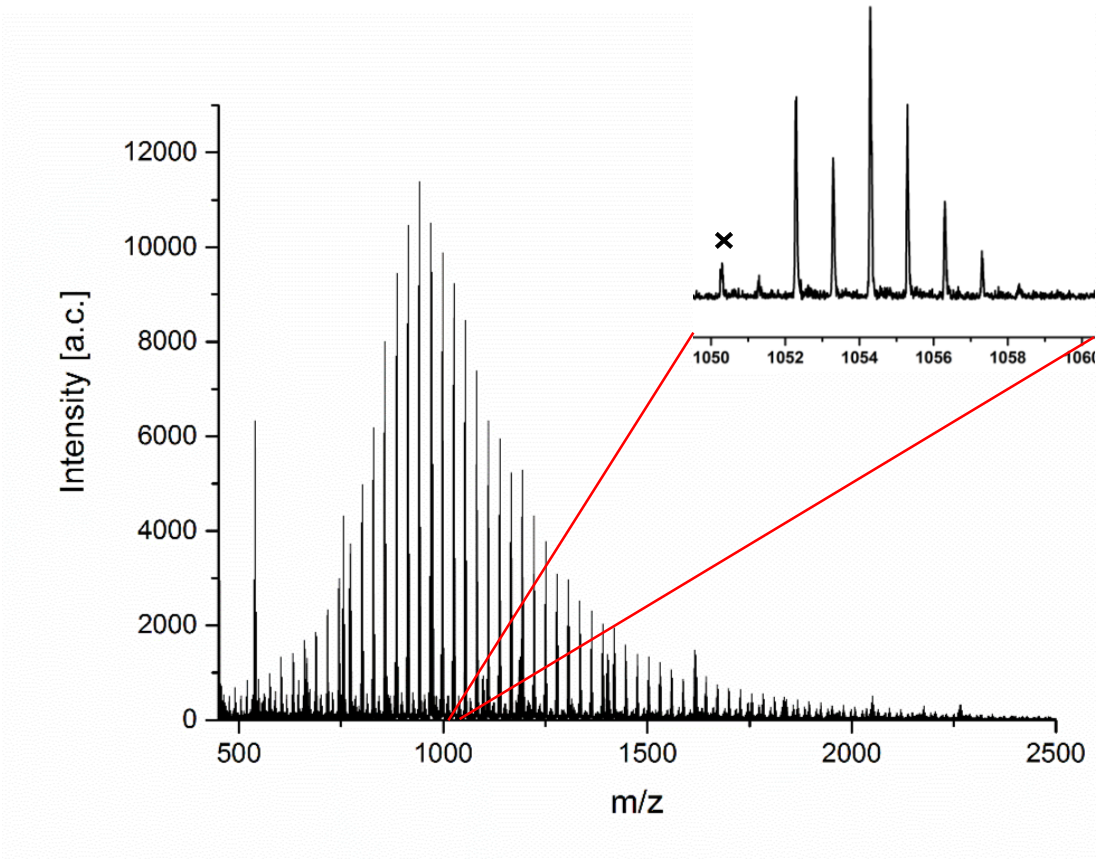

Figure 2.14: MALDI spectrum of PE-i-DIB

The MALDI mass spectra of EH-*i*-DIB were not acquired. The nature of statistical copolymers does not lead to coherent MALDI mass spectra due to the overlapping distributions, making relevant interpretation difficult. Regardless, it would not be expected that it would be impossible to identify the differences between PE and EH by MALDI as the addition of a hexene unit is the same as the addition of three ethylene units, and so the distributions would overlap.

2.6 Ethylene copolymers with dodecene

The robustness of the reaction set up was tested with the use of higher α-olefin dodecene to investigate if the observed trends are consistent with longer side chain branches.

Table 2.5 Copolymerisations of ethylene and dodecene with 1,3-DIB in presence of hydrogen.

RUN [a]	Comonomer 1	Comonomer 2	[Comon.1] (mol/L)	[Comon.2] (mol/L)	Catalyst	M_p (g/mol) [b]	M_w (g/mol)	M_n (g/mol)	Đ	Yield (g)	Productivity [c]	Comonomer Incorp. (mol%) [d]
1	DIB	DODEC	2.07	0.48	$ZrCp_2Cl_2$	4500	9000	4100	2.2	11.3	14000	4.6
2	DIB	DODEC	2.07	0.48	$(^iPr\text{-}Cp)_2ZrCl_2$	5100	8800	4000	2.2	8.6	10000	6.7
3	DIB	DODEC	2.07	0.48	$(n\text{-}BuCp)_2\,ZrCl_2$	5500	10000	4300	2.4	6.7	8000	6.6
4	DIB	DODEC	2.07	0.48	rac-EBI$ZrCl_2$	18000	21500	8600	2.5	2.3	3000	9.3

[a] Reaction Conditions: $Cp_2ZrCl_2 = 2.5\times10^{-6}$ mol; MAO = 1800 equivalents; C_2H_4 partial pressure = 32 psi except where indicated; solvent = toluene; reaction volume = 90 ml; reaction time = 20 min; reaction temperature = 60°C.
[b] GPC data were based on universal calibration from PS standards
[c] (kg polymer/(mol[Zr].h))
[d] Comonomer incorporation determined via ^1H method

In Table 2.5 a series of polymerisations of DIB and DODEC, conducted with the same range of catalysts used previously (*vide supra*), is listed. Through these reactions, comonomer concentration was maintained while the catalyst was altered. The molecular weights of the copolymers produced by $ZrCp_2Cl_2$, $(n\text{-}BuCp)_2\,ZrCl_2$ and $(^iP\text{-}Cp)_2ZrCl_2$ were very similar but were significantly higher when the ansa-bridged zirconocene catalyst was employed. This was also observed when using a hexene comonomer. Additionally the incorporation of dodecene was found to follow similar trends as found with the ethylene/hexene copolymerisations.

2.7 Hafnocene catalysed polymerisations

Metallocene catalysts based on hafnium were of interest due to a reported higher incorporation of 1-hexene and other α-olefins.[32] These hafnocene catalysts have been seldom used due to a low polymer productivity using MAO activation. Hafnocene is also known to produce polymers with significantly higher molecular weights in homogeneous conditions.[33] Nevertheless a series of copolymerisations of ethylene and 1,3-DIB catalysed by hafnocene dichloride were conducted. However the products of polymerisation were unexpected and of little practical use. The results of these polymerisations are summarised in Appendix A.

2.8 Short chain analogues of functional polyolefins

In addition to increasing solubility of the block copolymer by increasing PE chain branching, it would also be prudent to explore increasing solubility through the lowering of the molecular weight of the olefin segment block. The CHIP mechanism allows control of the molecular weight of the polymers produced by manipulating the gaseous partial pressures of dihydrogen and ethylene. However, the practical lower limit of molecular weight had already been achieved. As such a new method for production of low molecular weight analogues of isopropenyl functionalised polyethylene materials was conceived.

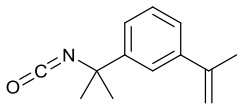

Figure 2.15: 3-isopropenyl-α,α-dimethylbenzyl isocyanate

An AMS derivative, 3-isopropenyl-α,α-dimethylbenzyl isocyanate (Figure 2.15) the isocyanate functional group in a reaction with long chain linear alcohols, catalysed by dibutyltin dilurate to form the carbamate product which bears a isopropenyl functionalised alkane product as shown in Scheme 2.3 below. 1-docosanol (also known as behenyl alcohol) was the long chain alcohol used in stoichiometric quantities with the isocyanate, the monomers were combined at 50° in the presence of the catalyst for 18 h, and precipitated into methanol to form a white powder.

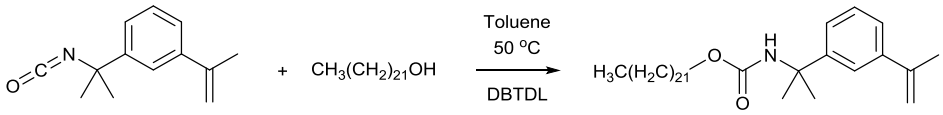

Scheme 2.3: Reaction of functional isocyanate with alcohol materials

The crystalline white solid product formed in this reaction is in essence a short chain analogue of PE-i-DIB and displays an increased solubility as compared with the long chain polymers. Electrospray mass spectra of the product were consistent with the formation of the proposed structure with a strong peak at m/z 550.30 Da for $[C_{35}H_{61}NO_2 + Na]^+$.

The products were also analysed by ^1H NMR and the acquired spectrum of this is shown in Figure 2.16. From the spectrum it can be seen that complete conversion of the 1-docosanol has been achieved and that any residual isocyanate has been removed. The characteristic isopropenyl peaks can be seen at 5.35 & 5.08 ppm, though the peak at 5.08 ppm overlaps with the proton of the secondary amine.

Attempts to use this material as a macromonomer in free radical polymerisations were unsuccessful since it proved very challenging to separate from homopolymer.

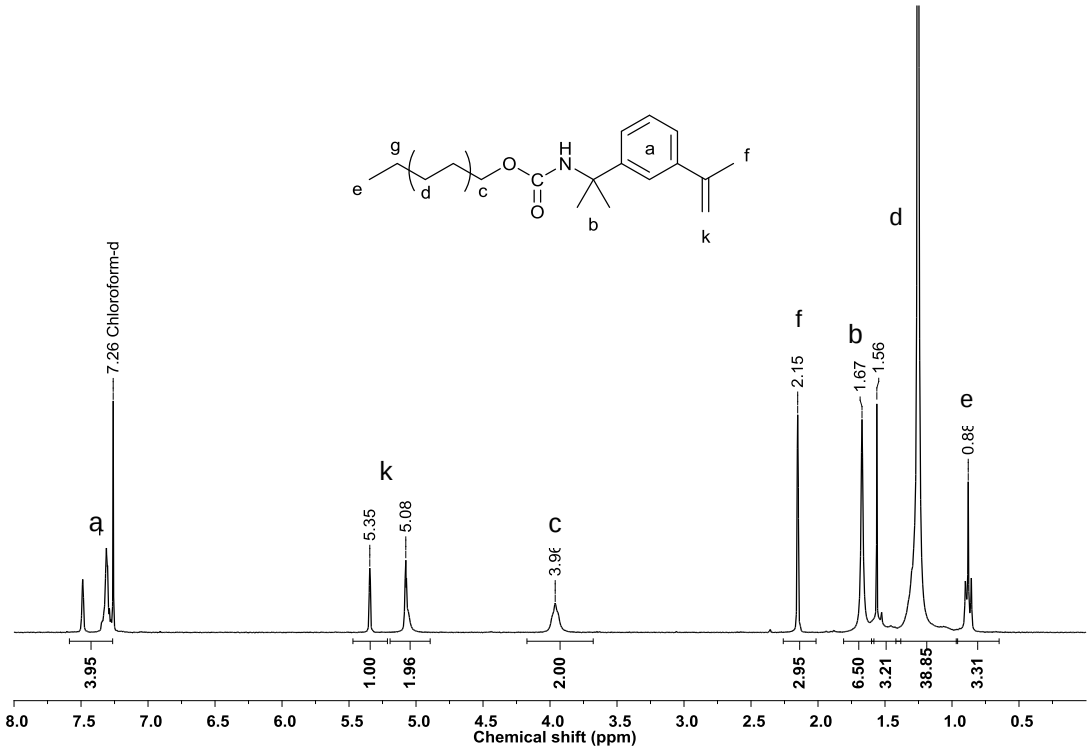

Figure 2.16: ^{1}H NMR spectrum of BeCa in d^2-TCE.

2.9 Conclusions

The CHIP mechanism has been successfully used to synthesise end functional EH and LLDPE materials in high yields and with high end group fidelities. Using a range of comonomer concentrations and a number of catalysts, polyolefin copolymers with a range of comonomer incorporations between 2 and 21 mol% was achieved. These values were determined through detailed integration of ^{13}C NMR and EGF was estimated from this information. The synthesis of these materials was shown to be robust and copolymers of ethylene and dodecene were also produced.

The thermal properties of these materials were investigated and it was found, as expected, that the melting temperature decreases with increasing comonomer

content and that the undercooling was largely unaffected, indicating that nucleation of crystalline PE domains is not substantially inhibited by the increasing hexene content.

MALDI mass spectra were acquired for PE-*i*-AMS and PE-*i*-DIB. The spectra show the distribution of PE with the respective attached end group functionalities. To the best of our knowledge MALDI spectra of PE materials of this quality have not been seen in literature.

Finally short chain analogues of functionalised PE were synthesised through reaction of long chain alcohols with a functional isocyanate species catalysed by dibutyltin dilurate. The complete conversion of these species was confirmed by NMR and ESI mass spectrometry.

2.10 References

1. W. Kaminsky and A. Laban, *Appl. Catal., A*, 2001, 222, 47-61.
2. J. R. Severn, J. C. Chadwick, R. Duchateau and N. Friederichs, *Chem. Rev.*, 2005, 105, 4073-4147.
3. L. Wu, J.-M. Zhou, D. T. Lynch and S. E. Wanke, *Appl. Catal., A*, 2005, 293, 180-191.
4. D. Ribour, V. Monteil and R. Spitz, *J. Polym. Sci., Part A: Polym. Chem.*, 2009, 47, 5784-5791.
5. N. Senso, P. Praserthdam, B. Jongsomjit, T. Taniike and M. Terano, *Polym. Bull.*, 2011, 67, 1979-1989.
6. G. B. Galland, M. Seferin, R. S. Mauler and J. H. Z. Dos Santos, *Polym. Int.*, 1999, 48, 660-664.
7. C. Schwecke and W. Kaminsky, *Macromol. Rapid Commun.*, 2001, 22, 508-512.
8. C. Kay, PhD Thesis, University of Warwick, 2014.
9. P. J. Chirik and J. E. Bercaw, *Organometallics*, 2005, 24, 5407-5423.
10. D. Schwahn, D. Richter, P. J. Wright, C. Symon, L. J. Fetters and M. Lin, *Macromolecules*, 2002, 35, 861-870.
11. R. Quijada, J. Dupont, M. S. L. Miranda, R. B. Scipioni and G. B. Galland, *Macromol. Chem. Phys.*, 1995, 196, 3991-4000.
12. I. Camurati, B. Cavicchi, T. Dall'Occo and F. Piemontesi, *Macromolecular Chemistry and Physics*, 2001, 202, 701-709.

13. P. Lehmus, O. Härkki, R. Leino, H. J. G. Luttikhedde, J. H. Näsman and J. V. Seppälä, *Macromolecular Chemistry and Physics*, 1998, 199, 1965-1972.
14. I. Bruaseth, M. Bahr, D. Gerhard and E. Rytter, *J. Polym. Sci., Part A: Polym. Chem.*, 2005, 43, 2584-2597.
15. H. Wigum, L. Tangen, J. A. Støvneng and E. Rytter, *J. Polym. Sci., Part A: Polym. Chem.*, 2000, 38, 3161-3172.
16. I. Bruaseth and E. Rytter, *Macromolecules*, 2003, 36, 3026-3034.
17. M. De Pooter, P. B. Smith, K. K. Dohrer, K. F. Bennett, M. D. Meadows, C. G. Smith, H. P. Schouwenaars and R. A. Geerards, *J. Appl. Polym. Sci.*, 1991, 42, 399-408.
18. H. Morita and H. M. Rice, *Anal. Chem.*, 1955, 27, 336-339.
19. B. Ke, *J. Polym. Sci.* , 1960, 42, 15-23.
20. P. Badrinarayanan and M. R. Kessler, *J. Chem. Educ.*, 2010, 87, 1396-1398.
21. R. P. Quirk and M. A. A. Alsamarraie, *Polymer Handbook*, John Wiley & Sons, Inc, New York, 3rd edn., 1989.
22. K. Cho, F. Li and J. Choi, *Polymer*, 1999, 40, 1719-1729.
23. Y. Kong and J. N. Hay, *Polymer*, 2002, 43, 3873-3878.
24. V. A. Kryuchkov, J.-C. Daigle, K. M. Skupov, J. P. Claverie and F. M. Winnik, *J. Am. Chem. Soc.*, 2010, 132, 15573-15579.
25. R. P. Quirk and M. A. A. Alsamarraie, eds. J. Brandrup, E. H. Immergut and J. W. S. Inc, New York, 3rd edn., 1989, ch. V, pp. 15-26.
26. B. Wunderlich, *Thermal Analysis*, Academic Press, Inc., London, 1990.
27. R. Chen, T. Yalcin, W. E. Wallace, C. M. Guttman and L. Li, *J. Am. Soc. Mass. Spectrom.*, 2001, 12, 1186-1192.
28. R. Chen and L. Li, *J. Am. Soc. Mass. Spectrom.*, 2001, 12, 367-375.
29. M. S. Kahr and C. L. Wilkins, *J. Am. Soc. Mass. Spectrom.*, 1993, 4, 453-460.
30. S. F. Macha and P. A. Limbach, *Curr. Opin. Solid State Mater. Sci.*, 2002, 6, 213-220.
31. D. C. Schriemer and L. Li, *Anal. Chem.*, 1997, 69, 4176-4183.
32. A. Laine, M. Linnolahti, T. A. Pakkanen, J. R. Severn, E. Kokko and A. Pakkanen, *Organometallics*, 2011, 30, 1350-1358.
33. V. Busico, R. Cipullo, R. Pellecchia, G. Talarico and A. Razavi, *Macromolecules*, 2009, 42, 1789-1791.

Chapter 3

Free radical polymerization as a route to LLDPE block copolymers

3.1 Introduction

α-Methylstyrene (AMS) is commonly used as a end capping agent in free radical polymerizations.[1, 2] This is due to the highly stable tertiary benzylic radical which forms from the addition of AMS unit to the end of a growing polymer chain. AMS also has a high chain transfer to monomer constant ($C_m = k_{tr} / k_p$), arising from a low propagation rate (k_p).[2] This, combined with the low ceiling temperature[3] means that the AMS unit adds rapidly to the end of the polymer radical but any additional propagation is relatively slow, particularly at higher temperatures. A theoretical investigation of the polymerization of styrene in the presence of small quantities of AMS[4] also found that high concentrations of AMS monomer should yield products with a high fraction of AMS end groups.[5]

AMS monomer has also been used to give end chain functionality to styrenic and acrylate type polymers in catalytic chain transfer polymerizations (CCTP) using e.g. bis(boron difluorodimethylglyoximate)cobaltate(II) (COBF); a terminal vinylic end group is produced.[2, 4, 6-8] The copolymerisation of styrene and AMS in a CCTP process using COBF found that chain transfer to AMS was the primary termination mechanism, with the use of only 1% AMS gave an AMS end group fidelity of 89%.[4] This method of generating end capped polymers is shown to work with many

monomers including *n*-butyl acrylate to produce P(*n*-BA) terminated with AMS (Scheme 3.1).[2, 8]

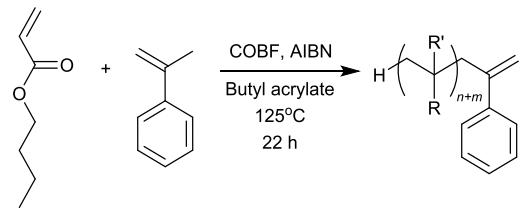

Scheme 3.1: Copolymerisation of n-BA and AMS in the presence of COBF.[2]

In addition, it has been shown that AMS also end-caps styrene-maleic anhydride copolymers produced via CCTP (Scheme 3.2) and yields a vinylic end group with was viable in a number of further reactions.[9]

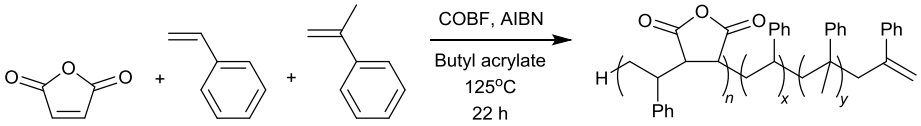

Scheme 3.2: Copolymerisation of maleic anhydride, styrene and AMS in the presence of COBF.[9]

These literature reports led Scott *et al.* [10] to the idea that PE-*i*-DIB could act in the same manner as AMS in order to yield polyethylene copolymers, noting that the double bond reactivity in the macromonomer is expected to be similar to that of the corresponding monomer.[11] This chapter will explore and describe the development of EH-Polar block copolymers utilising EH-*i*-DIB as an end capping agent in copolymerisations with suitable polar monomers in free radical polymerization conditions.

3.2 Copolymerisation of EH-*i*-DIB with n-butyl acrylate

Copolymerisations of EH-*i*-DIB with a range of concentrations of n-butyl acrylate were carried out in toluene at 125°C to ensure the solubility of the EH-i-DIB and promote end-capping.[1, 2] Benzoyl peroxide was selected as the initiator due to its short half-life at the reaction temperature;[12] this has the effect of generating a high concentration of radicals, and thus many propagating chains early in the reaction. This has previously been shown to give faster conversion of PE-*i*-DIB.[10]

For each run detailed in Table 3.1, several ampoules were set up in parallel and the progress of the polymerization was monitored by stopping one of the reactions at chosen intervals by plunging the ampoule into liquid nitrogen and subsequently opening to air. The resulting polymer mixture was then poured into an excess of methanol to precipitate the product.

The relative insolubility of the EH block as compared with the polar P(*n*-BA) block meant that precipitation and purification of the copolymers was very simple. Pouring into methanol caused the precipitation of the copolymers while any acrylate monomer or homopolymer remained in solution, as evidenced by ^{1}H NMR spectra (*vide infra*).

Following this purification, and drying under vacuum overnight, the isolated samples were analysed by NMR and GPC so that macromonomer conversion and polymer growth could be monitored. Conversion of the EH macromonomer was determined by comparison of the integrals of the sharp vinylidene proton signals (at 5.07 and 5.34 ppm) which arise from the DIB end group in each precipitated sample and the starting EH macromonomer.

Table 3.1: Copolymerisations of EH-*i*-DIB with n-butyl acrylate

Run	Time (min)	Initiator	n-BA: EH-*i*-DIB	M_p [d]	M_w [d]	M_n [d]	Đ [d]	Yield	EH-i-DIB Conversion (%) [e]	DP of n-BA /EH-i-DIB [e]
A	128	0	200	4400	14000	4100	3.5	0.23	21	1:1
B	960	BP	0	4300	7000	3900	1.8	0.1	36	n/a
1 [a]	2	BP	50	4900	9800	3500	2.8	0.21	11	0:1
	4	BP	50	9000	12760	4400	2.9	0.22	63	2:1
	8	BP	50	11000	12000	4800	2.5	0.25	94	4:1
	16	BP	50	10000	13000	5000	2.6	0.24	100	5:1
	32	BP	50	9400	10810	4700	2.3	0.23	100	7:1
	64	BP	50	10000	11500	5000	2.3	0.25	100	7:1
	128	BP	50	10000	13800	6000	2.3	0.28	100	16:1
2 [b]	2	BP	100	4800	9600	3400	2.8	0.21	27	0:1
	4	BP	100	4900	12000	4200	2.9	0.25	86	2:1
	8	BP	100	16000	18000	6000	2.9	0.35	100	7:1
	16	BP	100	15000	20000	7400	2.7	0.39	100	18:1
	32	BP	100	14000	19000	7000	2.7	0.39	100	20:1
	64	BP	100	12000	17000	6000	2.7	0.41	100	22:1
	128	BP	100	15000	19000	7800	2.4	0.42	100	21:1
3 [c]	2	BP	500	4800	6300	3200	2.0	0.22	62	9:1
	4	BP	500	11000	14100	7000	2.0	0.87	99	125:1
	8	BP	500	53000	107000	22000	4.8	1.95	100	258:1
	16	BP	500	58000	110000	22000	4.9	2.13	100	288:1
	32	BP	500	52000	102000	23000	4.4	2.22	100	255:1
	64	BP	500	59000	115000	25000	4.6	2.16	100	263:1
	128	BP	500	51000	110000	22000	5.2	2.43	100	242:1

[a] Polymerization conditions: EH-*i*-DIB = 0.20 g; *M*n = 3900 g/mol, Đ = 2.2; [EH-*i*-DIB] = 5.13×10^{-5} mol/L; *n*-BA added = 50 equivalents, 0.33 g (0.36 mL); [Initiator] = 5.13×10^{-4} mol/L; solvent = toluene; reaction volume = 8.2 mL; temperature = 125°C.

[b] *n*-BA added = 100 equivalents, 0.65 g (0.73 mL)

[c] *n*-BA added = 500 equivalents, 3.25 g (3.6 mL)

[d] GPC data obtained at 160°C in 1,2,4-trichlorobenzene using universal calibration from PS standards

[e] Calculated from ^{1}H NMR.

In a control reaction, EH-*i*-DIB and *n*-BA were combined in the absence of initiator (run A, Table 3.1). After t = 128 min the DIB end group conversion of the product was estimated to be 21% with the average of one *n*-BA monomer per polyolefin chain. Another control reaction between EH-*i*-DIB and BP, this time in the absence of *n*-BA monomer was conducted (run B, Table 3.1). Following an extended reaction time (16 h) there was no observed change in polymer molecular weight by GPC. This result is as expected due to the low ceiling temperature of AMS (66°C) compared with the reaction temperature.

Runs 1-3 in Table 3.1 detail the polymerizations of EH-*i*-DIB over time with increasing concentrations of *n*-BA monomer (50, 100 and 500 equivalents). In run 1 complete conversion of the macromonomer is achieved after 16 min, following which time molecular weights, dispersities and mass yields differ very little.

In run 2, an increase in monomer concentration to 100 × that of EH-*i*-DIB, was accompanied by an increase in the yields, molecular weights, dispersities and rate of conversion of end groups. Full conversion was, in this case, achieved after 8 min and beyond this molecular weights did not vary significantly.

Finally, in run 3, to further investigate the effect of increasing monomer concentration, a reaction was conducted with *n*-BA monomer concentration 500 × greater than EH-*i*-DIB. In this instance complete conversion of the EH-*i*-DIB macromonomer was achieved after only 8 min. Following this, M_n and M_w appear to plateau while observing a small increase in yield finally giving, after 128 min, a copolymer of M_n = 22000 g/mol ($Đ$ = 2.4). Despite an apparent lack of variation of molecular weight, the dispersites of these polymers are all broad after t = 8 min. This

increase in dispersity possibly arises from co-precipitation of a small amount of P(*n*-BA) homopolymer, due to its increased molecular weight.

From the filtrates of run 3 (Table 3.1) the methanol soluble P(*n*-BA) homopolymer was recovered from solution and analysed (Table 3.2). The ^{1}H NMR spectra the soluble fractions showed no EH containing products. Peaks indicative of vinyl terminated P(*n*-BA) were visible at 6.2 and 5.5 ppm. These groups are formed from backbiting in the propagating P(*n*-BA) radical which at temperatures greater than 90°C this is followed by β-scission.[7, 13, 14] Mass yields of homopolymer for 2 and 4 min reactions were insufficient for analysis. Following this time however, mass yields, molecular weights and dispersities were all broadly similar; most of the homopolymer is produced within 8 min.

Table 3.2: Comparison of P(n-BA) from runs with (3) and without (4) EH-*i*-DIB.

Run[a]	Time (min)	Yield (g)	M_p (g/mol)[b]	M_W (g/mol)[b]	M_n (g/mol)[b]	Đ
3	2	0.00	nd	nd	nd	nd
	4	0.03	nd	nd	nd	nd
	8	0.55	13000	13000	5800	2.3
	16	0.62	13000	14000	5300	2.7
	32	0.51	10000	11000	4500	2.4
	64	0.78	14000	15000	6300	2.4
	128	0.71	10000	9800	3900	2.5
4[c]	128	3.09	35000	88000	8000	11

[a] Polymerization conditions: comonomer = *n*-BA; [*n*-BA] = 3.3 mol/L; [Initiator] = 5.13x10^{-4} mol/L; solvent = toluene; reaction volume = 8.2 mL; temperature = 125°C.
[b] GPC data obtained on a chloroform system at room temperature and based on PMMA standard calibration.
[c] 0 EH-*i*-DIB

For comparison purposes, a homopolymerizations of *n*-BA was conducted (run 4) under the same circumstances as run 3, but without EH macromonomer present. The product was a more typical free-radical P(*n*-BA) homopolymer with high dispersity and molecular weight, and a mass conversion of 94%. Capture of the P(BA) radical

chains by EH-i-DIB appears to be very efficient, even under such conditions where all the polar monomer is present at the start of the reaction.

3.3 Copolymerisation mechanism

The observations made in the previous section are consistent with a mechanism involving cross-propagation of the EH-i-DIB macromonomer with the growing radical polar chain. A mechanism of the polymerization is shown below in Scheme 3.3.

Thermal decomposition of the benzoyl peroxide (BP) initiator generates two radicals (Init˙). These initiate the fast propagation of the (*n*-BA) with rate coefficient k_{11}, this produces the radial P(*n*-BA) polymer chains **I**.

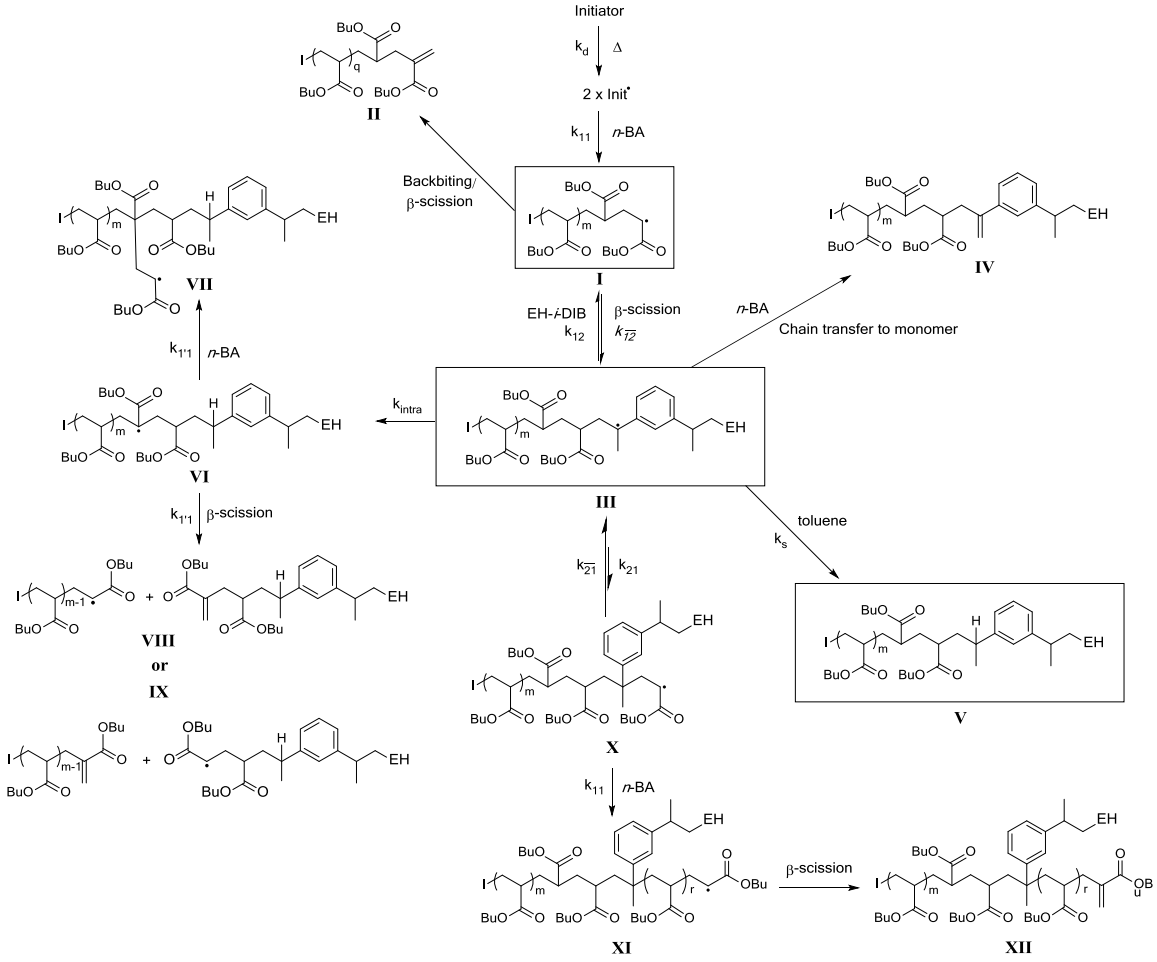

Scheme 3.3: Proposed mechanism for the free-radical copolymerisations of *n*-BA and EH-*i*-DIB

From here the radical polymer chain **I** may cross-propagate with the EH-*i*-DIB macromonomer to produce radical species **III**, at a rate coefficient k_{12}, expected to be 5 × greater than k_{11}.[15] The tertiary benzylic radical in product **III** is relatively stable[14, 16, 17] and is expected to be resistant to homopropagation as well as chain transfer processes, not least as a result of the added steric protection provided by the attached EH polymer chain. Propagation of species **III** with further EH-*i*-DIB is unlikely given the low concentrations, steric bulk and the instability of consecutive AMS monomer units.

At the high temperatures utilised in this reaction, unimolecular β-scission of **III** (rate constant $k_{\overline{12}}$) is realistic[8] and leads to reformation of **I** and the possibility of further propagation of the butyl acrylate homopolymer. A reversible process of **I** to **III** would allow the polar block to grow in a relatively controlled fashion, perhaps after consumption of the initiator. Following complete consumption of the monomer at *ca* 32 min, backbiting and subsequent β-scission of species **I** would predominate[7, 8, 13, 14] to give a propagating poly(butyl acrylate) radical as well as **II** which comprises the methanol soluble fraction recovered.

In n-BA homopolymerization, the backbiting reaction which transfers the radical to a tertiary carbon is followed by propagation from this centre or β-scission,[18] although it has further been shown that mid chain radical migration is kinetically significant.[19] Based upon this we must also consider the possibility of an intramolecular chain transfer of the mid chain radical in **III** to give **VI.** From here the radical species **VI** is expected to undergo β-scission, rapidly,[7, 8, 13, 18] in either of two directions;[19, 20] of these, one possibility is copolymer **IX** which contains an oligomeric butyl acrylate block bearing a vinylic end group. ^{1}H NMR spectra of the isolated products do not show such polymers, indicating that if β-scission is occurring in

significant levels then all such species **IX** must be incorporated into the products or else converted. Given that the analogous butyl acrylate homopolymer **II** is present in significant quantities in the soluble fraction, it is unlikely that complete eradication of **IX** by these means is achieved, and so it can be concluded that intramolecular chain transfer of **III** to another tertiary carbon is very slow. The reaction of tertiary radical of species **VI** with monomer or macromonomer would lead to the formation of branched species such as **VII**. However high reaction temperatures would lead to significant fragmentation,[7] and indeed quaternary branch points in the P(*n*-BA) chain[18] are not observed in ^{1}H NMR spectra.

Under the reaction conditions used the rate (k_{21}) of cross propagation of **III** with the *n*-BA to produce copolymer **X** is expected to be low,[2] even before steric crowding of the radical centre by the polymer chain is taken into account. In a patent[21] by Moad *et al.*, it was shown that in *n*-BA homopolymerization, high reaction temperatures and low concentrations of AMS lead to AMS being incorporated as an end group due to the fact that the tertiary benzylic radical that is formed is unable to propagate at any significant rate.[21] Hence while the process **III** → **X** is unlikely, it is still feasible and in the event that it did occur, it would be followed by the rather fast process (k_{11}). Therefore, we are unable at this stage to exclude the possibility that the graft copolymer **XII** could be produced in this mechanism. However, should the graft 'through' polymer **XII** be formed it is expected that we would observe vinylic end groups from termination products in the ^{1}H NMR spectrum and such groups are not observed; additionally two-dimensional NMR studies (*vide infra*) are consistent with the final product **V** rather than the "graft through" products.

It is expected that chain transfer from **III** to the solvent, toluene would be slow,[15] however this reaction is still likely to be the main cause of eventual termination and route to the observed product **V**.

The mechanism above is comparable to that for nitroxide mediated polymerization (NMP), whereby the growing polymer chain reversibly forms dormant adducts with the control agent. The conditions utilised in these reactions have a similar molar concentration of EH-i-DIB end groups to that of nitroxide used in the typical reaction,[22] although as might be expected radical polymers are not as well mediated by EH-i-DIB as they are by TEMPO. Unavoidably then, some butyl acrylate homopolymer is produced during the early stages of the reaction which instead of terminating to EH-*i*-DIB reversibly, terminates irreversibly via back-biting and subsequent *β*-scission would predominate[7, 8, 13, 14, 20] leading to the formation of low molecular weight P(*n*-BA) as the soluble homopolymer product (Run 6, Table 3.2).

The notion that this terminated, inactive polymer is made in the early stages of the reaction is also indicated due to the fact that the yield and molecular weight of the homopolymer does not vary in any meaningful way after 8 min, additionally, the copolymer, having spent longer as part of the "living" process, had a substantially higher molecular weight in the polar block. Additionally the fact that the P(*n*-BA) side products show narrow dispersities as compared with P(*n*-BA) produced in the absence of EH-*i*-DIB suggests that the macromonomer plays some role in controlling the *n*-BA polymerization.

3.4 Structural analysis of copolymers of EH-*i*-DIB and *n*-BA

3.4.1 NMR Analysis

Possible structures of the copolymerisation of EH-*i*-DIB with polar monomers, as discussed in the previous section, are shown in Figure 3.1.

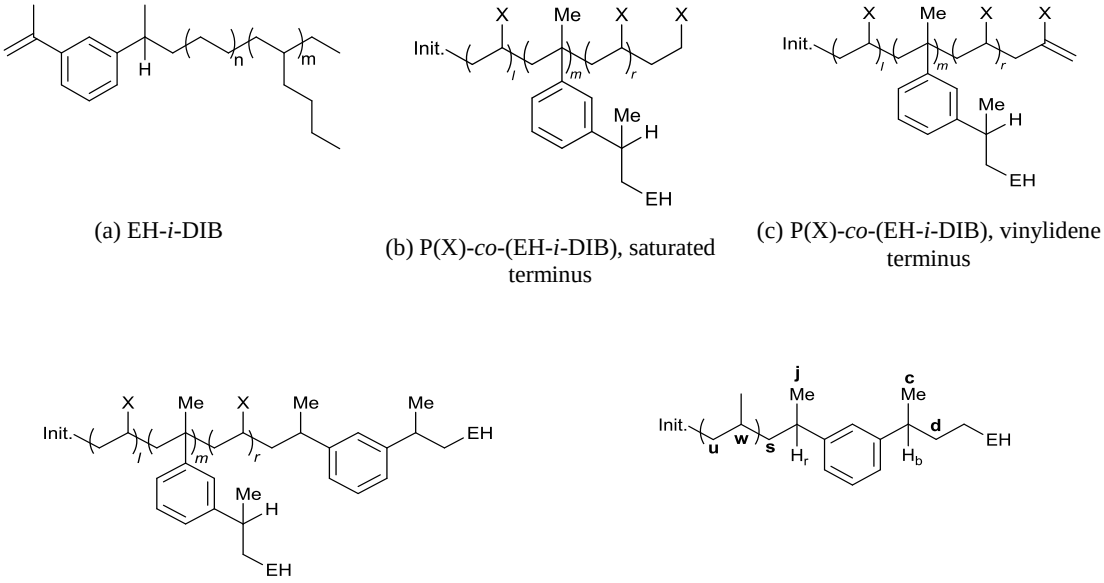

(a) EH-*i*-DIB

(b) P(X)-*co*-(EH-*i*-DIB), saturated terminus

(c) P(X)-*co*-(EH-*i*-DIB), vinylidene terminus

(d) P(X)-*co*-(EH-*i*-DIB)-*t*-EH-*i*-DIB

(e) P(X)-*b*-(EH-*i*-DIB)

Figure 3.1: EH-i-DIB and the expected structures from copolymerisation with polar monomers

Figure 3.2 shows the ^{1}H NMR spectrum (100°C) of the final product of run 1-128 from Table 3.1. The spectrum shows a peak at 1.30 ppm corresponding to EH backbone as well as peaks attributed to P(BA).[23] The absence of DIB end group vinylidene protons at 5.07 and 5.34 ppm indicates compete conversion of the EH-*i*-DIB macromonomer, creating either block (e) or graft (b)-(d) copolymer.

A growing polymer chain, **XI** (Scheme 3.3), from polymerization through **III** would be expected to undergo termination principally by the same mechanism as BA homopolymer i.e. backbiting/β-scission producing polymer (c). The absence of vinylic end groups in the ^{1}H NMR spectra of the purified polymers (5.51 and 6.15 ppm) excludes the presence of (c) and thus such a polymerization 'through' mechanism; additionally indicating successful separation of the copolymer from P(*n*-BA) homopolymer species.

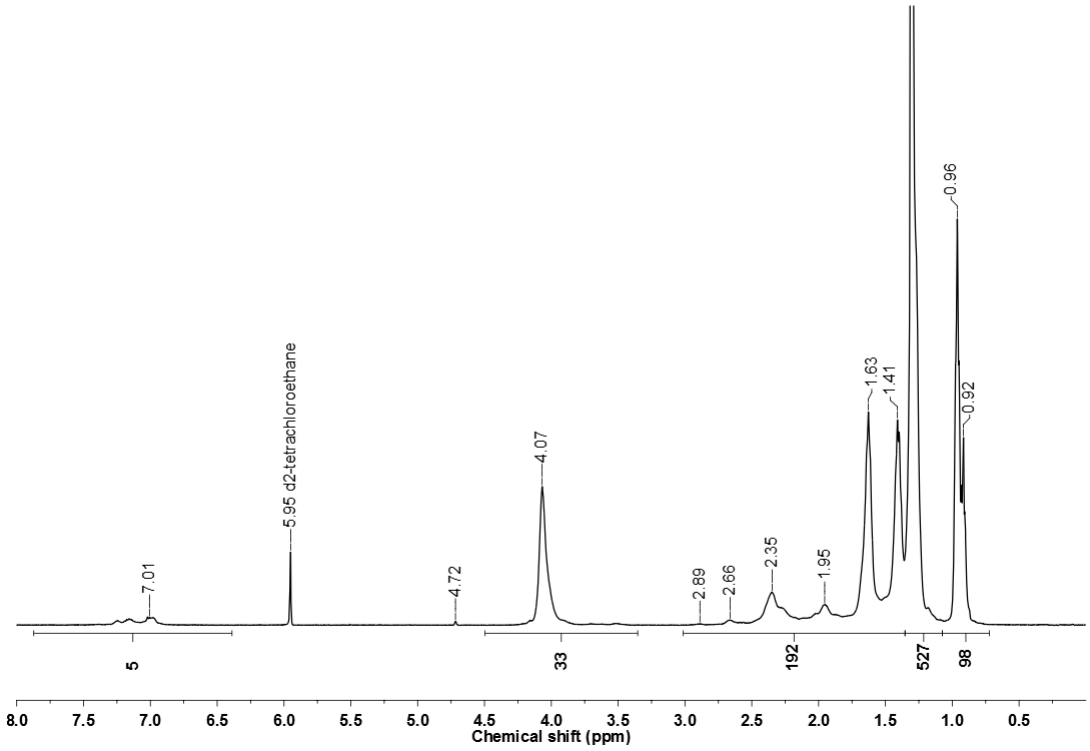

Figure 3.2: ^{1}H NMR spectrum of EH-P(*n*-BA) in d^{2}-TCE at 100°C (400 MHz). Relaxation delay = 1 s. Integral of the n-BA signal at 4.07 ppm is set according to the following: by assuming that an average of one EH-*i*-DIB macromonomer (M_n-3900 g/mol) is present in the copolymer chains (M_n-6000 g/mol), the contribution of *n*-BA to the M_n of the copolymer is *ca* 2100 g/mol. Hence integral of *ca* 2×(2100/128.2) = 33 H.

In the ^{1}H NMR spectra of these materials there is significant overlap between the EH main chain at *ca* 1.30 ppm and the P(BA) side chain methylene signals at *ca* 1.4 ppm. Similarly there is an overlap of the EH methyl peaks with the P(BA) side

chain methyl groups at *ca* 0.9 ppm. This precludes meaningful integration of the spectra for direct estimation of the DP of either block.

Nonetheless, by assuming for the moment that the copolymer (M_n = 6000 g/mol by GPC, universal calibration) contains only a single unit of EH-i-DIB macromonomer (3900 g/mol), the expected integral of the P(*n*-BA) ester CH_2 resonance at *ca* 4.1 ppm can be calculated (Figure 3.2) to be *ca* 33 H. Using this value, the relative integrals of the remaining groups are found to correspond closely to expectations: (i) the overlapping peaks ranging from 2.7 to 1.3 ppm have an integral of 619 H (expected 671 H) and the relative integral of the EH main chain peak at 1.3 ppm was appropriate, with an integral of 527 H (expected 557 H); (ii) the isolated P(*n*-BA) and EH methyl signals at *ca* 1.0 ppm had an integral of 98 H (expected 116 H); (iii) finally the signal from the aromatic region at *ca.* 6.9-7.3 ppm has an integral of 5 H (4 H expected). Therefore, the assumption that the copolymer contains a single EH-*i*-DIB macromonomer unit is consistent with integration values in high temperature ^{1}H NMR spectra. This is inconsistent with the presence of significant quantities of polymer (d) can be excluded (Figure 3.1) where polymerisation through EH-i-DIB on *m* occasions has been followed by termination to EH-i-DIB. It is also inconsistent with the presence of polymers (b) or (c) where $m > 1$.

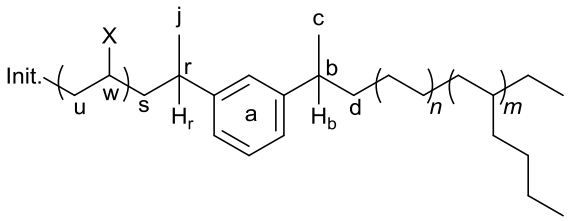

Figure 3.3: Structure of EH-b-P(X) block copolymer

For the final architecture type, block copolymers (e) it is expected that there will be two inequivalent benzylic proton signals (**H_b** and **H_r**) appearing at *ca* 2.7 ppm.

Indeed these peaks are observed within the spectra shown in Figure 3.4, however there is significant overlap of these small signals with the adjacent, large P(*n*-BA) methine signal at 2.35 ppm, making integration untenable. The comparison of the benzylic signals is shown in Figure 3.4. The sharp benzylic signals (**H_b**) from the EH-*i*-DIB spectra are centred at 2.70 ppm, while the broader signal, arising in the copolymer, occurs at *ca* 2.66 ppm (**H_b/H_r**).

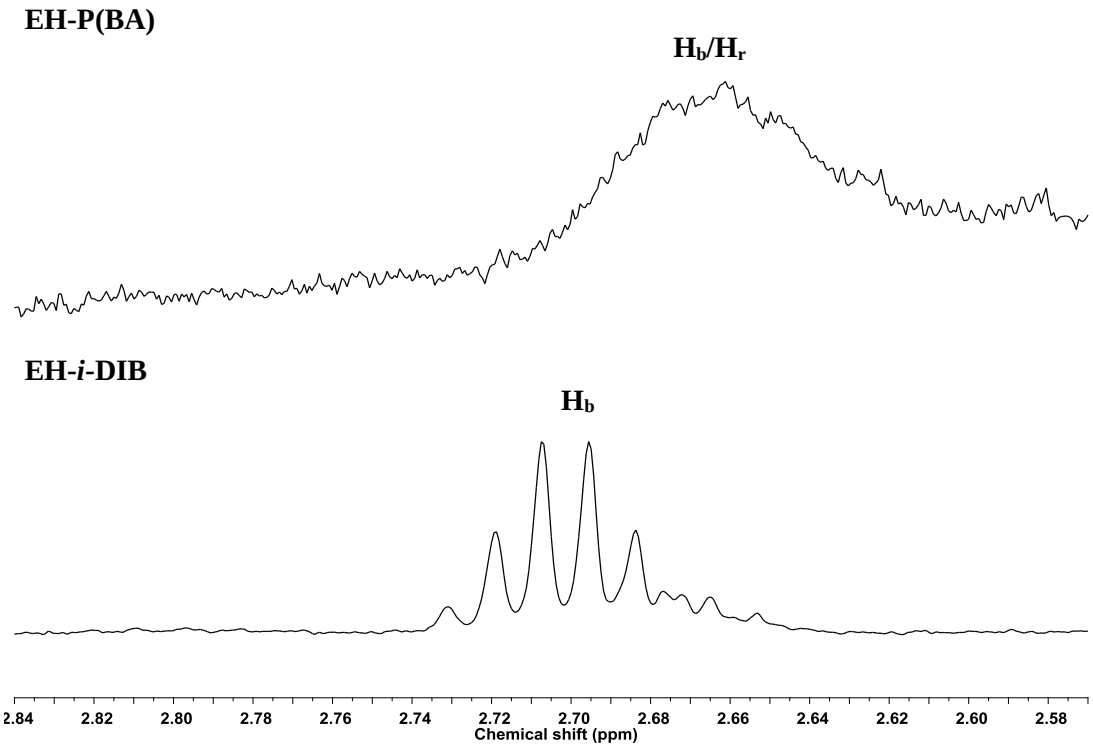

Figure 3.4: ^{1}H NMR spectra of EH-*i*-DIB and the copolymer recovered from run 2 (Table 2.1) in d^2-TCE at 100°C focusing on the benzylic methine region

3.4.2 Two-Dimensional NMR analysis

Figure 3.5 is a segment of the ^{1}H-^{1}H COSY spectrum, attained under the same conditions described previously, and shows that benzylic signal described above gives a diagonally elongated cross-peak correlating with signals at *ca* 1.2-1.25 ppm. While

these individual correlations are not resolved, this is still indicative of coupling between benzylic proton environments **H_b** and **H_r** coupling to the methyl environments **Me_c** and **Me_j.**

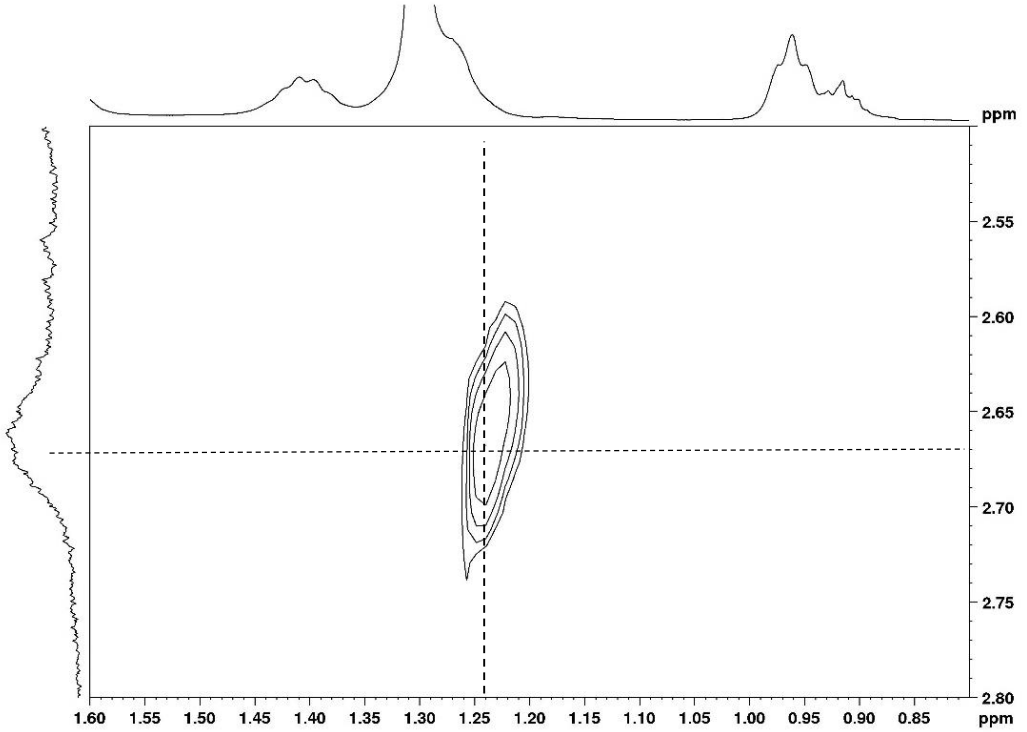

Figure 3.5: Detail of a ^{1}H-^{1}H COSY NMR of EH-*b*-PBA in *d*^{2}-TCE at 100°C (500MHz).

Also detectable within the ^{1}H-^{1}H COSY (Figure 3.6) were two sets of diastereotopic correlations, the first set being a coupling between the benzylic proton **H_b** (2.64 ppm) and the neighbouring EH diastereotopic methylene proton environment **H_d** at *ca* 1.55/1.59 ppm. Additionally a second pair of correlations occurs between the benzylic proton **H_r** (2.67 ppm) and the adjacent diastereotopic P(*n*-BA) methylene proton environment **H_s** at *ca* 1.76/1.78 ppm. The nature of these correlations is consistent with the block copolymer structure (Figure 3.1 (e))

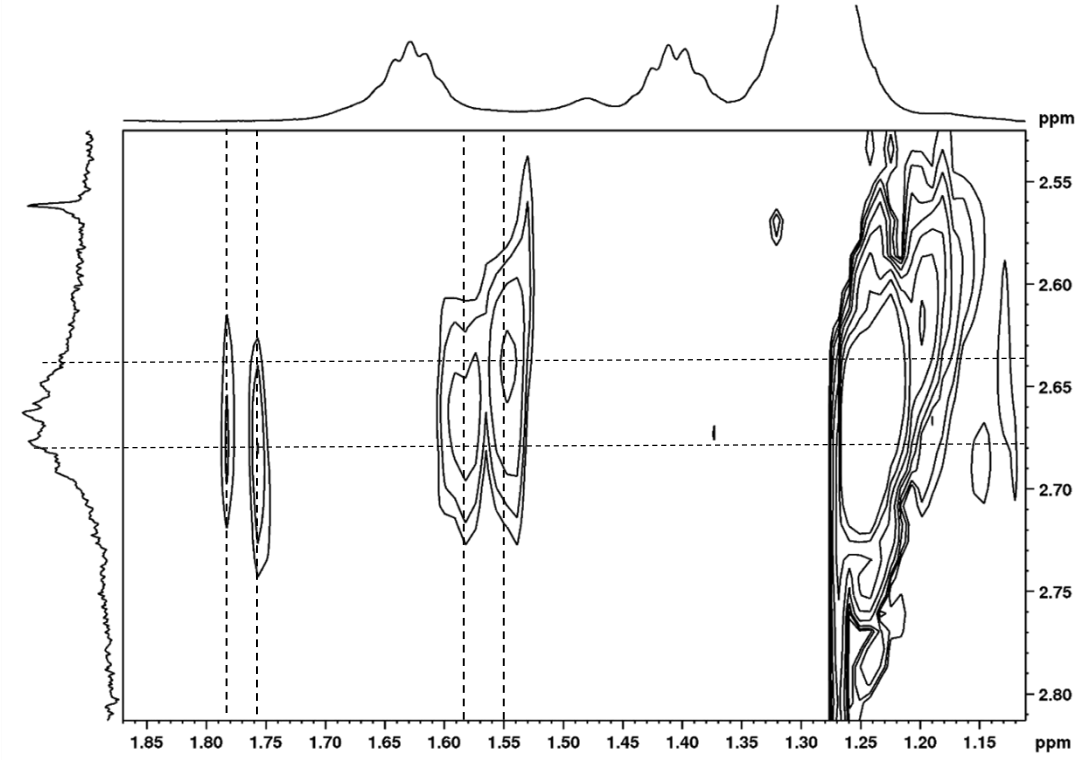

Figure 3.6: Detail of a ^{1}H-^{1}H COSY NMR of EH-*b*-PBA in *d*^{2}-TCE at 100°C (500MHz).

Table 3.3: EH-*b*-P(*n*-BA) NMR assignments

Proton environment	Predictions[a]			
	^{1}H (ppm)	Error (±)	^{13}C (ppm)	Error (±)
b	2.75	0.64	40.1	2.41
r	2.75	0.64	38.1	5.28
d	1.76	0.54	40.2	5.61
s	1.64	0.40	43.7	11.78
u	1.14	0.47	42.0	5.28
w	2.44	0.47	45.3	5.44
j	1.27	0.23	23.6	2.74
c	1.16	0.23	22.8	2.18

[a] Expected ^{1}H and ^{13}C chemical shifts for EH-b-P(BA) calculated by ACD/I-LAB

^{1}H-^{13}C HMQC spectrum (Figure 3.7) appears to show a cross peak between the benzylic region and what appear to be two small environments in the ^{13}C NMR, one at *ca* 39.10, which we expect to be $\mathbf{C_r}$, and another at *ca* 41 ppm, $\mathbf{C_b}$. Both are within the expected range for the expected shifts shown in Table 3.3 and provides evidence of the presence of two benzylic environments.

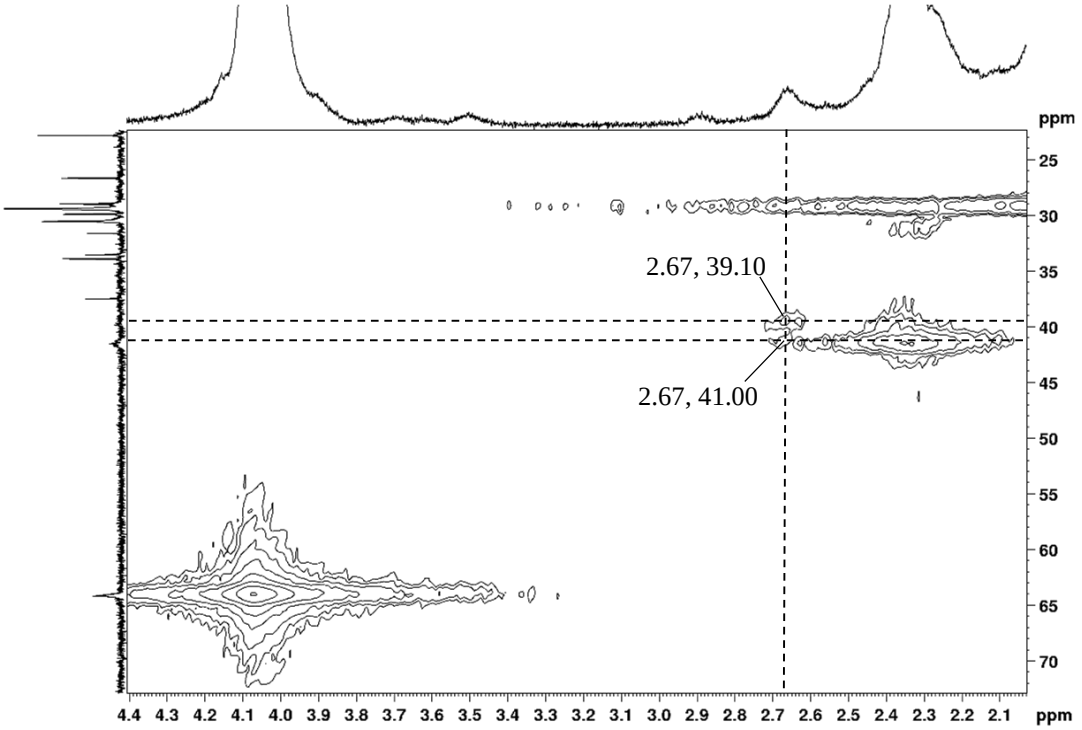

Figure 3.7: Detail of a ^{1}H-^{13}C HMQC NMR of EH-*b*-PBA in *d*^{2}-TCE at 100°C (500MHz).

3.5 Copolymerisation of functionalised LLDPE with vinyl acetate

Ethylene-vinyl acetate copolymers (EVAs) have many applications in materials science engineering, [24] and as noted in chapter 1, they are used as wax crystal modifiers in fuels and other hydrocarbon fluids. The properties of EVA materials can be modified substantially by changing the ethylene to vinyl acetate ratio.[25,26,27] More

recently the prospect of synthesis of block like PE-P(VAc) materials has emerged with the works of Monteil and Detrembleur,[28,29] however such copolymerisations are very rare.

EH-*i*-DIB (M_n = 3900 g/mol, $Đ$ = 2.1) was heated with 500 equivalents of vinyl acetate in toluene at 125°C in the presence of benzoyl peroxide initiator (Run 1, Table 3.4). The resultant mixture of polymeric materials was separable by precipitation in ethanol. The ethanol soluble fraction was shown by ^{1}H NMR spectroscopy to be P(VAc) homopolymer. No EH-containing material was detected in this fraction. Samples were dried overnight *in vacuo* prior to analysis. The ^{1}H NMR spectrum of the precipitated product of run 1 (Table 3.4) showed complete conversion of the EH-*i*-DIB macromonomer and the presence of signals corresponding to both EH and P(VAc), even after multiple reprecipitations (*vide infra*). GPC analysis gave M_n = 6600 g/mol (Đ = 2.6).

As detailed in section 3.4, kinetic experiments (runs 2 and 3, Table 3.4) were conducted by setting up several ampoules in parallel with individual reactions being stopped at pre-defined intervals. The polymers were purified by precipitation in ethanol as before. Complete recovery of the EH component was verified by the absence of signals corresponding to EH in the NMR spectrum of the soluble fraction. The end group conversions (Table 3.4) were calculated by comparison of integrals of the vinylidene proton signals corresponding to the DIB end group at 5.07 and 5.34 ppm in each sample to those in the NMR spectrum of the EH-*i*-DIB macromonomer.

Table 3.4: Copolymerisations of EH-*i*-DIB with vinyl acetate

Run	Time (min)	Initiator	VAc: EH-*i*-DIB	M_{p} [d]	M_{w} [d]	M_{n} [d]	Đ [d]	Yield	EH-i-DIB Conversion (%)[e]	DP of VAc/ EH-i-DIB[e]
1 [a]	128	BP	500	8600	17000	6600	2.6	0.42	100	33:1
2 [b]	2	BP	100	5700	8000	4000	2.0	0.2	53	1:1
	4	BP	100	5900	8400	4000	2.1	0.22	74	1:1
	8	BP	100	6500	8600	4100	2.1	0.22	89	2:1
	16	BP	100	7200	8200	4300	1.9	0.23	100	4:1
	32	BP	100	6800	8800	4200	2.1	0.27	100	5:1
	64	BP	100	6900	9700	4400	2.2	0.28	100	6:1
	128	BP	100	6800	10400	4500	2.3	0.29	100	7:1
3 [c]	2	BP	200	6400	8800	4000	2.2	0.22	0	1:1
	4	BP	200	6500	8000	4200	1.9	0.24	86	3:1
	8	BP	200	6600	8000	4200	1.9	0.25	100	4:1
	16	BP	200	6700	9000	4500	2.0	0.26	100	7:1
	32	BP	200	7000	11000	4700	2.3	0.29	100	9:1
	64	BP	200	7000	11000	5000	2.2	0.31	100	13:1
	128	BP	200	7100	10400	5200	2.0	0.32	100	15:1

[a] Polymerization conditions: EH-*i*-DIB = 0.20 g; M_n = 3900 g/mol, Đ = 2.2; [EH-*i*-DIB] = 5.13×10^{-5} mol/L (0.2 g); VAc added = 500 equivalents, 2.16 g (2.3 mL); [Initiator] = 5.13×10^{-4} mol/L; solvent = toluene; reaction volume = 8.2 mL; temperature = 125°C.

[b] Mass VAc added = 100 equivalents, 0.4 g (0.47 mL)

[c] Mass VAc added = 200 equivalents, 0.8 g (0.94 mL)

[d] GPC data obtained at 160°C in 1,2,4-trichlorobenzene using universal calibration from PS standards

[e] Calculated from ^{1}H NMR.

Runs 2 & 3 (Table 3.4) the copolymerisation of EH-*i*-DIB with 100 and 200 equivalents of vinyl acetate respectively. In Run 2, the EH-*i*-DIB the EH-*i*-DIB macromonomer was converted after t = 16 min, determined by the ^{1}H NMR spectrum. Following this time, mass yields, molecular weights and dispersities did not change significantly, indicating that following macromonomer conversion there is little

further change in copolymer properties, which is consistent with observations made for copolymerisations with *n*-BA. In Run 3 conversion of the EH-*i*-DIB macromomer was complete after t = 8 min, this quicker conversion is due to the higher concentration of propagating P(VAc) chains and concurrently we observe higher copolymer molecular weights and larger mass yields.

3.5.1 EH-b-P(VAc) NMR analysis

NMR spectroscopy was once again used to investigate the structure of the copolymers produced, as to whether they occur as graft (b)-(d) or block (e) copolymers (Figure 3.1). Figure 3.9 shows the ^{1}H NMR spectrum of run 1 (Table 3.4). The EH methyl end group peaks appear as a resolved triplet peak at 0.91 ppm while the EH backbone methylene protons are observed to and as a peak at 1.30 ppm. Additionally, peaks arising from the P(VAc) segments are observed,[30] including the pendant methylene protons at 4.90 ppm.

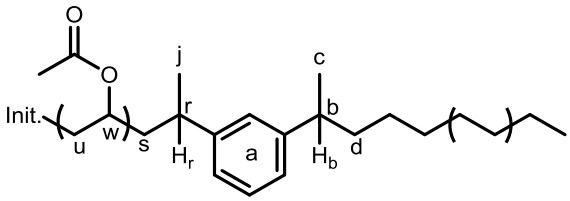

Figure 3.8: Labelled structure of EH-*b*-P(VAc)

As previously described, the complete conversion of the EH-*i*-DIB macrmonomer was determined by the absence of the vinylidene protons at 5.07 and 5.34 ppm. Figure 3.9 shows the ^{1}H NMR spectrum of EH-P(VAc) copolymer produced in run 1 (Table 3.4). In some crude samples it was possible to detect a small

peak at *ca* 4.1 ppm, arising due to the methylene end groups of P(VAc) homopolymer which co-precipitates from the polymerization mixture. The homopolymer impurity can be removed by reprecipitation from toluene to ethanol. This P(VAc) methylene end group assignment was verified by 2D NMR experiments on the homopolymer and has been shown to occur after termination *via* chain transfer by H abstraction.[30, 31] While these methylene end groups could also arise from termination by disproportionation it would be accompanied by an equivalent number of vinylic end groups which would have also been observed in the ^{1}H NMR spectra.[31] That such vinylic signals are absent, indicates that disproportionation does not occur in significant quantities under these conditions and is suggestive of termination by chain transfer. As such we can exclude polymerization 'through' EH-*i*-DIB followed by termination by disproportionation to form copolymer architecture (c) (Figure 3.1). Given also that the methylene end groups appear only in the homopolymer and not the copolymer suggests that polymerization 'through' followed by chain transfer to form

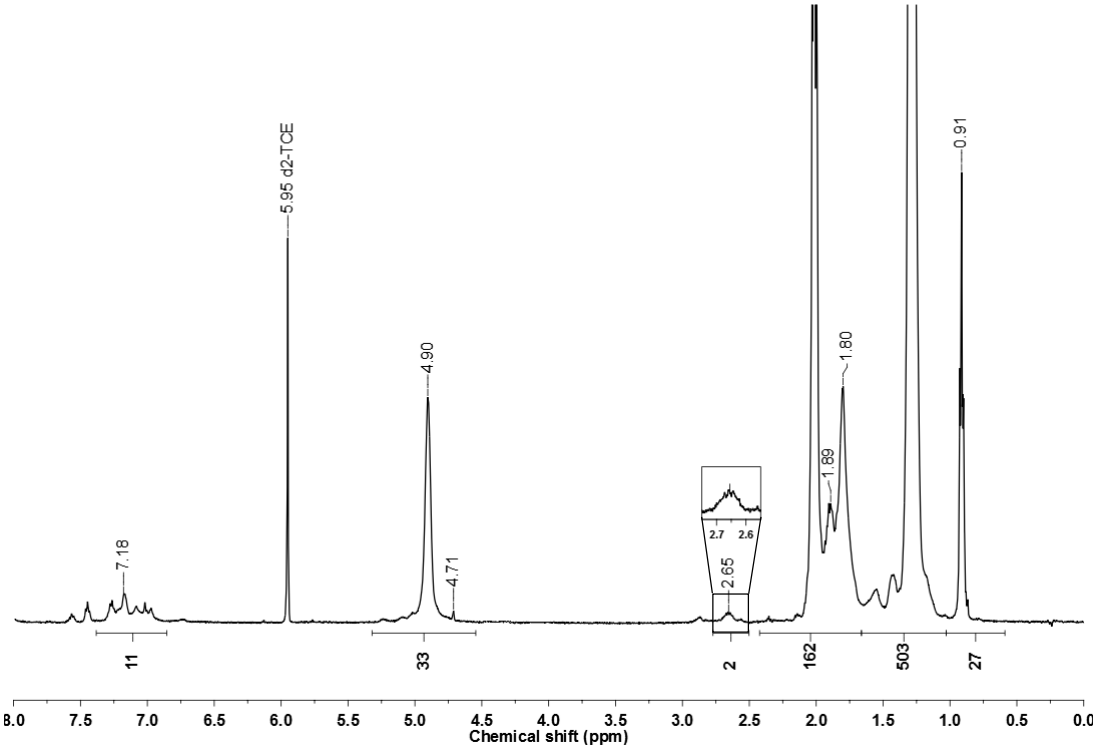

Figure 3.9: ^{1}H NMR of EH-*b*-P(VAc) in d^{2}-TCE at 100°C (400 MHz). Relaxation delay = 1 s

architecture (b) does not occur and is consistent with P(VAc) termination to the macromonomer.

With regard to integration of EH-b-P(VAc) ^{1}H NMR spectra, we note that the benzylic proton resonance at 2.69 ppm is far more isolated then for EH-*b*-P(BA) (*vide supra*). Utilising this and the resonance of the P(VAc) backbone methine group at 4.91 ppm we are able to estimate the copolymer molecular weight in a more direct fashion. From this the degree of polymerization of vinyl acetate block was estimated by having the benzylic peak integral set to 2H, which is equivalent to the number of protons which would be present in a block copolymer structure. This lead to a peak integral of the methine protons in the P(VAc) backbone of 33 H, meaning the degree of polymerization of the VAc of 33. We then calculate the M_n of the copolymer to be 6700 g/mol (M_n = 6600 g/mol by GPC).

Additionally, we can calculate the relative resonance integrals in the same manner described for EH-*b*-P(BA). As before, we initially assume the copolymer (M_n = 6600 g/mol by universal calibration of GPC) contains only a single macromonomer unit (3900 g/mol), from this we calculate the expected integral of the P(VAc) ester CH_2 signal at 4.91 ppm (Figure 3.10) to be 31 H. For the remaining groups the integrals were found to closely match with expectations, the overlapping peaks between *ca* 1.7 and 2.2 ppm have an integral of 154 H as compared with the expected 155 H. The signals between *ca* 1.2-1.6 ppm have an integral of 479 H, which gives the greatest deviation from the expected integral of 557 H. The EH methyl end groups signal at 0.9 ppm has an integral of 26 H (expected 20 H). Finally the isolated benzylic signal at 2.64 ppm has and integral of 2 H (expected 2H) and the aromatic signals had an integral of 11 H (expected 9H). Given the consistency of these integrations with the expected values seems to support the assumption of the presence of a single EH-*i*-DIB

macromonomer per copolymer chain. This would appear to preclude the presence of significant quantities of polymer (d) (Figure 3.1).

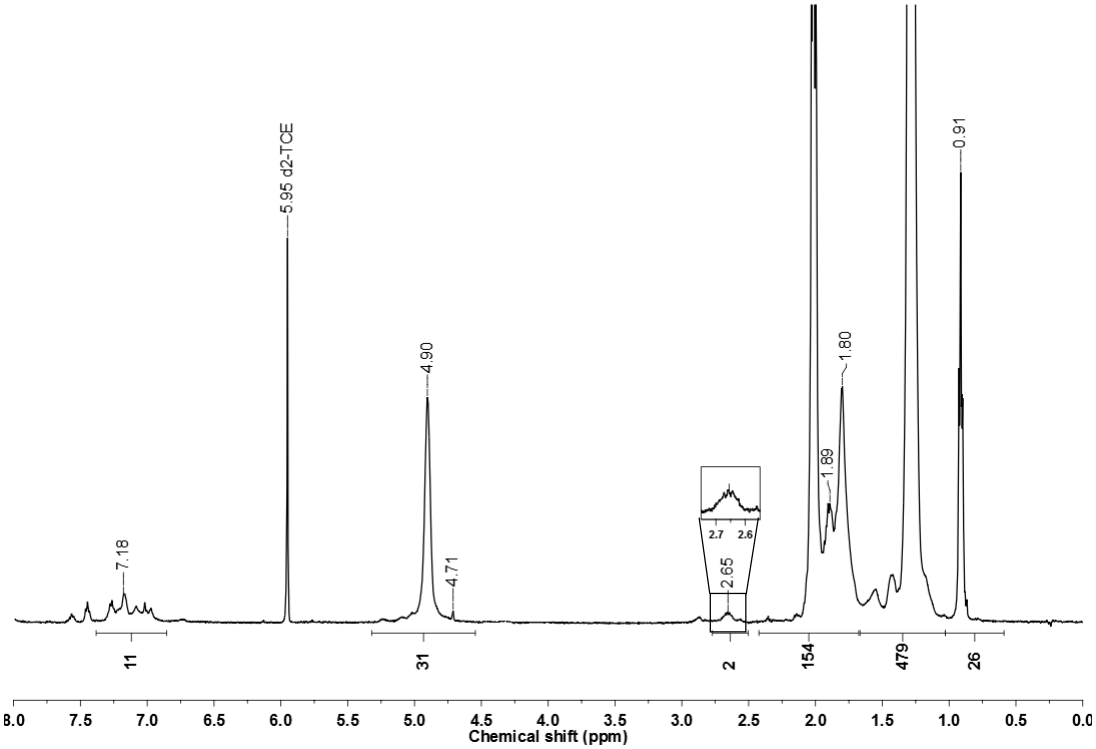

Figure 3.10: ^{1}H NMR spectrum of EH-P(VAc) in d^{2}-TCE at 100°C (400 MHz). Relaxation delay = 1 s. Integral of the P(VAc) signal at 4.90 ppm is set according to the following: by assuming that an average of one EH-*i*-DIB macromonomer (M_n-3900 g/mol) is present in the copolymer chains (M_n-6600 g/mol), the contribution of *n*-BA to the M_n of the copolymer is *ca* 2700 g/mol. Hence integral of *ca* (2700/86.1) = 31 H.

The comparison of the benzylic signals of EH-*b*-P(VAc) and EH-*i*-DIB is shown in Figure 3.11. The sharp benzylic signals (**H_b**) from the EH-*i*-DIB spectra are centred at 2.70 ppm, while the broader signal, arising in the copolymer, occurs at *ca* 2.66 ppm (**H_b/H_r**). As previously stated the copolymer benzylic signal is much better resolved than in the EH-*b*-P(BA) (*vide supra*).

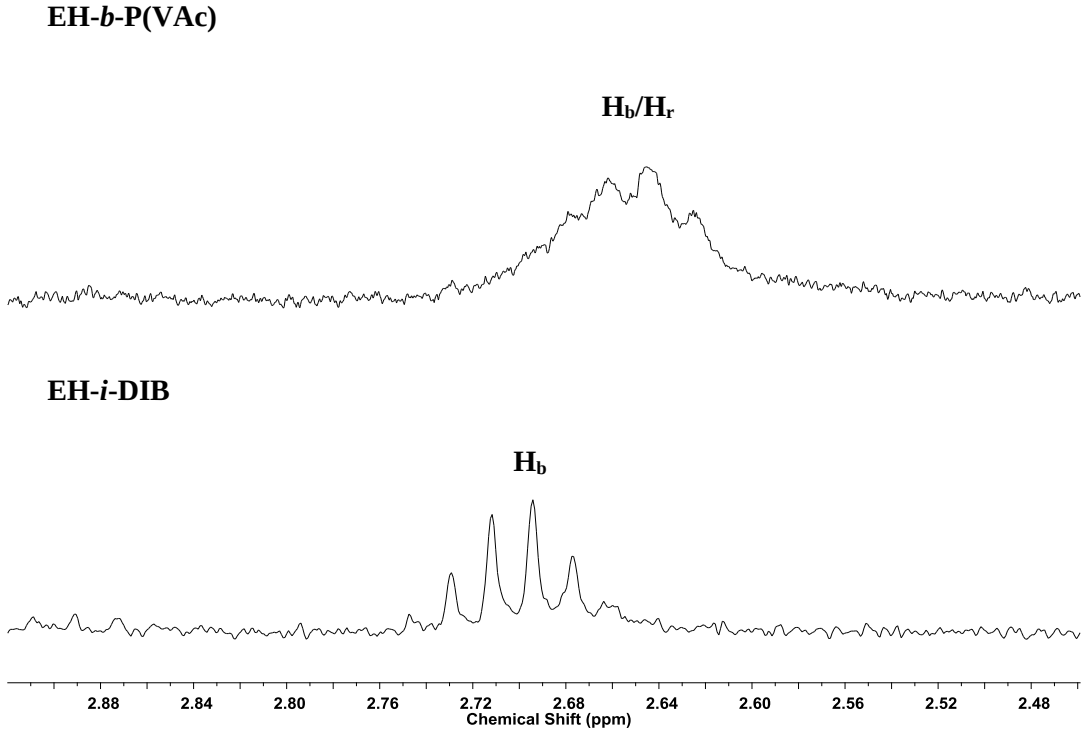

Figure 3.11 - ^{1}H NMR spectrum of EH-*i*-DIB and EH-*b*-P(VAc) in d^2-TCE at 100°C, focused on benzylic methine region (400 MHz).

3.5.2 Two-Dimensional NMR analysis

As with EH-*b*-P(BA), 2D NMR spectra were acquired for EH-*b*-P(VAc). Figure 3.12 is a segment of the ^{1}H-^{1}H COSY spectrum, attained under the same conditions described previously, shows that benzylic signal described above gives a pair of diagonally aligned cross-peaks correlating with signals at *ca* 1.2-1.25 ppm. Unlike with EH-b-P(BA) copolymers these individual correlations are resolved and are consistent with the benzylic proton environments $\mathbf{H_b}$ and $\mathbf{H_r}$ coupling to the methyl environments $\mathbf{Me_c}$ and $\mathbf{Me_j}$, either side of the aromatic ring, respectively.

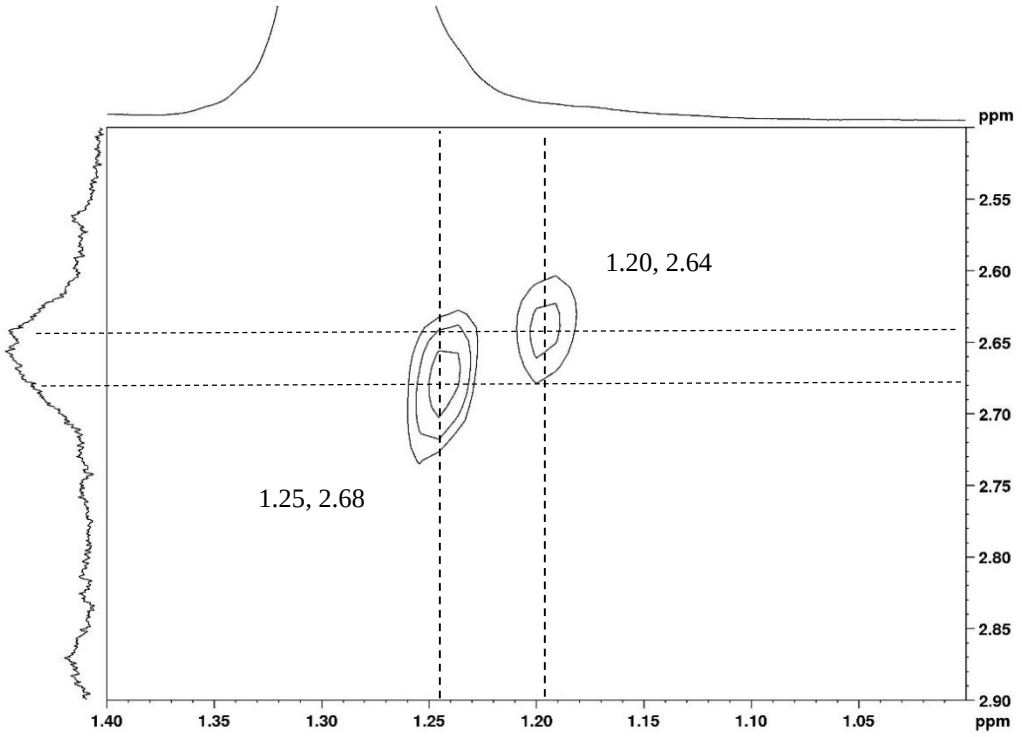

Figure 3.12: Detail of a ^{1}H-^{1}H COSY NMR of EH-b-P(VAc) in d^{2}-TCE at 100°C (500MHz).

Also detectable within the ^{1}H-^{1}H COSY (Figure 3.13) were two sets of diastereotopic correlations, the first set being a coupling between the benzylic proton $\mathbf{H_b}$ (2.65 ppm) and the neighbouring EH diastereotopic methylene proton environment $\mathbf{H_d}$ at *ca* 1.54/1.61 ppm. Additionally a second pair of correlations occurs between the benzylic proton $\mathbf{H_r}$ (2.67 ppm) and the adjacent diastereotopic P(*n*-BA) methylene proton environment $\mathbf{H_s}$ at *ca* 1.90/1.93 ppm. These observations are consistent with those made for EH-b-P(BA) and indicates that these materials possess a block copolymer structure (Figure 3.1 (e)).

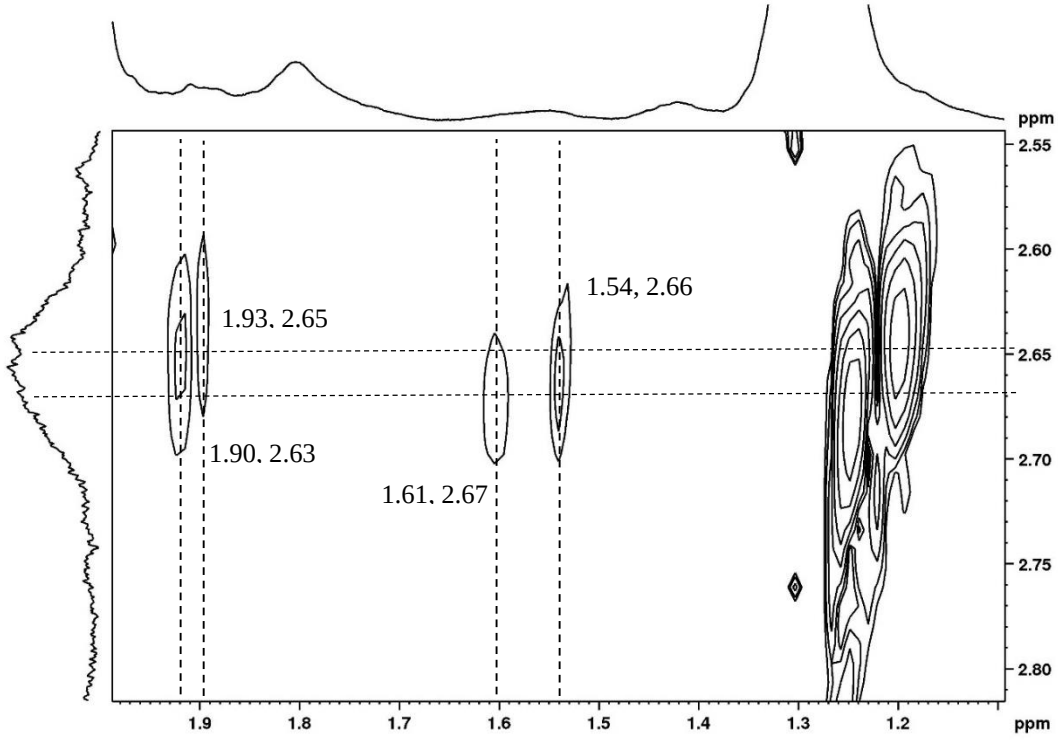

Figure 3.13: Detail of a ^{1}H-^{1}H COSY NMR of EH-b-P(VAc) in d^{2}-TCE at 100°C (500MHz).

The ^{1}H-^{13}C HMQC spectrum (Figure 3.14) shows an elongated cross peak between the benzylic region and what appear to be two small environments in the ^{13}C NMR at ca 39.7, which we expect to be $\mathbf{C_r}$, and $\mathbf{C_b}$. Both are within the range of the expected shifts listed in Table 3.5 and provides evidence of the presence of two benzylic environments.

Table 3.5: Assignments of EH-b-PVAc

Proton environment	Predictions[a]			
	^{1}H (ppm)	Error (±)	^{13}C (ppm)	Error (±)
b	2.75	0.64	40.13	2.41
r	3.07	0.64	36.73	5.15
d	1.52/1.76	0.54	40.15	5.61
s	1.75/1.94	0.40	44.53	2.51
u	1.73	0.58	39.47	4.37
w	4.98	0.24	67.88	2.72
j	1.25	0.22	22.61	2.26
c	1.16	0.23	22.79	0.91

[a] Expected ^{1}H and ^{13}C chemical shifts for EH-b-P(BA) calculated by ACD/I-LAB

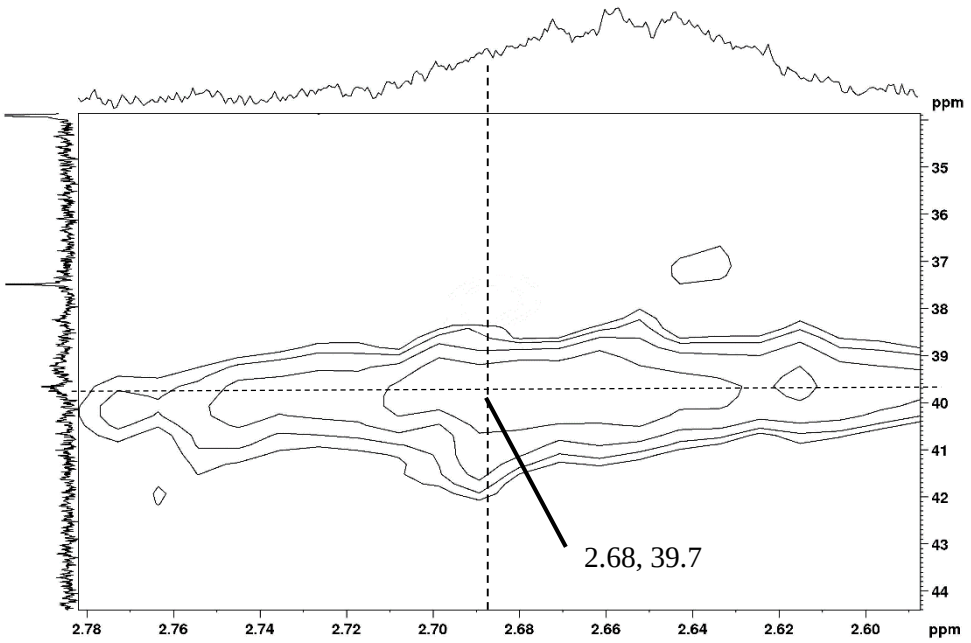

Figure 3.14: Detail of a ^{1}H-^{13}C HMQC NMR of EH-*b*-P(VAc) in d^{2}-TCE at 100°C (500MHz).

3.6 Hydrolysis of poly(vinyl acrylate) block copolymers to poly(vinyl alcohol)

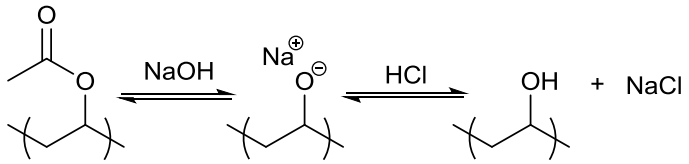

Scheme 3.4: Hydrolysis of P(VAc) to P(VA)

Hydrolysis of EH-*b*-P(VAc) (M_n = 5660 g/mol, $Đ$ = 2.0) was carried out in 70:30 toluene:isopropyl alcohol in the presence of potassium hydroxide, at 120°C over 16 h followed by neutralization with 1M HCl.[32] The polymer was precipitated in water and washed before drying *in vacuo*.

Table 3.6: Hydrolysis of EH-b-PVAc to EH-b-PVA

Run	Time (min)	Hydrolysing Agent	Conc	M_p	M_w	M_n	Đ	Yield	VAc Conversion (%)
CB241[a]	180	NaOH	0.27	8200	9200	4600	2.0	0.7	100
CB243[b]	180	NaOH	0.27	7800	8500	4100	2.1	0.8	100

[a] Starting material is sample CB237, 1 g, M_w-11305, M_n, 5660, Đ -2.0
[b] Starting material is sample CB239, 1 g, M_w-11866 M_n-5410, Đ -2.2

Conversion of the vinyl acetate block was examined by comparison of the infra-red spectra of both starting material and product (Figure 3.15). The spectra shown clearly the complete disappearance of the ν(CO) band at 1750 cm^{-1} with the simultaneous appearance of a broad hydroxyl stretch 3340 cm^{-1}, this shows that we have achieved complete conversion of the vinyl acetate to vinyl alcohol.

Table 3.7: Full IR spectral assignments for peaks observed in EH-*b*-PVAc and EH-*b*-PVA

Observed Wave Number & Rel. Intensity	**Assignments**
3338	O-H
2916	C-H
2848	C-H
1734	C=O stretching
1469	CH asym deformation
1370	CH_3 asym deformation
1231	C-H in plane bending
1115	C-O stretching
1021	CH_2 twisting
945	CH_3 wagging
830	C-O-C in plane bending
719	CH_2 rocking
604	C=O out of plane bending

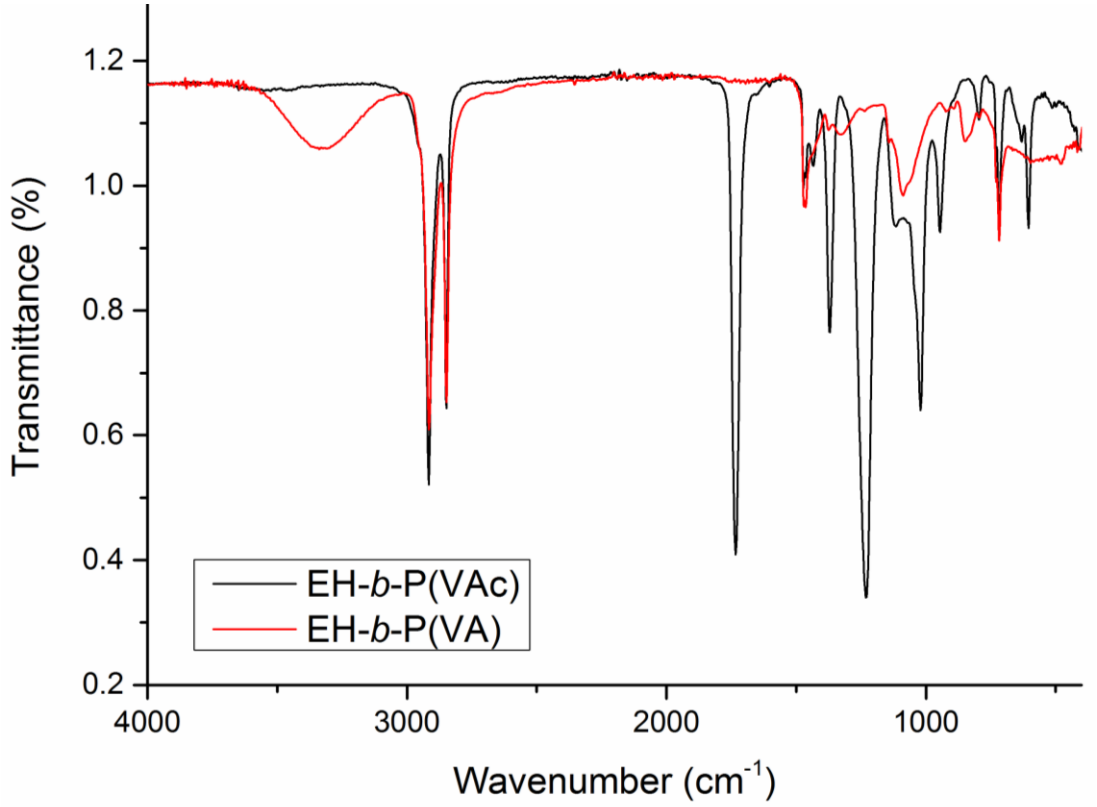

Figure 3.15: IR spectra for before and after EH-*b*-P(VAc) hydrolysis to EH-b-P(VA)

An assignment of the IR spectrum (Figure 3.15) of EH-*b*-P(VA) (Run 1, Table 3.6) is shown in Table 3.7. GPC data indicate a reduction of molecular weight expected upon loss of the acetyl groups. In run 1 (Table 3.6) the EH-*b*-P(VAc) starting material had a molecular weight of M_n = 5700 g/mol (GPC universal calibration) accounting for the EH component (3900 g/mol) gives a polar block molecular weight of 1800 g/mol and therefore a P(VAc) DP of 21 (1800/86.1). Hydrolysis of a VAc unit leads to a loss of 42 g/mol and so the reduction of molecular weight upon hydrolysis (Run 1, Table 3.7) would be 882 g/mol. Making this deduction we find the expected copolymer molecular weight for EH-*b*-P(VA) would be M_n = 4800 g/mol which matches closely with molecular weights recorded by GPC.

While the solubility of the material was greatly reduced following the hydrolysis the ^{1}H NMR spectrum was acquired. This shows a disappearance of the resonance for methine protons of the backbone of the vinyl acetate (4.86 ppm), and the appearance of a broad feature at *ca* 4.22 ppm, assigned to the hydroxyl groups.

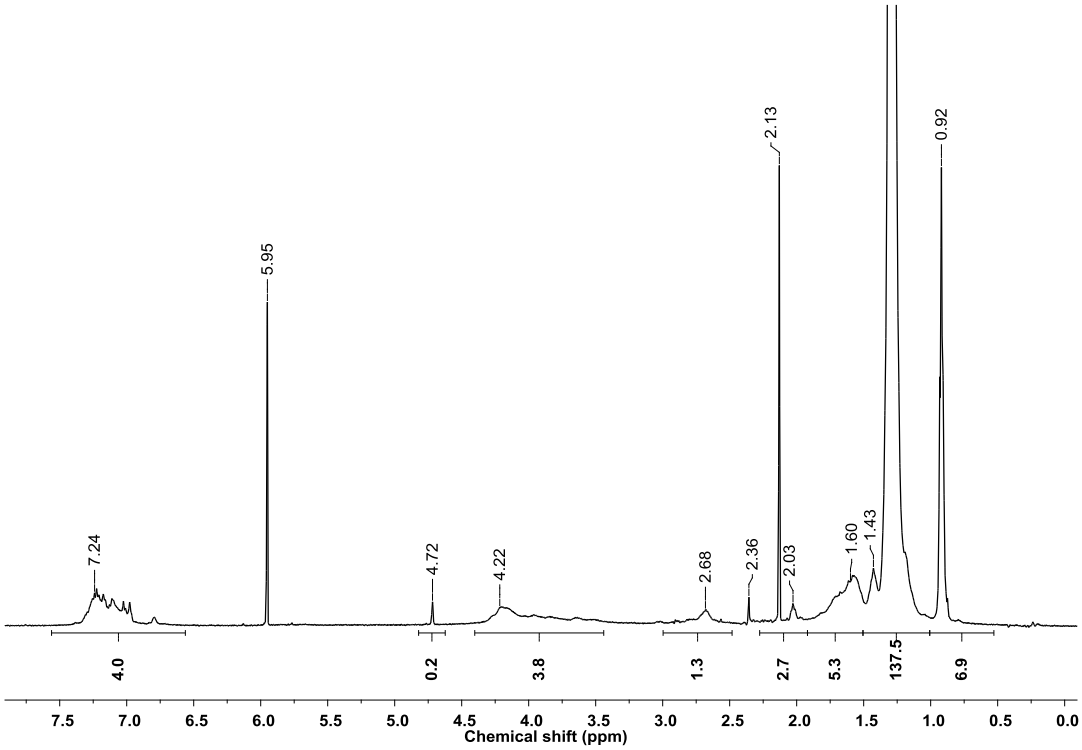

Figure 3.16: ^{1}H NMR of EH-*b*-P(VA) in d^{2}-TCE at 100°C (400 MHz). Relaxation delay = 1 s

3.7 Copolymerisations with other polar monomers.

3.7.1 Vinyl 2-ethylhexanoate

In comparison to EVAs copolymers of ethylene and vinyl esters bearing longer alkyl side chains are reported far less frequently in the academic literature. Nevertheless those materials have shown potential in a range of applications including for resins[33], adhesives[34] and in wax crystal modification in oils.[35, 36] Vinyl-2-ethylhexanoate

(V2EH) (Figure 3.17), has been frequently utilised in such applications and is commercially available.

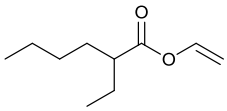

Figure 3.17: Vinyl-2-ethylhexanoate

Run 1 (Table 3.8) is a kinetic experiment conducted in the same manner as was described for the previous copolymerisations (*vide supra*) and details the progression of the reaction. EH-*i*-DIB (M_n = 3900 g/mol, $Đ$ = 2.1) was heated with 200 equivalents of V2EH (Run 1, Table 3.8) in toluene at 125°C using benzoyl peroxide as the initiator. The result was a polymeric mixture that was found to be separable by precipitation in acetone.

Table 3.8: Free radical polymerizations of V2EH in presence of EH-*i*-DIB

Run [a]	Time (min)	Initiator	V2EH: EH-*i*-DIB [b]	M_p [b]	M_w [b]	M_n [b]	Đ [b]	Yield	EH-i-DIB Conversion (%) [c]	DP of n-BA/EH-i-DIB [c]
1	2	BP	200	10000	12000	4300	2.9	0.22	92	2:1
	4	BP	200	11000	12000	4500	2.6	0.23	100	2:1
	8	BP	200	14000	16000	6000	2.7	0.31	100	18:1
	16	BP	200	19000	23000	9200	2.5	0.47	100	31:1
	32	BP	200	23000	27000	11000	2.5	0.56	100	41:1
	64	BP	200	25000	30000	12000	2.5	0.62	100	48:1
	128	BP	200	27000	31000	12000	2.6	0.61	100	47:1

[a] Polymerization conditions: EH-*i*-DIB = 0.20 g; M_n = 3900 g/mol, Đ = 2.2; [EH-*i*-DIB] = 5.13x10^{-5} mol/L (0.2 g); V2EH added = 200 equivalents, 1.75 g (2.0 mL); [Initiator] = 5.13x10^{-4} mol/L; solvent = toluene; reaction volume = 8.2 mL; temperature = 125°C.

[b] GPC data obtained at 160°C in 1,2,4-trichlorobenzene using universal calibration from PS standards

[c] Calculated from ^{1}H NMR.

The ^{1}H NMR spectrum of the precipitated product showed complete conversion of the of the EH-*i*-DIB macromonomer and the presence of signals corresponding to both EH and P(V2EH). GPC analysis indicated copolymer molecular weight of M_n = 12000 g/mol ($Đ$ = 2.6), at the end reaction time. The acetone soluble fraction was shown by ^{1}H NMR spectra to be P(V2EH) and, as before, no EH-containing material was detected in the soluble fraction. It was shown by ^{1}H NMR spectra that macromonomer conversion was complete after t = 4 min.

3.7.2 Myristyl Methacrylate

Another monomer of commercial significance, but which is also uncommon in academic literature, is myristyl methacrylate (C_{14}MA). C_{14}MA features in the field of wax crystal modification in both fuels and crude oil.[37] Its long pendant alkyl chain is expected to have good effect at inhibiting crystal agglomeration.

EH-*i*-DIB (M_n = 3900 g/mol, $Đ$ = 2.1) was reacted with 200 equivalents of C_{14}MA in the presence of BP initiator at 125°C (Run 1, Table 3.9). Separation of the resultant polymeric mixture was attempted by repeated precipitation in acetone from toluene. Complete macromonomer conversion was confirmed by the ^{1}H NMR spectrum with peaks assignable to EH and P(C_{14}MA). The ^{1}H NMR spectrum also showed the presence of this homopolymer with vinylidene end group signals (5.47 and 6.21 ppm) which occur as a result of chain transfer following H$^{\bullet}$ abstraction from the P(C_{14}MA) a-methyl group to solvent.[16] The GPC elution traces were shown to be broad which is consistent with the high dispersities reported. This suggests that significant amounts of homopolymer remain present in the product even following

multiple reprecipitations. The ^{1}H NMR spectra of the soluble fraction was found to contain both P(C_{14}MA) and C_{14}MA monomer.

Table 3.9: Free radical polymerization of C_{14}MA in presence of EH-*i*-DIB

Run [a]	Time (min)	Initiator	C14MA: EH-*i*-DIB [b]	M_p [c]	M_w [c]	M_n [c]	Đ [c]	Yield	EH-i-DIB Conversion (%) [d]	DP of C14MA /EH-i-DIB [d]
1	2	BP	200	4100	11000	4000	2.9	0.19	37	1:1
	4	BP	200	12000	30000	11000	2.7	0.58	72	25:1
	8	BP	200	21000	52000	20000	2.6	1.03	100	57:1
	16	BP	200	30000	72000	29000	2.5	1.49	100	89:1
	32	BP	200	32000	77000	31000	2.5	1.60	100	96:1
	64	BP	200	33000	80000	32000	2.5	1.62	100	99:1
	128	BP	200	35000	88000	34000	2.6	1.74	100	106:1

[a] Polymerization conditions: EH-*i*-DIB = 0.20 g; M_n = 3900 g/mol, Đ = 2.2; [EH-*i*-DIB] = 5.13x10^{-5} mol/L (0.2 g); C_{14}MAadded = 200 equivalents, 2.89 g (3.3 mL); [Initiator] = 5.13x10^{-4} mol/L; solvent = toluene; reaction volume = 8.2 mL; temperature = 125°C.

[b] GPC data obtained at 160°C in 1,2,4-trichlorobenzene using universal calibration from PS standards

[c] Calculated from ^{1}H NMR.

3.8 Conclusions

From the data presented in this chapter it is clear to see that the product of the free radical copolymerisation of EH-*i*-DIB and *n*-BA and other polar monomers presented here, is principally a block copolymer. The AMS type end group on the end of EH-*i*-DIB is used in the mechanism as an end capping agent which terminates to the growing radical polymer chain. The increase in polymer dispersity at high monomer concentrations, following complete macromonomer conversion, arose from co-precipitation of a small quantity of higher molecular weight homopolymer.

Macromonomers based on e.g. PS, PEO, PMMA have experienced extensive use in free radical copolymerisations[38] and as such it is striking that no such mechanism has been reported previously. In spite of this, there have been important related observations that have been made by others. When styrene was copolymerised with isopropenylbenzyl-terminated PEO macromonomer higher molecular weights were achieved than in the comparable homopolymerizations.[39] We suggest then that such observations are consistent with the presence of a persistent radical species such as the proposed species **III**. The detailed NMR studies conducted were consistent with the formation of a block copolymer structure.

The use of EH-i-DIB macromonomer in free radical copolymerisations is shown to be highly efficient and the simplicity of the purification steps make this system practical; especially since the synthesis of the macromonomer is so easily achieved. Given the context of the materials produced, the two step synthesis of these amphiphilic copolymers may indicate a significant advancement in the development of block copolymers.

The robustness of the EH-*i*-DIB macromonomer was tested in free-radical copolymerisation using a variety of different polar monomers. Copolymerisation of EH-i-DIB with *n*-BA, VAc, V2EH and C_{14}MA were conducted and the copolymers produced were isolated, purified and shown to give block copolymer architectures.

The overall simplicity of the production of these polymers and the wide range of compatible monomers, as well as the control available over the molecular weight of each block, make this a remarkably powerful and highly practical process which overcomes a lot of the drawbacks to the established routes to block copolymer development, as discussed in Chapter 1.

3.9 References

1. D. Kukulj, T. P. Davis and R. G. Gilbert, *Macromolecules*, 1998, 31, 994-999.
2. T. Y. J. Chiu, J. P. A. Heuts, T. P. Davis, M. H. Stenzel and C. Barner-Kowollik, *Macromol. Chem. Phys.*, 2004, 205, 752-761.
3. H. W. McCormick, *J. Polym. Sci.* , 1957, 25, 488-490.
4. D. Kukulj, J. P. A. Heuts and T. P. Davis, *Macromolecules*, 1998, 31, 6034-6041.
5. C. Barner-Kowollik and T. P. Davis, *Macromol. Theory Simul.*, 2001, 10, 255-261.
6. J. P. A. Heuts, D. A. Morrison and T. P. Davis, in *Controlled/Living Radical Polymerization*, American Chemical Society, 2000, vol. 768, ch. 22, pp. 313-331.
7. J. Chiefari, J. Jeffery, T. A. M. Roshan, G. Moad, E. Rizzardo and H. T. Sann, in *Controlled/Living Radical Polymerization*, American Chemical Society, 2000, vol. 768, ch. 21 pp. 297-312.
8. J. Chiefari, J. Jeffery, J. Krstina, C. L. Moad, G. Moad, A. Postma, E. Rizzardo and S. H. Thang, *Macromolecules*, 2005, 38, 9037-9054.
9. G. C. Sanders, R. Duchateau, C. Y. Lin, M. L. Coote and J. P. A. Heuts, *Macromolecules*, 2012, 45, 5923-5933.
10. C. Kay, PhD Thesis, University of Warwick, 2014.
11. G. Moad and D. H. Solomon, in *The Chemistry of Radical Polymerization (Second Edition)*, Elsevier Science Ltd, Oxford, 1995, DOI:
12. J. C. Salamone, *Polymeric materials encyclopedia*, CRC Press, 1996.
13. J. Chiefari, J. Jeffery, R. T. A. Mayadunne, G. Moad, E. Rizzardo and S. H. Thang, *Macromolecules*, 1999, 32, 7700-7702.
14. A. A. Gridnev and S. D. Ittel, *Chem. Rev.*, 2001, 101, 3611-3660.
15. T. J. Wang, M. J. Leamen, N. T. McManus and A. Penlidis, *J. Macromol. Sci., Pure Appl. Chem.*, 2004, 41, 1205-1220.
16. D. Kukulj and T. P. Davis, *Macromolecules*, 1998, 31, 5668-5680.
17. G. E. Roberts, J. P. A. Heuts and T. P. Davis, *Macromolecules*, 2000, 33, 7765-7768.
18. A. N. F. Peck and R. A. Hutchinson, *Macromolecules*, 2004, 37, 5944-5951.
19. J. Vandenbergh and T. Junkers, *Macromolecules*, 2012, 45, 6850-6856.
20. C. Barner-Kowollik and T. Junkers, *J. Polym. Sci., Part A: Polym. Chem.*, 2011, 49, 1293-1297.
21. G. Moad, E. Rizzardo, C. L. Moad, S. D. Ittel, L. Wilczek and A. A. Gridnev, Google Patents, 1997, WO1997031030A1.
22. C. J. Hawker, A. W. Bosman and E. Harth, *Chem. Rev.*, 2001, 101, 3661-3688.
23. H. Kaneyoshi, Y. Inoue and K. Matyjaszewski, *Macromolecules*, 2005, 38, 5425-5435.

24. A. M. Henderson, *IEEE Electrical Insulation Magazine*, 1993, 9, 30-38.
25. B. A. Wolf, B. Will, W. Obrecht, R. Casper, W. Baade, G. Sylvester, K. P. Meurer and H. Zimmermann, Google Patents, 1990, US4937303A.
26. G. G. Orphanides, Google Patents, 1986.
27. A. Arsac, C. Carrot and J. Guillet, *J. Appl. Polym. Sci.*, 1999, 74, 2625-2630.
28. C. Dommanget, F. D'Agosto and V. Monteil, *Angew. Chem., Int. Ed.*, 2014, 53, 6683-6686.
29. A. Kermagoret, A. Debuigne, C. Jérôme and C. Detrembleur, *Nat Chem*, 2014, 6, 179-187.
30. A. Debuigne, J.-R. Caille and R. Jérôme, *Macromolecules*, 2005, 38, 5452-5458.
31. D. Britton, F. Heatley and P. A. Lovell, *Macromolecules*, 1998, 31, 2828-2837.
32. H. Y. Erbil, *J. Appl. Polym. Sci.*, 1987, 33, 1397-1412.
33. A. J. Mclennan, P. M. Zeimentz and S. Laborda, Google Patents, 2011.
34. A. J. Mclennan and P. M. Zeimentz, Google Patents, 2010, CA2689190A1.
35. J. Lin and G. I. Brown, Google Patents, 2012.
36. B. W. Davies, R. J. Brod, J. Bock and T. Ibrahim, Google Patents, 1996.
37. R. A. Soldi, A. R. S. Oliveira, R. V. Barbosa and M. A. F. César-Oliveira, *Eur. Polym. J.*, 2007, 43, 3671-3678.
38. G. F. Meijs and E. Rizzardo, *J. Macromol. Sci., Polym. Rev.*, 1990, 30, 305-377.
39. P. Rempp, P. Lutz, P. Masson and P. Chaumont, *Makromol. Chem.*, 1985, 13, 47-66.

Chapter 4

Physical properties and applications of EH-b-PX copolymers.

4.1 Introduction

Waxes crystallise at lower temps from middle distillate fuels as large plate like structures (*ca* 100 μm) which aggregate into extended networks[1, 2] and may cause blockages in diesel engine filters and pumps potentially leading to failure of engine components.[3, 4]

Addition of copolymer additives to distillate fuel is the most common method for modification of wax crystals.[5] Types of additives commonly utilised include architectures such as random copolymers, like those composed of alkyl acrylates or methacrylates with α-olefins,[6-8] ethylene-vinyl ester, including ethylene-vinyl acetate (EVA),[4, 9] poly(vinyl ethers),[10] as well as more refined structures like comb[2, 11] and diblock copolymers.[12-14] These polymer additives may interact with wax via a number of different modes of action.[3] A nucleation mechanism usually involves polymer additives that contain crystalline regions which promote wax crystal growth, and amorphous regions which control or direct the growth. Typically the target is production of a large number of smaller crystals which do not inhibit fuel flow within the engine system. An adsorption mechanism, also known as growth arrest, occurs when an additive binds physically to the face of a growing wax crystal. This inhibits further growth in that facial direction and also prevents agglomeration of wax crystals.[4, 15-19]

This chapter will examine the physical properties of the new block copolymers, looking at both the thermal properties and their properties in solution. It will then move on to discuss the testing of the efficacy of these EH-polar block copolymers as fuel additives, as assessed by industry standard tests.

4.2 Variable temperature ^{1}H NMR

The ^{1}H NMR spectra shown in this thesis have all been obtained at 100°C. Here we utilise variable temperature ^{1}H NMR experiments to analyses EH-*b*-P(*n*-BA) samples (Run 3-128, Table 3.1).

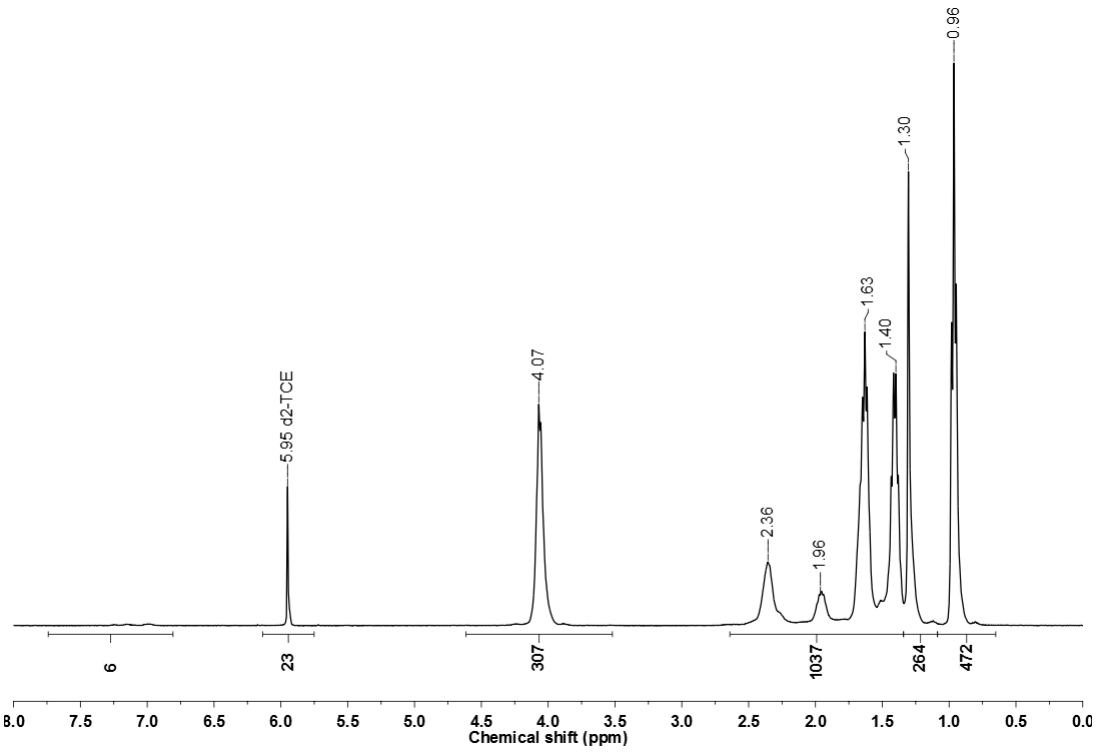

Figure 4.1 ^{1}H NMR of PE-b-P(n-BA) in d2-TCE at 100°C (400 MHz). Relaxation delay = 1 s.

Figure 4.1 and 4.2 are the 1H NMR spectra of EH-*b*-P(*n*-BA) recorded at 100°C and 25°C. While the polymer appeared to be soluble on visual inspection, it becomes clear that the chemical shifts and relative integrals of the two spectra differ

significantly. The solvent used was *d2*-TCE, with this resonance occurring at 5.95 ppm, and its integral is used as a reference. The integrals of the resonances of the P(n-BA) ester CH_2 (4.1 ppm) and the EH backbone CH_2 (1.30 ppm) occur in a ratio 1.15:1 in the spectrum recorded at 100°C, however this ratio changes to 1.5:1 in the spectrum recorded at 25°C.

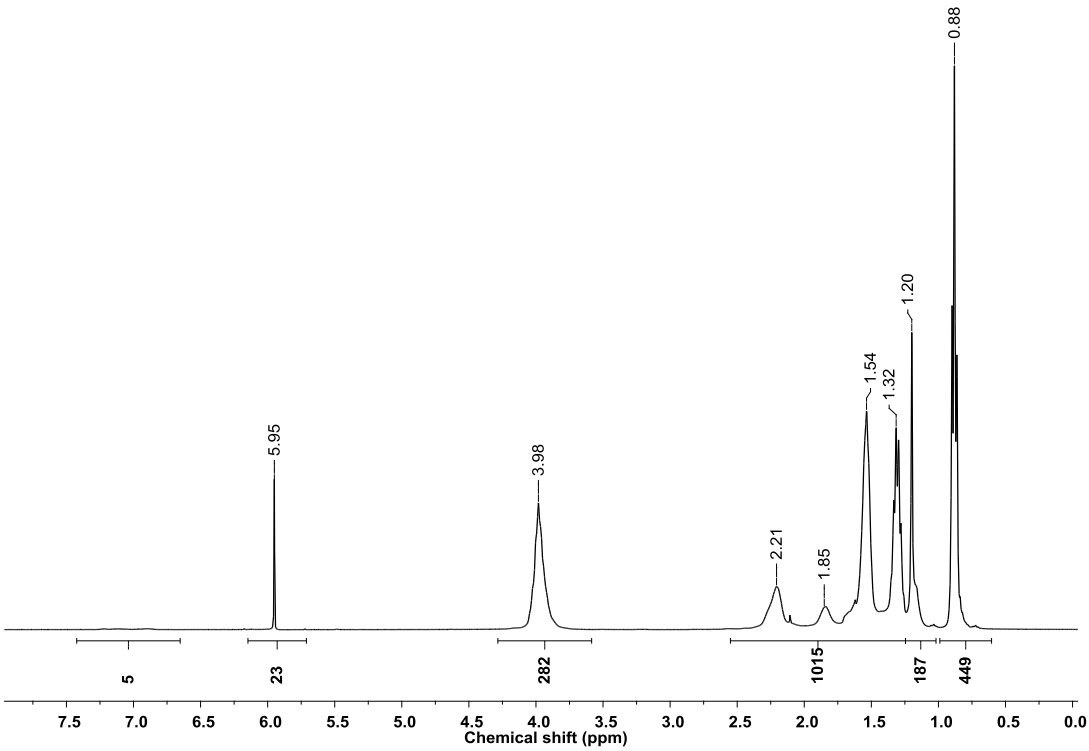

Figure 4.2 ^{1}H NMR of PE-b-P(n-BA) in d2-TCE at 25°C (400 MHz). Relaxation delay = 1 s.

With a decrease in temperature it is expected that the integrals of the resonances would be reduced,[20] however it is seen that the intensity of the EH signals is affected more greatly than the intensity of the P(*n*-BA) signals. These observations are consistent with the copolymers forming aggregates in solution. This is a phenomenon commonly observed when block copolymers are dissolved in selective solvents.[21] In such aggregates the insoluble EH block experiences reduced molecular motion as it is protected by the polar external component of the aggregates.

4.3 Block copolymer DLS analysis

As discussed above, ^{1}H NMR spectroscopy showed that at low temperatures the polyolefin copolymers appear to aggregate in solution. In order to further investigate the tendency for copolymer self-assembly in solution a selection of the samples recovered were analysed by dynamic light scattering (DLS). Each copolymer type was analysed and samples were selected based upon the complete conversion of the DIB end groups and the solubility of the copolymer. Three measurements were recorded for each sample following mild heating and vortex mixing. Sample preparation and analysis was repeated to ensure consistency. The samples readily dissolved in toluene at room temperature and correspondingly gave high dispersities, poor correlation plots[22] and high variation between measurements of the same sample. However when materials were dispersed in THF at 1 mg/ml a milky solution was formed which yielded much more consistent data.

The DLS plots of a number of well dispersed EH block copolymers are shown in Figure 4.3. The intensity signals recorded show monomodal nature and generally have narrow polydispersity index (PDI). Correlograms of the obtained DLS plots are detailed in Appendix B. Noting the assumptions that are made in regards to the shape, homogeneity, refractive index and precision of conversion of the intensity data to volume/mass distributions[22, 23] an effective spherical aggregate diameter is measured.

An estimation of copolymer chain length can be calculated via Equation 4.1 as proposed by Tanford.[24] This will give the maximum length (*l*max) for a chain with n_c' embedded carbon atoms, in angstroms. This value is calculated from the distance between alternate carbon atoms of a fully extended chain (2.53 Å), and addition of the

terminal methyl group van der Waals's radius (2.1 Å) as well as half the bond length to the first atom not positioned within the hydrophobic core (~0.6 Å).

$$l_{max} = 1.5 + 1.265n_c' \quad (4.1)$$

For example, EH-b-PBA (run 1-128, Table 3.1) had a molecular weight of 6000 g/mol, and comprises a PE core ($D_{PE} \approx 134$) and a soluble block of *ca* 16 units of *n*-BA. Performing this calculation and converting to nm, we calculate an expected chain length of *ca* 48 nm. This dimension is based upon a linear copolymer and does not account for the branched nature of the EH polymer core, as such this value is not unreasonable for an aggregate composed of such copolymers,[23, 24] and is consistent with those detected by DLS.

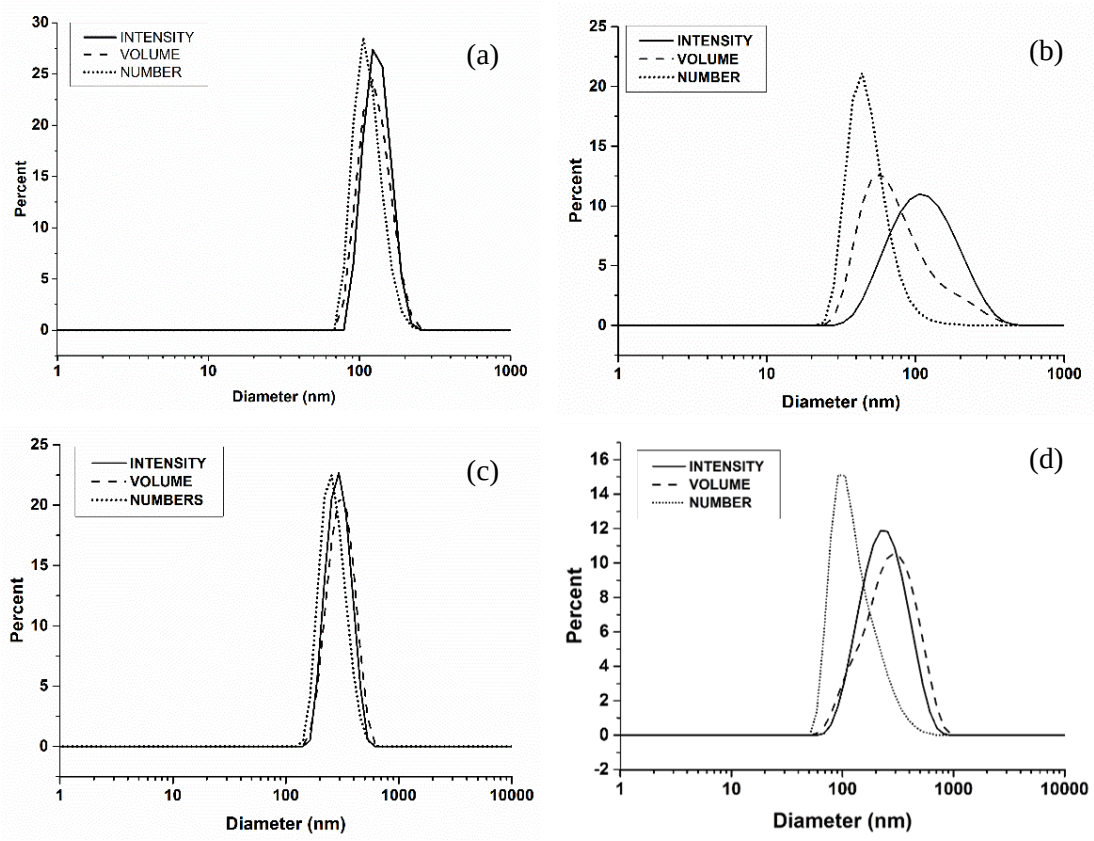

Figure 4.3: DLS intensity/volume/number size distributions of (a) EH-b-P(n-BA), (b) EH-b-P(VAc), (c) EH-b-P(V2EH) and (d) EH-b-P(C14MA) in THF (1mg/mL) (averages of three measurements).

The results for measured particle size and calculated chain length are summarised in Table 4.1. All samples had narrow polydispersity and regular correlograms. It is observed then that the experimentsl size measurements give gernerally good agreement with the calculated particle sizes. While the conclusions that can be made in terms of aggregate architecture are limited, it is possible to surmise that nanoscopic structures are formed in the selective solvent utilised. This information gives support to the observations made with regard to variable temperature NMR experiments.

Table 4.1: Summary of DLS values for analysed block copolymers

Sample	Observed size, number-average (nm)	PDI	Count rate (kcps)	Calculated chain length (nm)
EH-b-P(*n*-BA)	105	0.21	206	48
EH-b-P(VAc)	45	0.23	382	53
EH-b-P(V2EH)	255	0.03	409	58
EH-b-P(C_{14}MA)	90	0.26	257	77

4.4 Block copolymer TEM analysis

In order to support the data obtained from DLS (*vide supra*), the same solutions of the same samples detailed above (Table 3.1) were subsequently analysed by transmission electron microscopy (TEM). For the majority of the samples analysed the solubility of the polymers was insufficient for TEM analysis.

However the EH-*b*-P(BA) copolymer, sample 1-128 (Mn = 6000 g/mol) was able to be analysed and found to form spherical particles of *ca* 100-150 nm in width (Figure 4.4), and it is to be anticipated that these particles are composed of a polyolefin core and a polar, P(BA) shell in THF. While the contrast in some of the images

presented appears to be low and despite the low number of structures visible, it is nonetheless self-evident that when the copolymers are dispersed in this selective solvent that nanoscopic structures are formed. Additionally the aggregate structures that form remain intact following evaporation of dispersing solvent upon the TEM grid, however it is expected that they may have flattened and spread to some extent leading to an exaggeration of the particle size. Relating the TEM images to DLS data it is apparent that the structure sizes are consistent between the two techniques.

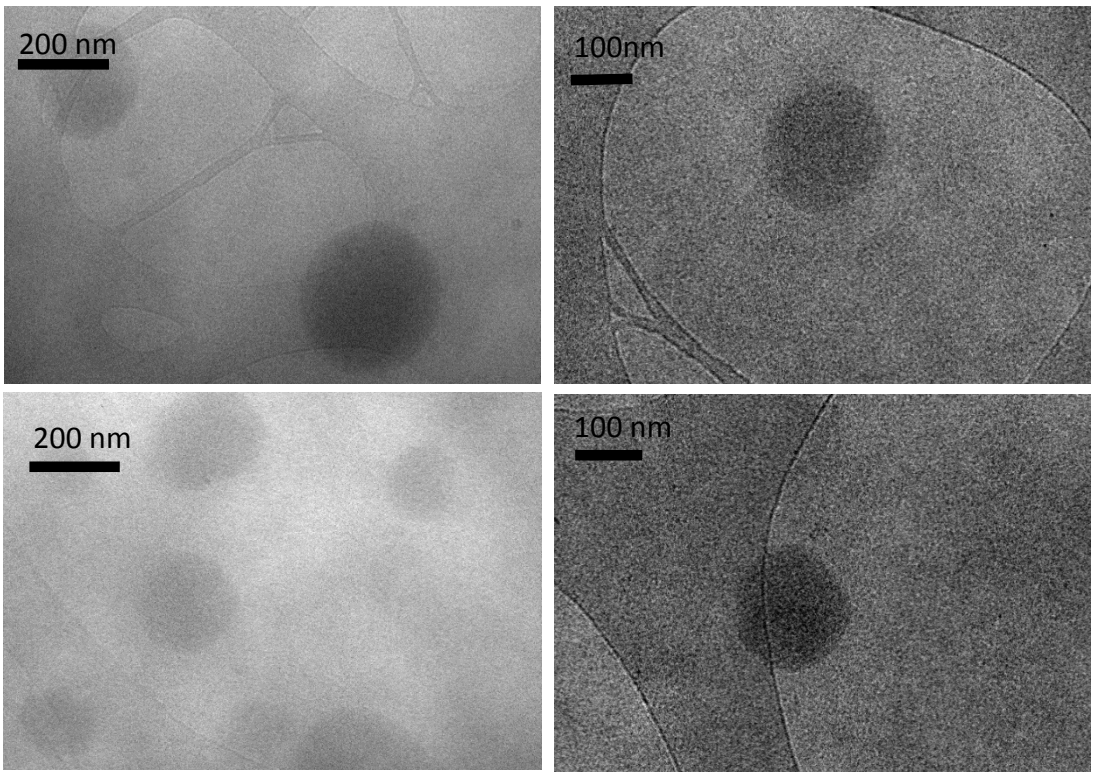

Figure 4.4: TEM image of particles formed from sample 1-128, Table 3.1 in THF (1 mg/mL)

4.5 Block copolymer DSC analysis

The isolated block copolymers are comprised of a semi-crystalline polyolefin segment and also an amorphous polar segment. To investigate the structure and phase separation behaviour of the block copolymers, thermal analysis was conducted by DSC.[25]

4.5.1 EH-*b*-P(*n*-BA)

Figure 4.5 compares the third heating curves* (a)-(d), of EH-i-DIB (run 2, Table 2.1, M_n=3900 g/mol) and copolymers with increasing polar block length (runs 1-128, 2-128 and 3-128 from Table 3.1 respectively).

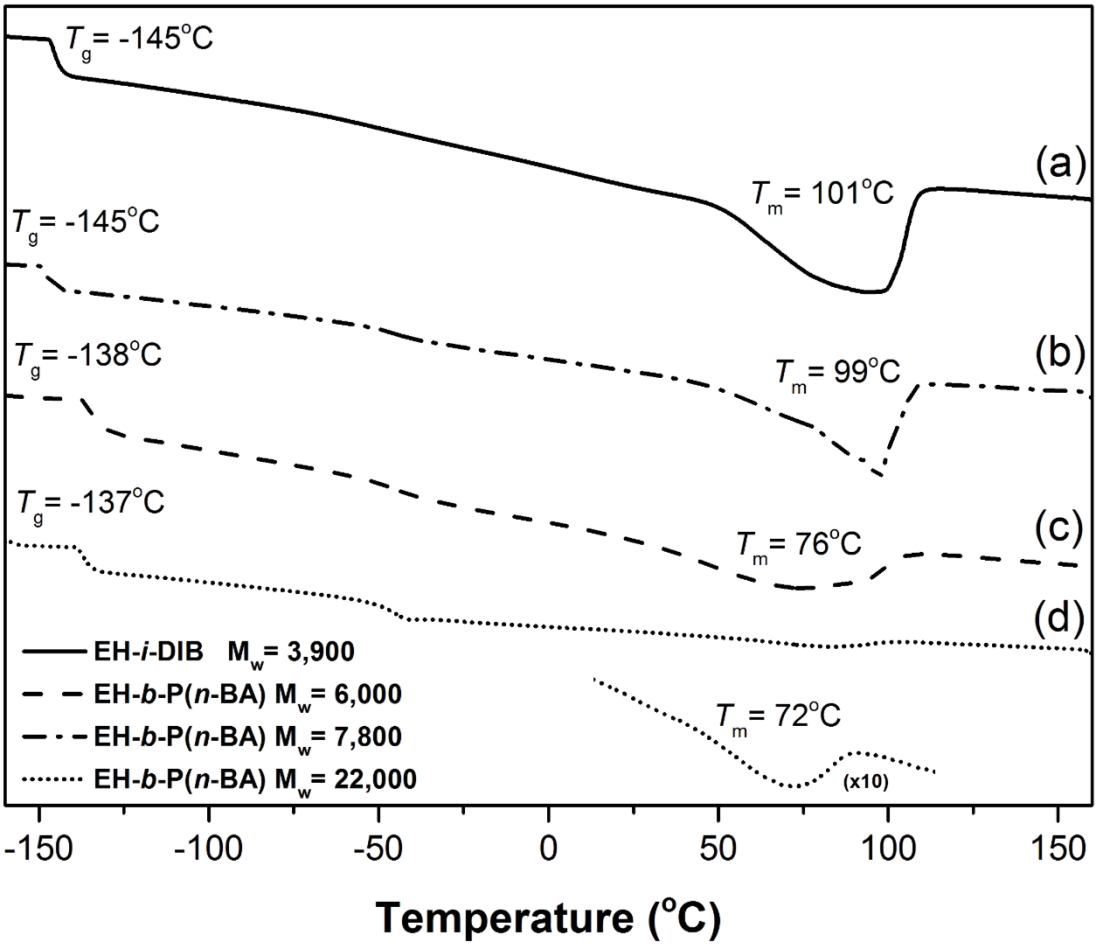

Figure 4.5: Third heating curves (10°C/min) from DSC traces of EH-i-DIB (run 2, Table 2.1), EH-*b*-P(BA) (run 1-128), EH-*b*-P(BA) (run 2-128), EH-*b*-P(BA) (run 3-128) (Table 3.1)

As detailed in Chapter 2, the EH-*i*-DIB macromonomer has a glass transition temperature (T_g) of -145°C and a broad melting temperature (T_m) peaking at 101°C**.** The EH-*i*-DIB trace shows a broad pre-melt starting at approximately 50°C which is

* The third and second heating curves were indistinguishable from each other.

caused by broad crystallite size distributions.[26] The glass transition temperatures (T_g) of the polyolefin segment of the block copolymers was largely unaffected by variations in molecular weight, and remained similar to the starting material, indicating that phase separation occurs between the polyolefin and the amorphous polar block. Given that it is also possible to observe a glass transition temperature around -50°C which corresponds to the glass transition temperature of the amorphous poly(butyl acrylate) in the copolymer, is further evidence of the phase separation behaviour of the block copolymers.

The melting temperatures of the block copolymers decreased slightly from 101°C in the EH-*i*-DIB down to 99°C upon the addition of a P(*n*-BA) block of *ca* 16 units in length (b). The T_m continued to decrease to 76°C and then 72°C as the (n-BA) block length was increased (c),(d).

It is possible to use DSC to measure the %-crystallinity of a polyolefin sample by comparing the theoretical enthalpy of melting of a 100% crystalline polyethylene (294 J/g)[26-29] with the enthalpy of melting of the sample. The enthalpies of fusion of totally crystalline PE and the test sample are denoted by ΔH_f^o (T_m^0) and $\Delta H_f(T_m)$ (Equation 4.2) and are measured in J/g. It is noted that the T_m values recorded, arise principally as a property of the polyolefin segment of the copolymers, and it is important to consider the fact that each of these copolymers contain different amounts of EH-*i*-DIB by mass,[30] this must be taken this into consideration in order to make a meaningful comparisons between the samples. The relative crystallinities of the EH blocks in each of the copolymers was estimated as follows: Initially the relative crystallinity of a sample is attained from the DSC measurement using the Equation 4.2. This value is then divided by the mass fraction of EH-*i*-DIB in the copolymer to

give the following crystallinity values. (a) EH-*i*-DIB, 46%; (b) run 1-128 *ca* 40%, (c) run 2-128 *ca* 32%; and (d) run 3-128 *ca* 17.5%.

$$\frac{\Delta H_f(T_m)}{\Delta H_f^0(T_m^0)} \times 100 \quad (4.2)$$

While acknowledging assumptions made within the calculations, it is clear that the crystallinity of the EH component is reduced substantially, from 46% in EH-*i*-DIB to *ca* 40% in the copolymer by addition of a P(*n*-BA) chain of M_n = 2100 g/mol, and that further extension to M_n = 18000 g/mol leads to a greater reduction in crystallinity to 17.5%.[31]

The observed drop in crystallinity from 46% to *ca* 17.5% is consistent with the loss of the relatively low-melting EH region, however following this the crystallinity is retained because of the phase-separation of the EH and amorphous P(*n*-BA) blocks.

The third DSC cooling curves of the EH-i-DIB and poly *n*-butyl acrylate copolymers are shown below in Figure 4.6. The crystallisation temperature (T_c) was shown to decrease with increasing P(BA) block length. The decreases in T_c were significantly larger than the decreases observed in the T_m in the heating curves, this disparity between the temperature decreases is referred to as undercooling.[32] The undercooling increases from 11°C in the EH starting material to 10, 21 and then 31°C in the block copolymers with increasing block length. It is therefore likely that the polyolefin block nucleation is inhibited by the presence of the amorphous P(BA) block and that this inhibition only increases with the block length of the polar segment.[32, 33]

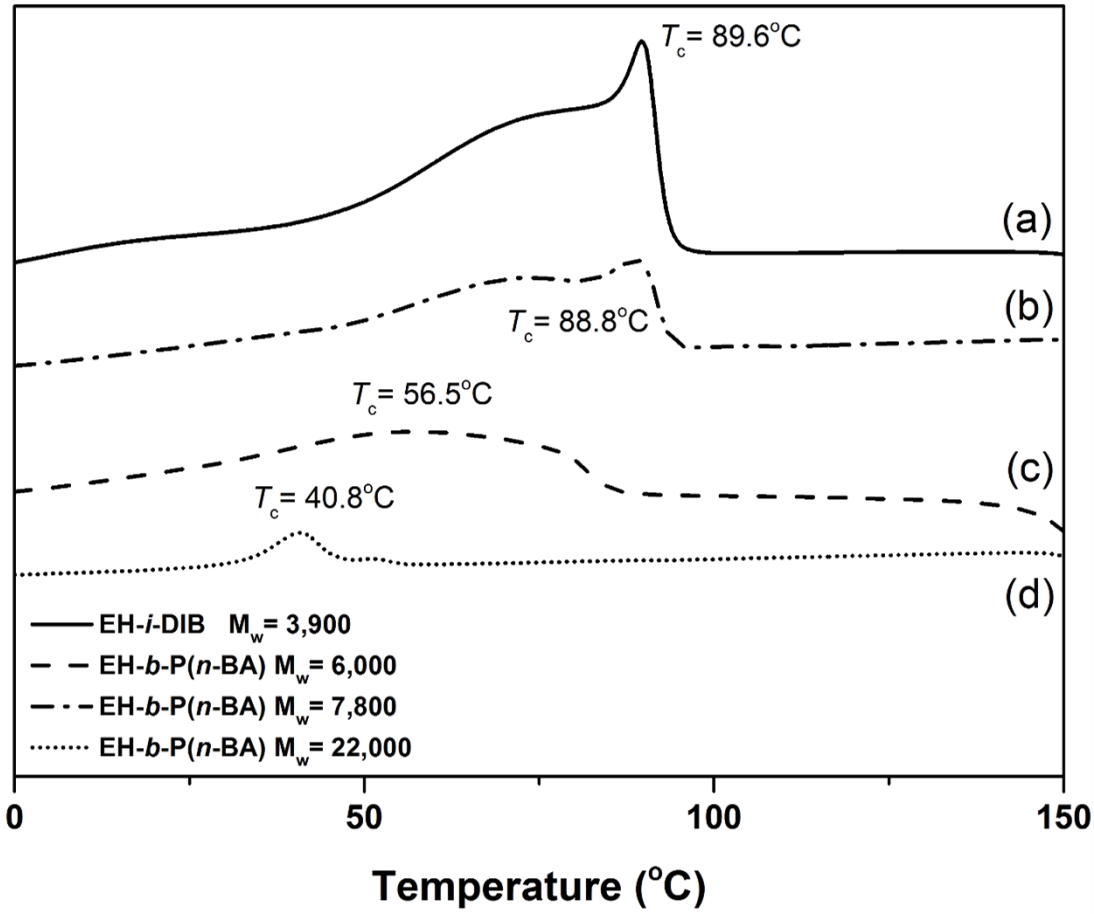

Figure 4.6: Third cooling curves (10°C/min) from DSC traces of EH-i-DIB (run 2, Table 2.1), EH-b-P(BA) (run 1-128), EH-b-P(BA) (run 2-128), EH-b-P(BA) (run 3-128) (Table 3.1)

4.5.2 EH-*b*-P(VAc)

Figure 4.7 examines the third heating curves of copolymers of EH and polyvinyl acetate with increasing molecular weight (runs 1-128, 2-128 and 3 from Table 3.4). The EH-i-DIB macromonomer is again shown for reference.

It is observed that the broad nature of the melting peaks makes assignment of T_m difficult, however there is an apparent trend of increase of T_m following addition of short P(VAc) blocks, which then falls again as block lengths increase. The glass transition temperature (T_g) is also largely unaffected - an indication of phase separation

The crystallinities of the EH blocks in each of the copolymers were estimated (as above) to be EH-*i*-DIB, 46%; then 43%, 32%, 29.5% for runs 2-128, 3-128 and 1 respectively (Table 3.4).

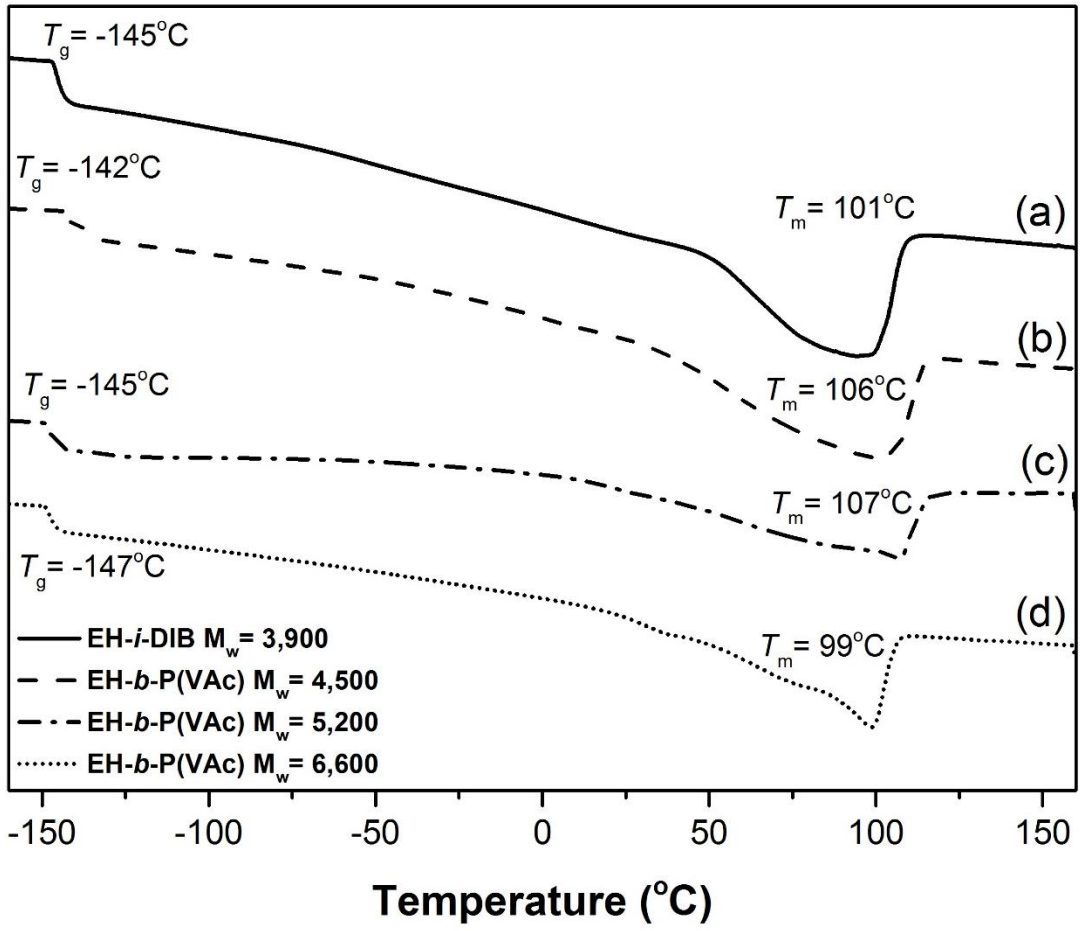

Figure 4.7: Third heating curves (10°C/min) from DSC traces of EH-i-DIB (run 2, Table 2.1), EH-*b*-P(VAc) (run 1-128), EH-*b*-P(VAc) (run 2-128), EH-*b*-P(VAc) (run 3) (Table 3.4)

The cooling curves of the EH-*b*-P(VAc) copolymers showed much the same trend for crystallization temperature of the block copolymer as with melting. The crystallisation temp of (b) increased from that of the EH-*i*-DIB macromonomer. Upon extension of the P(VAc) chain in traces (c) and (d), we note that the crystallisation temperature began to decrease.

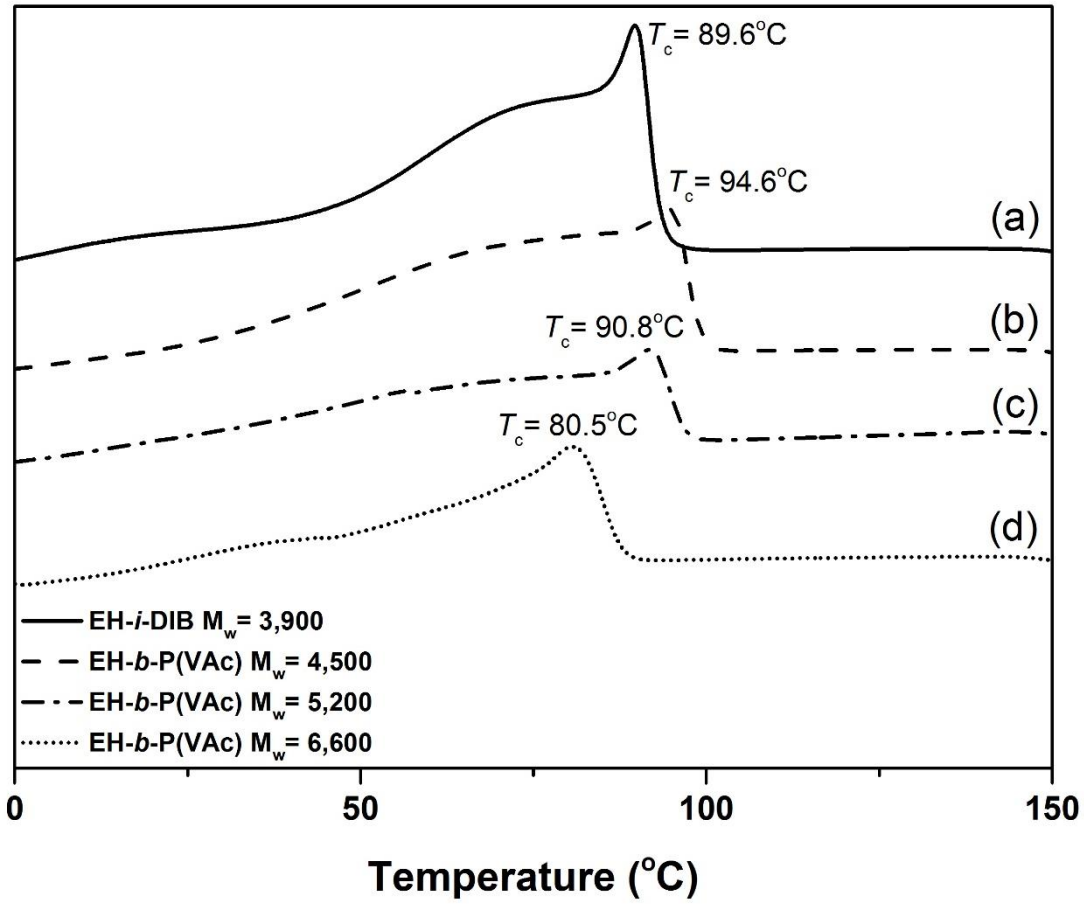

Figure 4.8: Third cooling curves (10°C/min) from DSC traces of EH-i-DIB (run 2, Table 2.1), EH-*b*-P(VAc) (run 1-128), EH-*b*-P(VAc) (run 2-128), EH-*b*-P(VAc) (run 3) (Table 3.4)

Measurement of the undercooling of the samples was difficult to determine as it requires subtraction of two values with large error. Nevertheless the undercooling for the EH-i-DIB starting material was calculated to be 11°C followed by 11.5°C, 16°C and then 18.5°C for (b)-(d) respectively.

4.5.3 Other EH-*b*-P(X) copolymers

All other block copolymer architectures described in this work displayed similar thermal properties to the two examples already shown. Whereby an increasing polar block length led to decreases in crystallising and melting temperatures and an increase

in the undercooling of the block copolymers. The glass transition temperature of the copolymers was also largely unaffected. Examples of the melt behaviour of the other copolymers is shown in Figure 4.9. The most striking of which is the EH-*b*-P(C_{14}MA) copolymer which has a large melt peak at -3.5°C and a small peak from the polyolefin melt at *ca* 99°C.

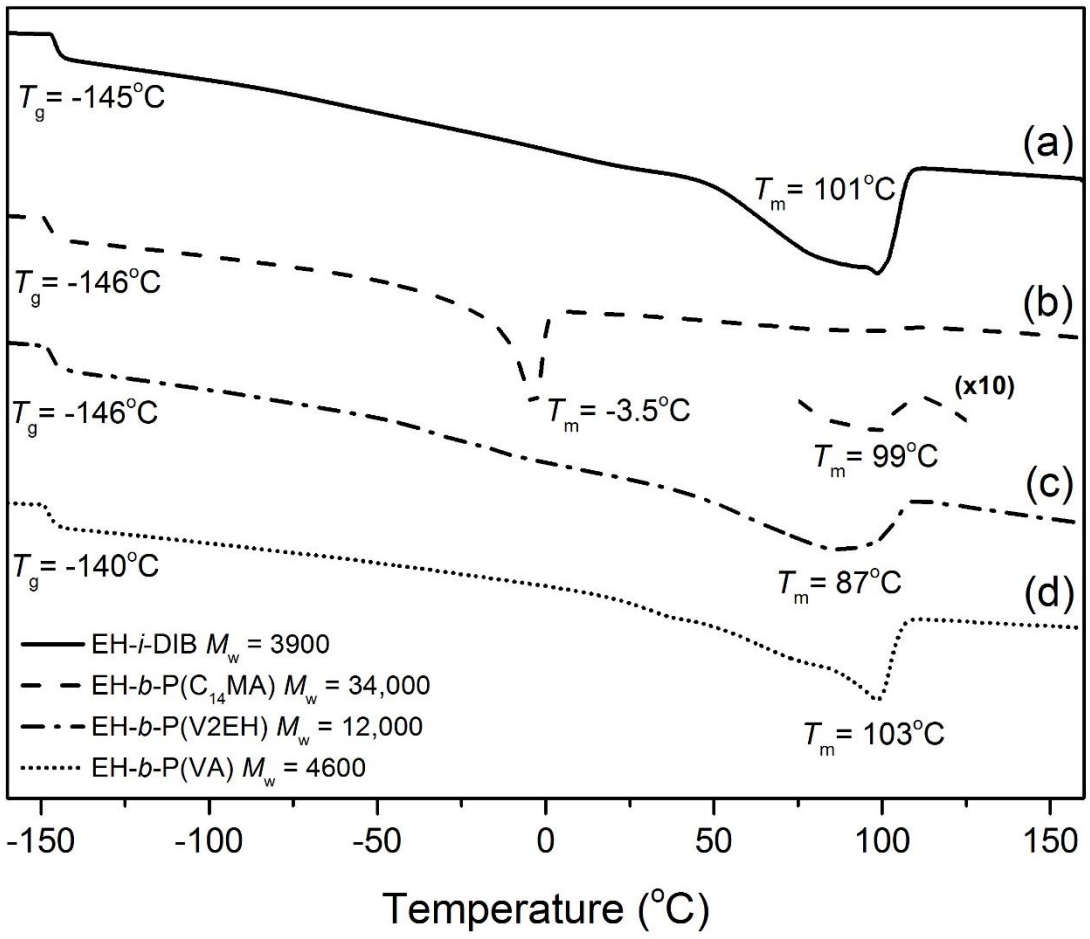

Figure 4.9: Third heating curves (10°C/min) from DSC traces of EH-i-DIB (run 2, Table 2.1), EH-*b*-P(C_{14}MA) (run 1-128, Table 3.9), EH-*b*-P(V2EH) (run 1-128, Table 3.8) and EH-*b*-P(VA) (run 1, Table 3.6)

Examining the thermal data for each of the copolymers shown (run 1-128, Table 3.9; run 1-128, Table 3.8; and run 1, Table 3.6), crystallinity values of the EH blocks for each were obtained. Within the EH-*b*-P(C_{14}MA) copolymer the EH

crystallinity was found to be 17.9%, while within the EH-*b*-P(V2EH) copolymer it was 10.1% and finally 30.8% within the EH-*b*-P(VA) copolymer.

4.6 Properties in Fuel

As discussed in the introduction the principle development goal of these materials was for their use as wax crystal modifiers in diesel fuel.

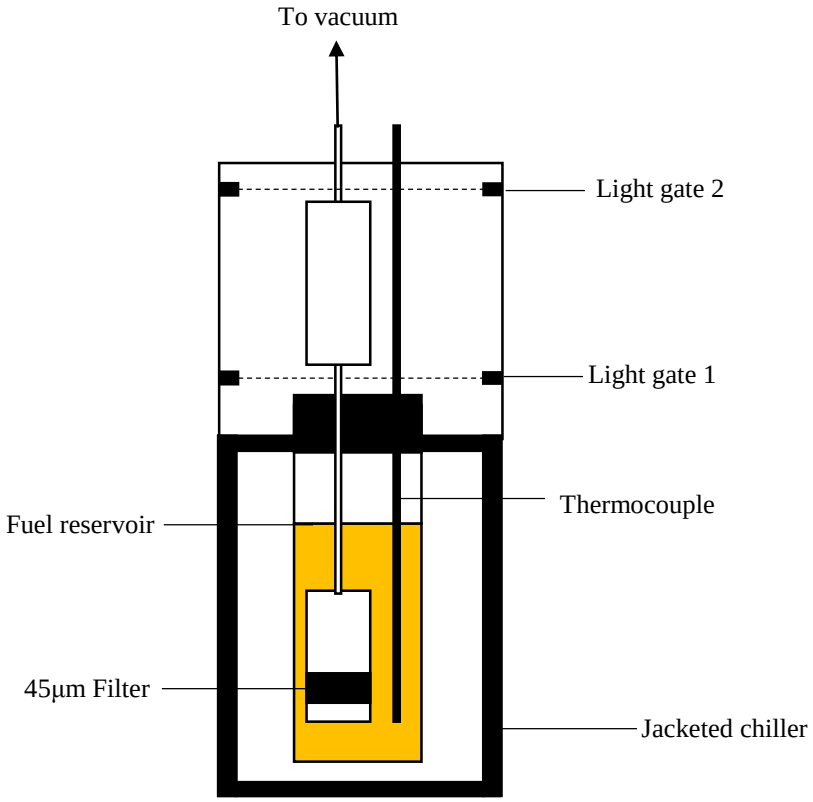

Figure 4.10: Schematic diagram of a CFPP unit

The principle industrial test used for this is the Cold Filter Plugging Point (CFPP), whereby a reservoir of fuel, treated or otherwise, is cooled and then drawn through a 45 µm filter under vacuum. By utilising light gates as detection, a set volume of fuel is drawn through the filter and the time measured, if the time taken for this volume to be drawn through the filter exceeds 60 s then the fuel is said to have fallen below the

point of operability and has failed the test. This gives the CFPP value for that fuel blend.

The doping of the fuel is achieved by first making a 10 wt% solution of polymer in Solvesso® 150; a hydrocarbon based solvent mixture with a high aromatic content and a boiling range of 175-205°C. An appropriate amount of fuel is filtered and doped with 250 ppm of the additive package. Additive packages can be pure polymer solution or mixtures with other commercial products in specific ratios. Samples were tested in duplicate, and as long as the values were within error (±2°C) no further repeats were conducted.

Table 4.2 shows the CFPP values for fuel samples which have been treated with various polymers. To lend these values some context, untreated fuel when tested in this manner, gives a CFPP value of -7°C, while addition of 250 ppm of commercial growth arrestor (GA) and nucleator (Nu) polymers led to CFPP values of -9°C and -14°C respectively.

From the results tabulated (Table 4.2) we can see that while addition of 250 ppm of EH-*b*-P(*n*-BA) alone reduced CFPP to -13°C, combination of this material at 50 ppm with 200 ppm of the above commercial growth arrestor (GA) led to CFPP of -23.5°C. In contrast, combination of EH-*b*-P(*n*-BA) with the commercial nucleator (Nu) led to CFPP of -15°C. On this basis we would associate the behaviour of EH-*b*-P(*n*-BA) as a nucleator. Noting that the polymer additives are, in all cases, more effective when packaged with the commercial growth arrestors this nucleation behaviour is true of all polymer types tested. EH-b-C_{14}MA copolymers are unique in that the efficacy of the neat polymer dope is significantly greater than in other cases.

Table 4.2: CFPP values for EH-*b*-P(X) copolymers

Description	CFPP Value (°C)		
	Neat Polymer	**Polymer : GA (20:80)**	**Polymer : Nu (80:20)**
	250 ppm	**250 ppm**	**250 ppm**
EH-*b*-P(*n*-BA)	-13	-23.5	-15
EH-*b*-P(VAc)	-14	-24	-15
EH-*b*-P(VA)	Polymer not soluble in fuel		
EH-*b*- P(V2-EH)	-14	-24	-15
EH-*b*-P(C_{14}MA)	-21.5	-23	-19.5

A more direct method for visualising the effectiveness of the polymer additives is achieved through microscopy. Shown in Figure 4.11 is an image of the wax crystals produced in untreated fuel. The image shows large plate like wax crystals in the size order of 100's of μm, which interlock and form these larger networks as discussed in the introduction.

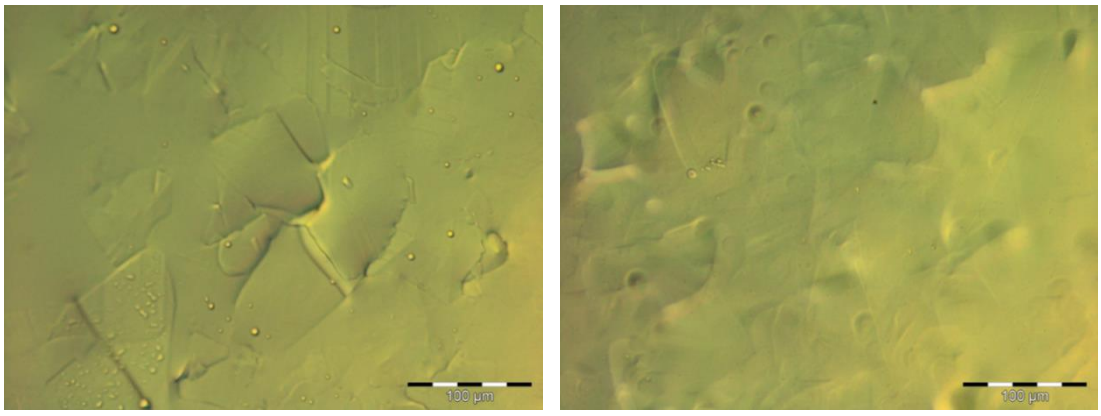

Figure 4.11: Optical microscopy image of wax crystals that precipitate from untreated diesel fuel.

Shown next in Figure 4.12 are the wax crystals that precipitate from fuels treated with neat copolymer EH-*b*-(C_{14}MA) and EH-*b*-(PBA) packages, as can be seen the crystal sizes have decreased dramatically with sizes now in the order of fewer than

10 μm. Additionally the precipitated crystals do not appear to be agglomerating to form networks as they have in untreated fuels. In particular image (b), which shows the EH-*b*-(C_{14}MA) doped fuel, shows an extremely small crystal size and excellent dispersion of these crystals, this supports the low CFPP value obtained for this polymer in Table 4.2.

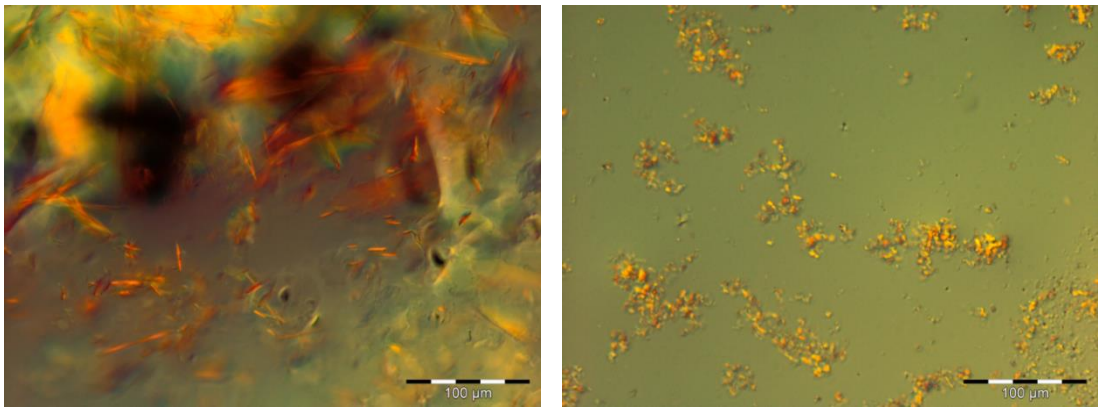

(a) (b)

Figure 4.12: Wax crystals precipitated from fuel doped with copolymer (a) EH-b-(PBA) (b) EH-b-(C_{14}MA)

Figure 4.13 shows microscopy image of fuels treated with the same polymer as above (Figure 4.12) however in this instance they are packaged with a commercial growth arresting agent. Once again we see an improvement in wax crystal size and dispersion which is consistent with the CFPP data obtained.

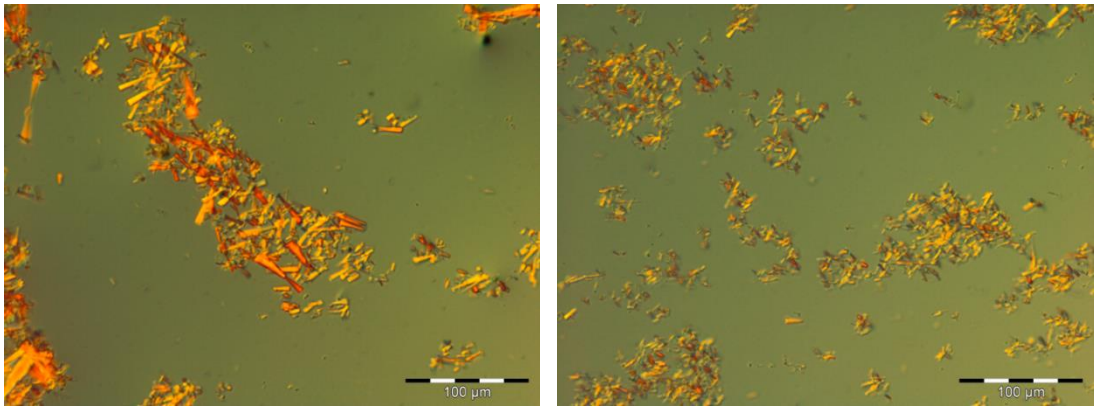

(a) (b)

Figure 4.13: Wax crystals precipitated from fuel doped with copolymer package with commercial GA and (a) EH-*b*-(PBA) (b) EH-*b*-(C_{14}MA)

4.7 Action of WCM additives examined by DSC

The effectiveness of the new polymers as wax modifiers was studied by DSC. Comparisons of the third cooling curves of untreated fuel as well as fuels doped with 250 ppm of the copolymer packages are detailed below.

The DSC crystallisation traces are used to examine numerous key properties of the fuel. The onset of crystallisation is known as the wax appearance temperature (WAT) and is the temperature at which wax crystals begin to precipitate from the fuel. The peak of the curve shows the point when the majority of the wax has precipitated. Finally for DSC thermograms that are normalised to sample weight (Wg^{-1}) the area under the curve is directly proportional to the mass of wax precipitated. All of these values are listed in Table 4.3.

In the thermograms presented below neat fuel is shown in each instance as a comparison. Neat fuel has the lowest crystallisation onset temperature at -10.8, the lowest peak height at -13.1 and the largest area. All of this indicates that neat fuel

precipitates the largest amount of wax of all samples tested and does so at lower temperatures.

Figure 4.14 shows the thermograms for fuels that have been treated with 250 ppm of block copolymer additive. In all instances less mass of wax is precipitated from the fuel and the WAT occurs at higher temperatures. This reinforces the idea that the polymer additives are acting as nucleating agents in the fuel. The polymers promote pre-nucleation of wax in fuel and provide a large number of nucleation sites leading to the formation of a larger number of smaller crystals.

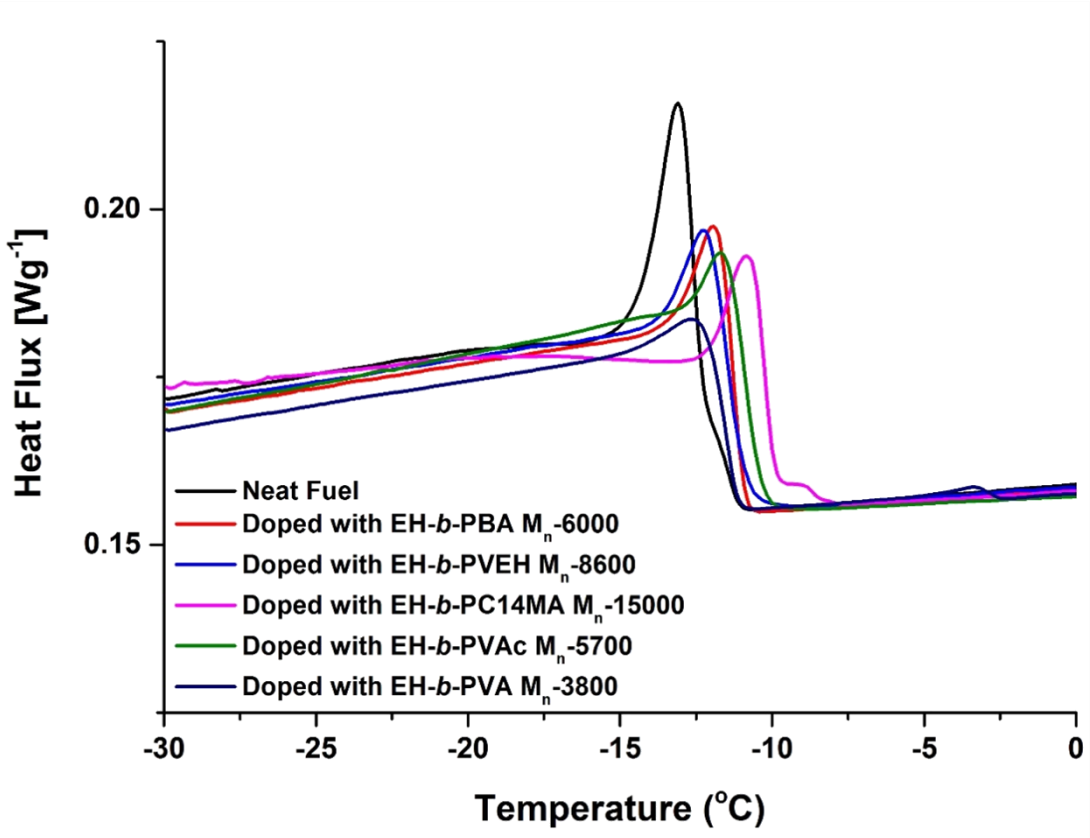

Figure 4.14: DSC traces of fuel samples treated with neat copolymer packages (250 ppm)

Table 4.3: Data values for DSC testing of doped fuels

Sample	Area			Onset			Peak Center		
	Neat Polymer	Polymer, Commercial Growth arrestor (20:80)	Polymer , Commercial nucleating agent (80:20)	Neat Polymer	Polymer, Commercial Growth arrestor (20:80)	Polymer , Commercial nucleating agent (80:20)	Neat Polymer	Polymer, Commercial Growth arrestor (80:20)	Polymer , Commercial nucleating agent (20:80)
Neat	0.51			-10.8			-13.1		
EH-*b*-P(BA)	0.49	0.47	0.48	-10.5	-10.7	-10.5	-11.9	-12.3	-9.2
EH-b-P(VAc)	0.47	0.56	0.46	-9.7	-9.8	-10.4	-11.7	-12.0	-12.5
EH-b-P(VA)	0.46	0.44	0.46	-10.8	-11.7	-10.0	-12.7	-13.1	-12.0
EH-*b*-P(VEH)	0.50	0.48	0.51	-8.8	-10.3	-10.3	-12.3	-12.3	-12.3
EH-*b*-P(C_{14}MA)	0.50	0.49	0.52	-7.8	-10.2	-10.5	-10.8	-12.0	-12.5

Copolymer additives which were packaged with a commercial growth arrestor (in a ratio 1:4) were shown to have given the best improvements in CFPP testing. Figure 4.15, shows the thermograms acquired for those samples. A WAT higher than untreated fuel is observed for all samples, however these values are not as greatly affected as with the pure copolymer packages. This is due to the presence of a lower concentration of the block copolymers present in the additive package. However, with the exception of EH-*b*-P(VAc), a decrease in the mass of wax to precipitate is seen for all copolymers

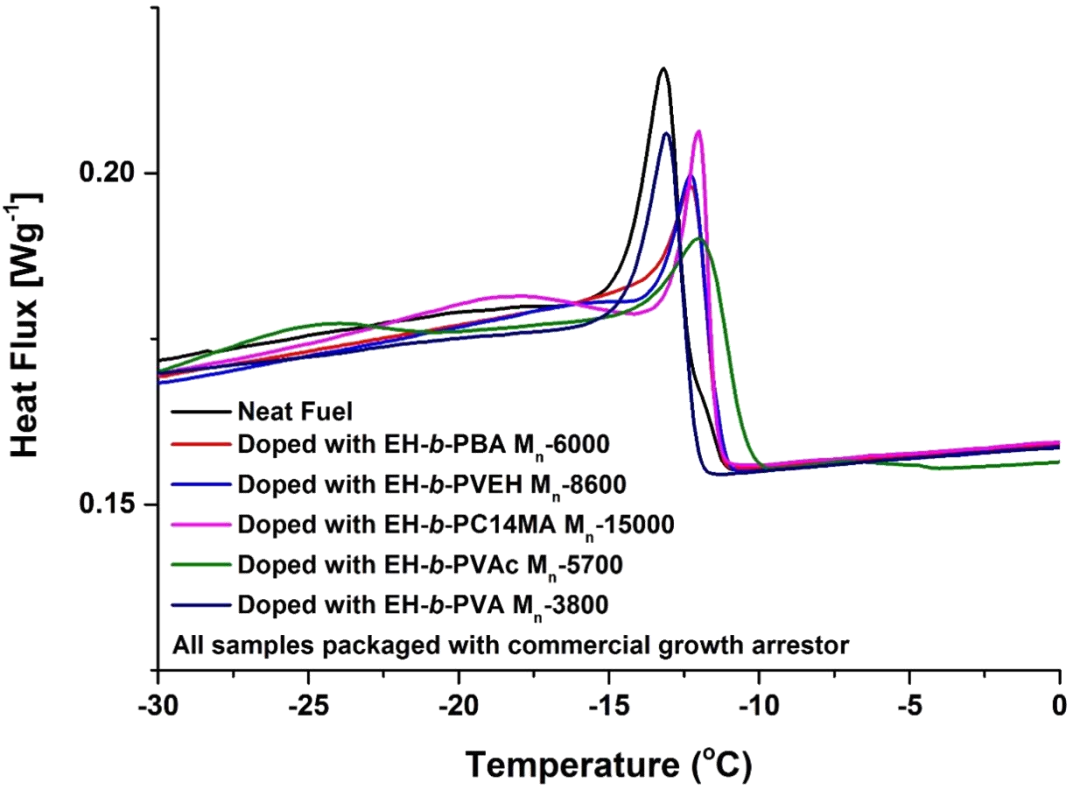

Figure 4.15: DSC traces of fuel samples treated with copolymers packaged with commercial growth arrestor (250 ppm)

Copolymers packaged with the commercial nucleating agent (4:1) were shown to present with only slight improvements to CFPP values. Examining the thermogram of these packages (Figure 4.16) we observe that the WAT of the treated fuels occurred at higher temperatures than untreated fuel, but again not as early as copolymer only packages. The total mass of wax precipitated from the fuel appears to be fairly consistent with the masses observed of samples doped with only copolymers. These observations are rather unsurprising as, in effect, the package represents a mixture of two different nucleating agents, with the majority of it being the block copolymer additive.

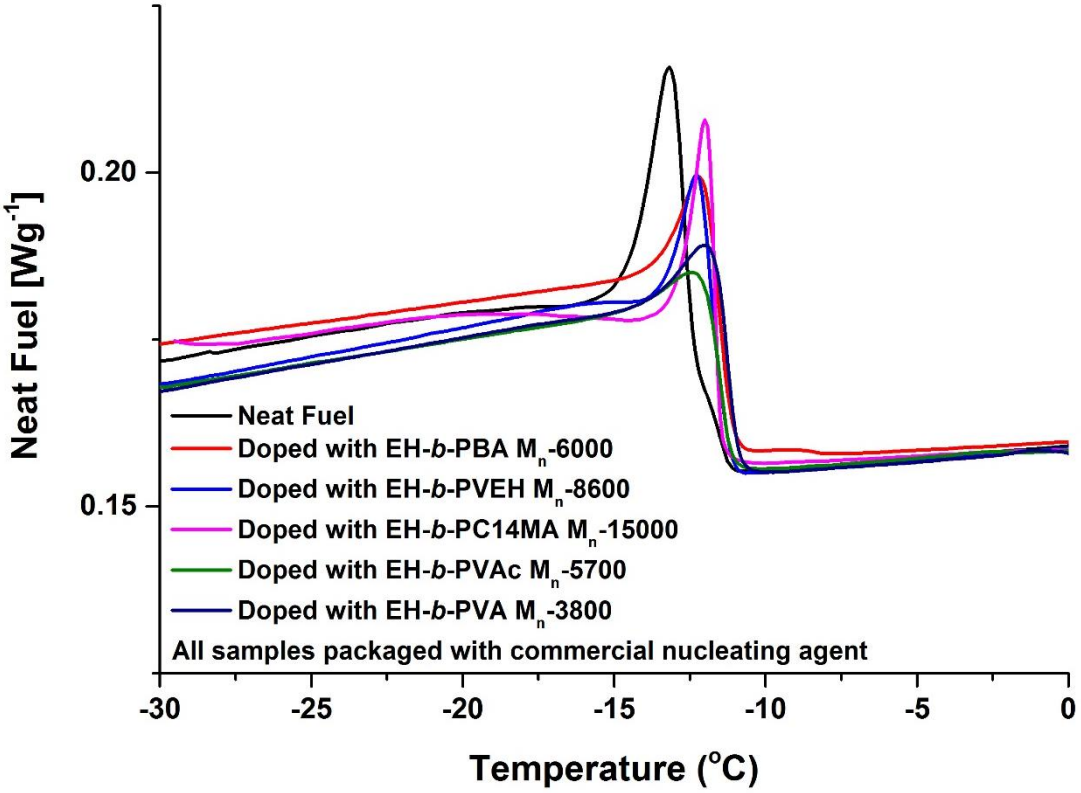

Figure 4.16: DSC traces of fuel samples treated with copolymers packaged with commercial nucleating agent (250 ppm)

4.8 Examination of solid wax doped with copolymers

Having established that the block copolymers are effective at modifying the structure of wax crystals in fuel, the nature and effects of the copolymer materials when dispersed in a polyethylene wax was investigated. Copolymer additives (10 wt%) were dissolved in molten PE wax. The wax was poured into a steel mould, and both faces of the disc would be tested for properties and composition.

Drop shape analysis (DSA) was conducted on the wax discs to investigate whether the blended polymer had affected the hydrophilicity of the surface. EH-*b*-PVA was chosen as the principle copolymer of interest as it was likely to give the greatest effect on the contact angle due to the polarity of the poly(vinyl acetate) block.

Table 4.4: DSA contact angle measurements of solid wax doped with EH-b-PVAc

Sample	**Contact Angle (°)**	
	Left	**Right**
Commercial PE Wax	108.5	108.5
Commercial PE Wax + 10wt% EH-PVAc (top face)	106.5	106.5
Commercial PE Wax + 10wt% EH-PVAc (bottom)	99.8	99.8

The contact angles measured are shown in Table 4.4. The untreated commercial PE wax disc produced a contact angle of 108.5° on both faces of the disc. Changes in the contact angles observed for the doped wax disc surfaces were moderate, the top surface reported a 2° depression of contact angle (106.5°) and the bottom surface gave an angle of 99.8°; a depression of 8.7°. The discrepancy between contact angle values for the two sides of the disc may be due to the copolymer precipitating from the wax as it cooled and then settling to the bottom of the mould.

Regardless of the disparity in the contact angle, the effect of the copolymer upon the wax surface contact angle was not as significant as was expected. This led to the question of whether the polymer additive resides at the disc surface, or whether the copolymers aggregate and reside within the bulk of the wax.

X-ray Photoelectron Spectroscopy (XPS) is a surface sensitive spectroscopic technique which is used to measure the elemental composition of a material. This technique was used to investigate oxygen concentrations on the internal and external surfaces to determine where the copolymer is within the wax disc, the results of which are presented in Table 4.5.

Table 4.5: XPS results for commercial PE wax disc doped with 10wt% of EH-b-PVAc

ID	Surface	C (%)	O (%)	Si (%)
Commercial PE Wax	Internal	99.3	0.7	0
Commercial PE Wax + 10 wt% EH-P(VAc)	Internal	85.3	13.1	1.6
Commercial PE Wax + 10 wt% EH-P(VAc)	Top	94.3	3.5	2.3
	Bottom	92.7	4.2	3.1

Samples were prepared by fracturing in an oxygen free environment. An untreated PE wax disc was prepared as a control, and showed that 99.3% of the analysed surface was carbon, with only 0.7% oxygen content. Conversely the treated disc showed between 3 and 4% oxygen content at the surface of the disc. This is a small increase but likely accounts for the small change in contact angle observed. It is further seen that the oxygen content for the internal face of the wax disc possesses 13% oxygen content, seeming to indicate that the majority of the polymer additive is dispersed in the bulk of the wax.

Table 4.6: Measurements of the content of the chemical bonds present within solid wax

Sample	Surface	Polyethylene	C-C / C-H (atmospheric)	C-OH /C-O-C/ C-NH	C=O	O=C-O /CaCO3/ Na2CO3
		Atomic %	Atomic %	Atomic %	Atomic %	Atomic %
1	Internal	58.5	39.7	1.0	0.7	0
2	Internal	14.7	54.9	14.5	9.6	4.8
	Top	79.3	17.7	1.8	0.8	0.5
	Bottom	88.8	8.3	1.7	0.7	0.6

A more detailed examination of the type of chemical bonds present in the wax (Table 4.6) was measured and it was found, unsurprisingly, that the untreated PE wax was composed near entirely by polyethylene and C-C/C-H bonds (98.3%). Within the treated disc we see that the oxygen containing bonds arise from C-OH /C-O-C and C=O bonds, which are the bonds present in P(VAc). Once again we observe that the content of these bonds is greater in the internal face of the disc.

These results indicate then, that while the polymers as they are, may be useful for compatibilisation/blending of materials, they do not lend themselves effectively to surface modification. This could possibly be addressed and improved upon by modification of the polymer properties such as molecular weight, relative block lengths, polymer type etc.

4.9 Conclusion

Evidence of aggregation of block copolymers in solution was obtained from ^{1}H NMR and DLS analysis, suggesting that these copolymers assemble into micelles in selective solvents with a polyolefin core, behaviour typical of block copolymers. TEM images supported this and suggest that in some instances these micelles are spherical in nature. DSC investigations showed evidence of phase separation of crystalline polyolefin and amorphous polar blocks.

Block copolymer performance as wax crystal modifiers in middle distillate fuels were investigated and it was found that the greatest effect was given when copolymer additives were packaged with a commercial GA and gave CFPP values significantly improved from untreated fuel. Microscopy images and thermal investigations (DSC) were consistent with copolymer additives behaving as nucleating

agents during the wax crystallization process, exemplified by the presence of high numbers of smaller crystals and an early onset of crystallization temperature.

The effects on the surface properties of solid wax doped with copolymer additives was investigated and it was found that certain copolymer architectures were able to give modest modification of the hydrophobicity/hydrophilicity of the surface. XPS experiments indicated that this was because the copolymer additive is dispersed primarily in the bulk of the wax.

4.10 References

1. B. Wei, *Journal of Petroleum Exploration and Production Technology*, 2015, 5, 391-401.
2. H. P. Soni, Kiranbala, K. S. Agrawal, A. Nagar and D. P. Bharambe, *Fuel Process. Technol.*, 2010, 91, 997-1004.
3. H. S. Ashbaugh, A. Radulescu, R. K. Prud'homme, D. Schwahn, D. Richter and L. J. Fetters, *Macromolecules*, 2002, 35, 7044-7053.
4. H. S. Ashbaugh, X. Guo, D. Schwahn, R. K. Prud'homme, D. Richter and L. J. Fetters, *Energy Fuels*, 2005, 19, 138-144.
5. J. Zhang, C. Wu, W. Li, Y. Wang and Z. Han, *Fuel*, 2003, 82, 1419-1426.
6. A. M. Nassar and N. S. Ahmed, *Int. J. Polymer. Mater.*, 2006, 55, 947-955.
7. R. A. Soldi, A. R. S. Oliveira, R. V. Barbosa and M. A. F. César-Oliveira, *Eur. Polym. J.*, 2007, 43, 3671-3678.
8. R. K. Farag, *Int. J. Polymer. Mater.*, 2008, 57, 189-202.
9. L. V. Castro and F. Vazquez, *Energy Fuels*, 2008, 22, 4006-4011.
10. A. K. Chatterjee, P. K. Chaturvedi, P. S. N. Murthy and G. C. Joshi, *Macromol. Rep.*, 1996, A33, 23-31.
11. T. T. Khidr, *Pet. Sci. Technol.*, 2007, 25, 671-681.
12. D. Richter, D. Schneiders, M. Monkenbusch, L. Willner, L. J. Fetters, J. S. Huang, M. Lin, K. Mortensen and B. Farago, *Macromolecules*, 1997, 30, 1053-1068.
13. A. Radulescu, D. Schwahn, J. Stellbrink, E. Kentzinger, M. Heiderich, D. Richter and L. J. Fetters, *Macromolecules*, 2006, 39, 6142-6151.
14. W. Leube, M. Monkenbusch, D. Schneiders, D. Richter, D. Adamson, L. Fetters, P. Dounis and R. Lovegrove, *Energy Fuels*, 2000, 14, 419-430.
15. G. A. Holder and J. Winkler, *Nature*, 1965, 207, 719-721.
16. J. A. P. Coutinho, C. Dauphin and J. L. Daridon, *Fuel*, 2000, 79, 607-616.
17. I. M. El-Gamal, T. T. Khidr and F. M. Ghuiba, *Fuel*, 1998, 77, 375-385.

18. I. M. El-Gamal and A. M. Al-Sabbagh, *Fuel*, 1996, 75, 743-750.
19. J. W. Qian, X. Wang, G. R. Qi and C. Wu, *Macromolecules*, 1997, 30, 3283-3287.
20. P. A. Mirau, *A practical guide to understanding the NMR of polymers*, Wiley-Interscience, 2005.
21. I. Hamley, in *Block Copolymers in Solution: Fundamentals and Applications*, John Wiley & Sons, Ltd, 2005, DOI: 10.1002/9780470016985.ch2, pp. 7-104.
22. H. C. Van de Hulst, *Light Scattering by Small Particles*, Dover Publ., 1982.
23. B. J. Berne and R. Pecora, *Dynamic Light Scattering: with Applications to Chemistry, Biology, and Physics*, Wiley-Interscience, 1975.
24. C. Tanford, *The Hydrophobic Effect: Formation of Micelles and Biological Membranes. 2nd Ed*, Wiley, 1980.
25. H. Kaneyoshi, Y. Inoue and K. Matyjaszewski, *Macromolecules*, 2005, 38, 5425-5435.
26. T. Hatakeyama and F. X. Quinn, in *Thermal Analysis: Fundamentals and Applications to Polymer Science*, John Wiley & Sons Ltd, Chichester, England, 2nd edn., 1999, ch. 5, pp. 102-109.
27. Y. Kong and J. N. Hay, *Polymer*, 2002, 43, 3873-3878.
28. R. P. Quirk and M. A. A. Alsamarraie, eds. J. Brandrup, E. H. Immergut and J. W. S. Inc, New York, 3rd edn., 1989, ch. V, pp. 15-26.
29. V. A. Kryuchkov, J.-C. Daigle, K. M. Skupov, J. P. Claverie and F. M. Winnik, *J. Am. Chem. Soc.*, 2010, 132, 15573-15579.
30. C. Kay, PhD Thesis, University of Warwick, 2014.
31. T. Matsugi, S.-I. Kojoh, N. Kawahara, S. Matsuo, H. Kaneko and N. Kashiwa, *J. Polym. Sci., Part A: Polym. Chem.*, 2003, 41, 3965-3973.
32. B. Wunderlich, *Thermal Analysis*, Academic Press, Inc., London, 1990.
33. B. Wunderlich, Springer Berlin, 2005, ch. 7, pp. 705-776.

Chapter 5

Experimental

5.1 General Considerations

When it was necessary the work detailed below was carried out in an inert atmosphere of argon, using standard Schlenk techniques. Glassware, syringes, cannulae etc. were all dried for at least 24 h prior to use at 125°C. Toluene and other solvents were dried by reflux over drying agents for three days prior to distillation. These solvents were then freeze-thaw degassed three times prior to use. Unless otherwise stated, deuterated solvents and reagents were purchased from Sigma Aldrich and used as purchased. To remove inhibitors, monomers were passed through a column of alumina and, in the case of 1,3-DIB (97% Sigma Aldrich/ 97% TCI Europe), transferred into glass ampoules and dried over 4Å molecular sieves before use. Methylaluminoxane (AXION CA 310) 10 wt% solution in toluene was purchased from Chemtura and was transferred in small quantities into a graduated glass ampoule by cannula and used as supplied. Research grade ethylene (BOC) was passed, prior to entering the burettes system, through a drying train consisting of BASF R3-11G deoxygenating agent and 3 Å molecular sieves and subsequently stored in pressurised burette system (Figure 5.1). High purity hydrogen (99.995%, BOC) was used as received. Tetrachloroethane-d^2 (99.6%, Cambridge Isotope Laboratories Inc.) was used as received. Catalytic metal complexes were stored under inert atmosphere in an MBraun glovebox containing <5 ppm O_2.

^{1}H NMR spectra were recorded on a Bruker DPX-400 or DRX-500 spectrometers at 100°C in 1,1,2,2-tetrachloroethane-d^2. Residual protio-solvent was used as an internal reference.[1, 2] ^{13}C NMR spectra of polyolefin samples were recorded on a Bruker DRX-500 at 125 MHs in 1,1,2,2-tetrachloroethane-d^2 (>10,000 scans, 4 s relaxation time, 100°C). NMR assignments were supported *via* ^{1}H-^{1}H (COSY), ^{13}C-^{1}H (HMQC) and ^{13}C-^{1}H (HMBC) correlation experiments where necessary.

High temperature GPC measurements were performed in 1,2,4-trichlorobenzene (≥99% Aldrich) containing 250 ppm 2,6-di-tert-butyl-4-methylphenol (BHT) (Aldrich) as antioxidant at 160°C at a flow rate of 1 ml/min. The instrument was a Polymer Labs PL220 equipped with a 5 cm PLgel guard column (5 μM) and two PLgel 30 cm mixed-C columns (5 μM) as well as differential refractive index (DRI), viscometry (VS) and dual angle light scatter (LS 90 + 15) detectors. Universal calibration was achieved using Polymer Labs polystyrene Easivial Standards. Universal calibration was selected for use on polyolefin containing materials as it is not chemically comparative as with standard GPC techniques. Conventional techniques consequently over estimate PE samples when compared to PS standards, as the hydrodynamic volume of PE with an equivalent molecular weight is greater. Universal calibration utilises a concentration response from the RI detector and the intrinsic viscosity (calculated from viscometer response) to generate a calibration curve of log (intrinsic viscosity × molecular weight) vs retention time. As is shown in work by Benoit *et al*,[3] the samples are separated by size in solution so the same calibration curve is produced irrespective of the chemical nature of the standards used to generate it. During sample analysis, the concentration of the sample is entered, and thus specific viscosity is calculated based on the response from the viscometer. From this the intrinsic viscosity is derived and along with the retention time, is

compared to the calibration curve to establish the molecular weight of the sample. PS standards were often run in conjunction with analysed samples in order to verify the accuracy of the calibration and generally had agreement with 5-10%. Where solubility and circumstance allowed, room temperature GPC was carried out in chloroform at 30°C at a flow rate of 1 ml/min on a Varian 390LC fitted with PLgel mixed-D columns (5 μM). In this case, calibration is created using Polymer Labs PMMA-M Easival Standards.

Particle size distributions were measured by dynamic light scattering (DLS) using a Malvern Zetasizer Nano ZS. Samples were prepared as follows; 10 mg of each polymer was dissolved in solvent (toluene or THF) to create a solution with a concentration of 1 mg/mL. These solutions are then passed through a 0.22 μm filter to remove dust and other large particles. Heating and vortex mixing were applied in order to aid the dissolution of polymer. Polymer solutions were transferred to a quartz cuvette with two clear faces (1 cm depth). A equilibration time of two min was used to allow the temperature to stabilise at 25°C. Particle sizing measurements were conducted in triplicate with 15 scans each and it is the average of these measurements that is reported.

Transmission electron microscopy (TEM) analyses were performed on a Jeol 2010F TEM (200kV FEG) instrument equipped with a Gatan UltraScan 4000 camera. TEM samples were prepared on by evapouration of a drop of block copolymer solution (see sample prep for DLS measurements) in THF (1 mg/mL) on a grid of graphene oxide coated Lacey-carbon 400 mesh copper grids purchased from Agar Scientific (AGS166-4H-GO).

Thermal analyses were carried out on a Mettler Toledo DSC1-400 system. The analysis was conducted under an atmosphere of dinitrogen. The samples were heated

to 160°C at 10°C/min, and cooled to -160°C at 10°C/min for recrystallisation. This cycle is then repeated 3 times in order to erase thermal history (non-uniform crystals/regions arising from crystallization events during sample synthesis/processing). Following this, all successive thermograms were identical. For thermal analysis of diesel samples, the samples were heated to 60°C before cooling to -30°C at a rate of 5°C/min under a nitrogen atmosphere, a hold time of 2min was applied after each heating/cooling segment. The heat cycle was repeated three times as before to erase thermal history and the successive thermograms were identical.

Cold filter plugging points (CFPP) of diesel samples were determined using an ISL CFPP 5GS instrument. Untreated diesel was initially filtered through 30 μm filter paper to remove dust and other contaminants. 50 g samples were prepared and doped with known concentrations of a 10wt% solution of copolymer additive in Solvesso® 150. CFPP experiments were carried out according to the standard procedure outlined in ASTM D6371.[4]

MALDI mass spectrum analysis was carried out using a Bruker Ultraflex II Extreme MALDI TOF/TOF using 9-nitroanthracene as the organic matrix and silver trifluoroacetate salts to promote cation formation in the polymer samples.

Drop shape analysis and contact angle measurements were made using a KRÜSS DSA100 measuring system. The liquid used was deionised water, which was loaded into a syringe and mounted to a stepper motor which was used to deposit drops on the surface.

Software used in the project included Cambridgesoft ChemOffice, Endnote X7, Microsoft Office 2013, OriginPro 8.5, ImageJ and PolymerLabs Cirrus software.

5.1.1 Table Values and Equations

The values tabulated in chapters 2-5 were calculated as follows. M_n, M_w, and Đ were calculated via GPC.

$$M_n = \frac{\Sigma MiNi}{\Sigma Ni} \qquad M_w = \frac{\Sigma Mi^2 Ni}{\Sigma MiNi} \qquad PD = \frac{M_w}{M_n}$$

Throughout this work, monomer conversion was determined gravimetrically where possible or otherwise by ^{1}H NMR spectroscopy (see Chapter 4). Productivity measurements were calculated using equation (1).

$$Productivity = \frac{kg\ polymer}{moles\ catalyst\ \times\ hours} \tag{1}$$

5.1.2 Gas burette system used to measure ethylene uptake during polymerisation

A gas pressure burette system, previously constructed by members of this research group to provide ethylene uptake measurements during the polymerisation reaction,[5] was used to gain information on catalyst lifetime and determine productivity of the catalysts. The system allows gas to flow from a storage burette into the reaction vessel *via* a pressure regulator. Measurements of the pressure change in the storage tank, enables calculation of the gas uptake (in moles) by the reaction (*vide infra*).

The system schematic is shown in Figure 5.1 while component details are given in Appendix C. The equipment is operated as follows: the burette system is filled prior to a reaction, with ethylene that has been passed through a drying train consisting of BASF R3-11G deoxygenating agent and 3 Å molecular sieves (E-2) and a filter (E-

3). It is then stored in either a 300, 1000 or 2250 cm^3 pressure burette (E-4, E-5, or E-6) at *ca* 16 bar. The supply valve (V-5) is closed during reactions, and gas flows from the storage burette into the reaction vessel (E-8) through the regulator (V-8) at the required pressure.

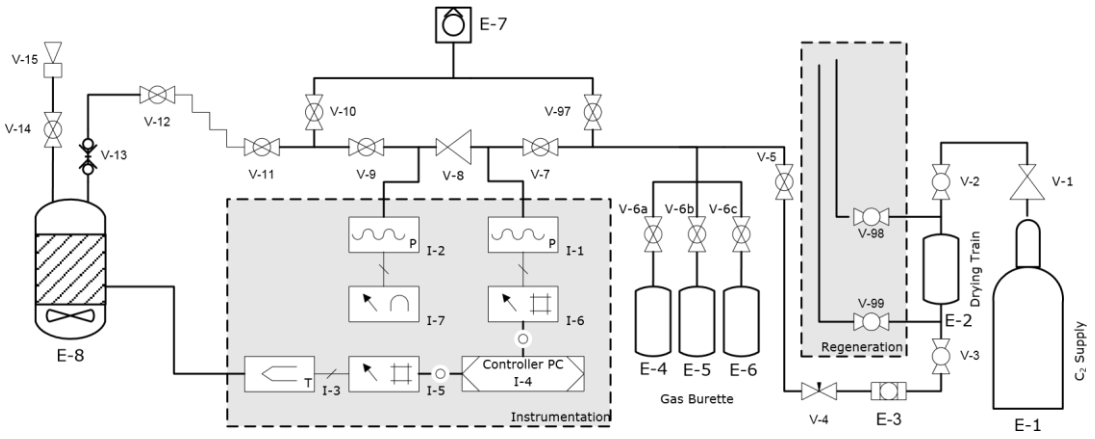

Figure 5.1: Gas pressure burette schematic[5]

5.1.3 Data Acquisition and Processing

The pressure transducer (I-1) monitors the pressure in the gas burette, and the reactor temperature is monitored by thermocouple (I-3). Data from the sensors is passed to process meters (I-5 and I-6), and recorded by an attached computer (I-4).

Data acquisition software (Polymeister) was custom made for this function by a previous member of this research group using Java programming language. The software displays a graph of ethylene uptake and temperature during the course of each polymerisation. Data from this software is output in the CSV format which is readily tabulated in spreadsheet software. The control software also calculates the conversion of the measured ethylene pressure remaining in the burette and moles of

gas consumed by the reaction, by applying the second order virial equation of state[6] shown in equation (2), due to the non-ideal behaviour of ethylene.

$$\rho V_m = RT\left(1 + \frac{B}{V_m}\right) \tag{2}$$

This equation can then be rearranged into the quadratic form (3), which is then solved using the standard numerical quadratic solution. This gives the equation (4), which is solved by the software for each data point recorded.

$$\left(\frac{B}{V}\right) = n^2 + n + \frac{-\rho V}{RT} \tag{3}$$

$$n = \frac{-1 \pm \sqrt{1 - 4\left(\frac{\mathrm{B}}{V}\right)\left(\frac{-\rho V}{RT}\right)}}{2\left(\frac{B}{V}\right)} \tag{4}$$

$\mathrm{B} = 2^{nd}$ virial coefficient

$\mathrm{n} = \mathrm{Number\ of\ Moles}$

$\mathrm{P} = \mathrm{Pressure}$

$\mathrm{R} = \mathrm{Gas\ Constant}$

$\mathrm{T} = \mathrm{Temperature}$

$\mathrm{V} = \mathrm{Total\ volume}$

$V_m = \mathrm{Molar\ volume}$

5.2 General procedure for polymerisation with monitored gas uptake

Polymerisations were conducted in a 250 mL stainless steel Parr reactor fitted with an internal cooling coil and equipped with a thermocouple. The reactor is also connected

to the burette system (*vide supra*) in order to monitor the gas delivery at fixed pressure. The reactor was dried under vacuum at 100°C for 1 hour following storage in an oven. Once dried and evacuated, the comonomer solution consisting of toluene, 1,3-DIB (33 ml, 0.19 mol) and MAO solution (3 ml, 1800 equivalents relative to catalyst) is transferred to the reactor *via* cannula. The reactor is heated initially to 50°C and then purged with dihydrogen for 10 min before subsequent addition of ethylene. Ethylene was stirred into the reaction solution until the uptake had stabilised. Following this a toluene solution of metallocene catalyst (2.5×10^{-6} mol), which was prepared in the glovebox, was injected using an overpressure of argon. Polymeister software was used to monitor the temperature and gas uptake following addition of catalyst solution. The exotherm that results from catalyst injection is controlled by use of a cold water feed connected to the internal cooling coil, a balance of this and a laboratory hot plate fitted beneath the reactor were used to maintain the desired temperature (typically 60°C). At the appropriate time, the reaction is terminated by first shutting off the ethylene supply, followed then by cooling and the careful addition of methanol (2 × 10 ml) to the vented reactor. The resultant polymer product was precipitated by pouring into a solution of acidified methanol (5% HCl) with stirring for 1 h. The product was recovered by filtration, and purified where necessary by reprecipitation from toluene. Products were dried by heating to 70°C *in vacuo* for 24 h.

5.3 General procedure for free radical polymerisations

In a typical example of a free radical polymerisation, a 10 ml ampoule equipped with a stirrer bar was charged in air with 1,3-diisopropenylbenzene initiated EH (EH-*i*-DIB) (0.2 g. 5.13×10^{-5} mol), *n*-butyl acrylate (0.8 ml, 5.1×10^{-3} mol), dibenzoylperoxide (75% in H_2O) (1.6×10^{-2} g, 5.1×10^{-5} mol), and made up to 8.2 ml with toluene. The

ampoule is then sealed and air is removed by freeze-thaw degassing three times. Following this the ampoule is stirred and heated to 125°C using an aluminium heating block. At the proper time, the reaction is terminated by opening the mixture to air and pouring into methanol (600 ml) with stirring to precipitate the product. The precipitate is then allowed to settle and the solvent is decanted off. The crude product may then be purified by reprecipitation 3 times from toluene/methanol if required and is dried *in vacuo* overnight.

5.4 General procedure for synthesis of short chain carbamates

A 250 ml 3-neck round bottom flask equipped with a stirrer bar, condenser (with N_2 bubbler) and two rubber seals was charged in air with a solution of docosanol (5.8g, 0.018 mol) in toluene (100 ml). The system was purged by bubbling argon through the reaction mixture using a needle connected to a Schlenk line with stirring at 50°C. After purging, the inert atmosphere was maintained with dinitrogen from the bubbler. Separately, a solution of 3-isopropenyl-α,α-dimethylbenzyl isocyanate (3.5 ml, 0.018 mol) and dibutyltin dilaurate in toluene (50 ml) was prepared in a 100 ml RBF and was purged as previously described. After purging, the solution was transferred to the 3-neck RBF *via* cannula under a positive pressure of argon. The reaction was conducted over 16 *h* following equilibration of the reaction temperature. The reaction was terminated by opening to air and the products were isolated by precipitation in methanol and collected by vacuum filtration.

5.5 References

1. H. E. Gottlieb, V. Kotlyar and A. Nudelman, *J. Org. Chem.*, 1997, 62, 7512-7515.

2. G. R. Fulmer, A. J. M. Miller, N. H. Sherden, H. E. Gottlieb, A. Nudelman, B. M. Stoltz, J. E. Bercaw and K. I. Goldberg, *Organometallics*, 2010, 29, 2176-2179.
3. Z. Grubisic, P. Rempp and H. Benoit, *J. Polym. Sci., Part B: Polym. Phys.*, 1967, 5, 753-759.
4. Standard Test Method for Cold Filter Plugging Point of Diesel and Heating Fuels in *ASTM Standard D6371* ASTM International, West Conshohocken, PA, 2016.
5. M. L. Hammond, PhD Thesis, University of Warwick, 2006.
6. P. W. Atkins, *Physical Chemistry*, Oxford University Press, Oxford, 1992.

Appendix A

Investigation of Hafnocene catalysts

Hafnocene catalysts have been seldom used due to a low polymer productivity while using MAO activation.[1-3] This low activity likely arises from the presence of TMA in the reaction mixture. Hafnocene dichloride and TMA are capable of forming the dinuclear methyl bridge species $[Cp_2Hf(\mu\text{-}Me_2)AlMe_2]^+$.[4] This bridged compound has been shown to be far more stable than the zirconium equivalent, arising from stronger M-C bonds,[5] and is considered to be in a resting state.[6] Hafnocene is also known to produce polymers with significantly higher molecular weights in homogeneous conditions.[7]

A.1 Polymerisation with hafnocene catalysts

A series of copolymerisations between ethylene and AMS type comonomers, in the presence of hydrogen, were conducted in the same manner as described previously (Table 2.1). As anticipated the reaction productivity was greatly reduced, and only small amounts of material were recovered following precipitation in methanol.

Run 1 is an ethylene polymerisation by hafnocene which yielded 2.2 g of polyethylene with higher molecular weight than the comparable polymer produced by zirconocene, so high in fact that it could not be dissolved for GPC analysis.

Runs 2-5 are the polymerisations of ethylene and DIB or AMS, at two different concentration levels, in the presence of hydrogen. From the results, we can observe that in both cases, the reaction productivity increases with increasing monomer concentration, along with a decrease in the dispersity and M_w of the polymers.

Table A.1 Copolymerisations of ethylene and α-methylstyrene monomers in the presence of hydrogen and ethylene.

RUN [a]	Comonomer 1	[Comon.1] (mol/L)	Catalyst	M_p (g/mol) [b]	M_w (g/mol)	M_n (g/mol)	Đ	Yield (g)	Productivity [c]
1	-	-	$HfCp_2Cl_2$	nd	nd	nd	nd	2.2	2600
2	DIB	1.01	$HfCp_2Cl_2$	4400	8800	2800	3.1	0.4	480
3	DIB	2.07	$HfCp_2Cl_2$	2700	3300	2200	1.5	1.2	1400
4	AMS	1.01	$HfCp_2Cl_2$	5500	5700	4200	1.4	0.1	130
5	AMS	2.07	$HfCp_2Cl_2$	2300	2500	2300	1.1	0.5	520

[a] Reaction Conditions: $Cp_2HfCl_2 = 2.5\times10^{-6}$ mol; MAO = 1800 equivalents; C_2H_4 partial pressure = 32 psi except where indicated; solvent = toluene; reaction volume = 90 ml; reaction time = 20 min; reaction temperature = 60°C.
[b] GPC data were based on universal calibration from PS standards
[c] (kg polymer/(mol[Zr].h))

A.2 ^{1}H NMR analysis

The ^{1}H NMR spectrum of the product of run 3 (Table A.1) is shown in Figure A.1. A number of distinct differences from the typical spectrum for end functionalised PE-*i*-DIB were observed. The large increase of the integral of the aromatic region, *ca* 14 H, rather than the typical 4 H for zirconocene catalysed systems, indicates the presence of additional aromatic species within the product.

The vinylidene region typically contains two sharp peaks at 5.34 and 5.07 ppm arising from the DIB end group, a number of additional broad peaks are seen within this region shown in insert (a). Insert (b) shows an additional peak (2.76 ppm) between the benzylic peak at 2.69 ppm and the peak resulting from the aryl group which occurs in hydrogenated DIB end groups at 2.89 ppm.

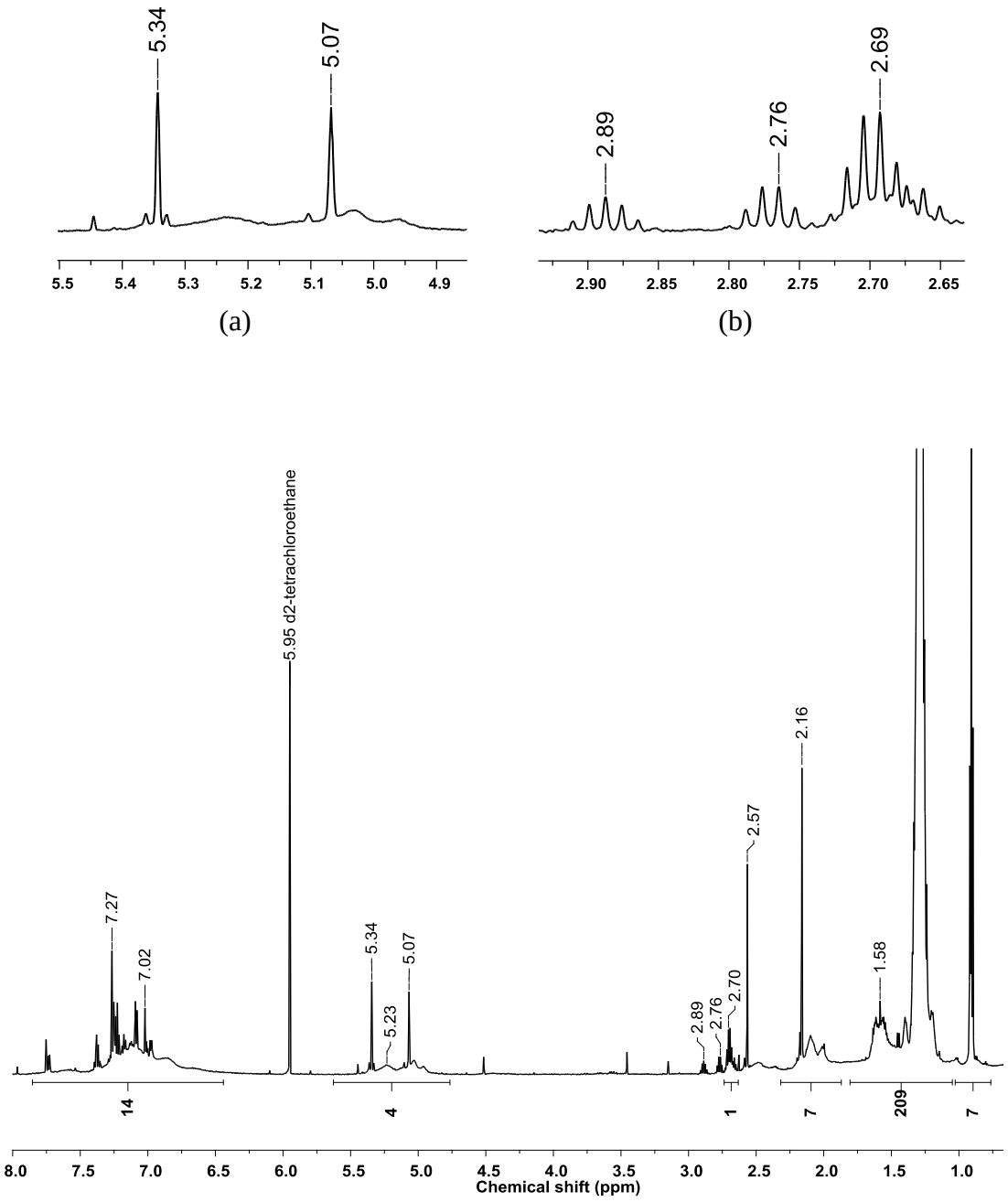

Figure A.1: ^{1}H NMR spectrum of the copolymerisation of ethylene and 1,3-DIB in the presence of hydrogen with inserts of (a) the vinylidene region and (b) the benzylic region

Further investigation of the structure of these materials was conducted due to the possibility that the NMR spectra may indicate in-chain incorporation of the 1,3-DIB functional group.

In other experiments α-methylstyrene monomer was used in place of 1,3-DIB as it does not bear the pendant isopropenyl group that occurs in 1,3-DIB (runs 4-5, Table A.1).

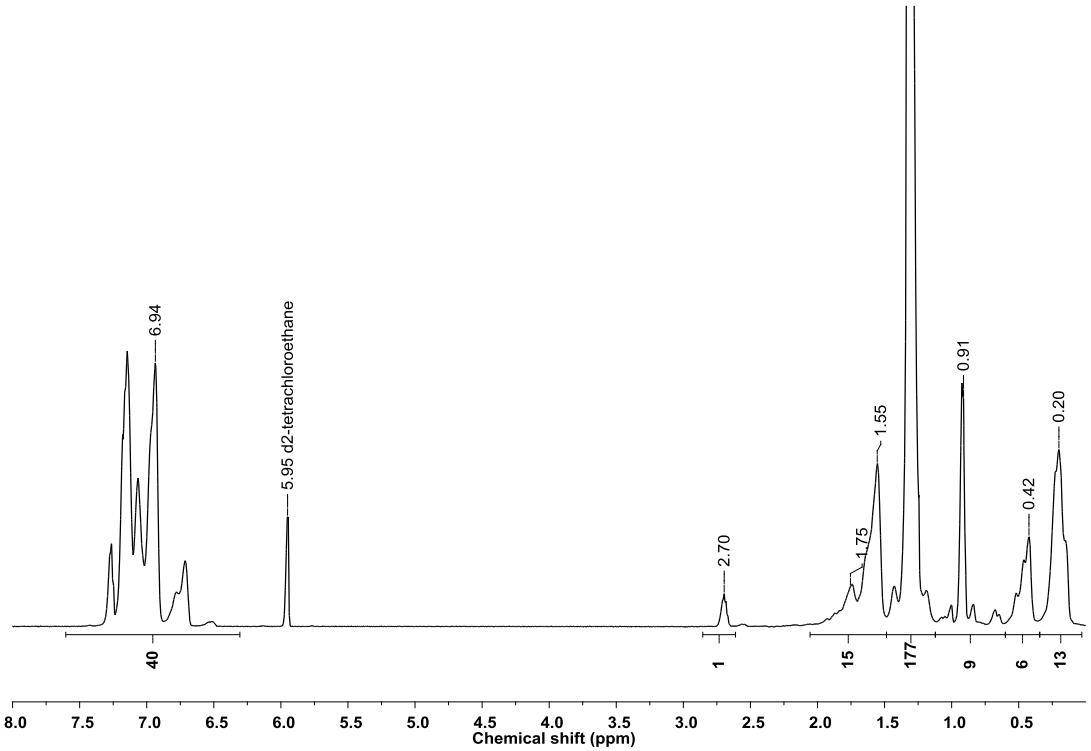

Figure A.2: ^{1}H NMR spectrum of PE/PAMS (run 5 Table 2.1) in d^2-TCE at 25°C (400 MHz). Relaxation delay = 1 s.

The NMR spectra of run 5, Table A.1, (Figure A.2) shows again a large aromatic region integral. Additionally, we observe peaks occurring at 0.42 and 0.20 ppm. Still visible in the spectrum is the peak at 2.70 ppm for the benzylic protons occurring from end termination of an AMS group.

A.3 DOSY NMR analysis

Diffusion-ordered NMR spectroscopy (DOSY) is a powerful spectroscopic technique that allows convenient analysis of complex mixtures without the need for prior

chemical separation.[8, 9] It uses the principle that in addition to temperature and viscosity, diffusion of molecules in solution depends heavily on the size and shape of the molecule. And so two different compounds should present two different diffusion coefficients.

Diffusion coefficients (*D*) of species can be described by the Stokes-Einstein equation (Equation A.1) assuming a spherical particle shape. A smaller molecule will move more quickly and therefore will have larger diffusion coefficients, while larger molecules will have smaller diffusion coefficients. In equation A.1, k is the Boltzmann constant, T is the temperature and η is viscosity of the liquid and r_s is the hydrodynamic radius of the molecule.

$$D = \frac{\kappa T}{6\pi\eta r_s} \quad \textbf{(A.1)}$$

For the analysis of polymers, diffusion coefficients are related to hydrodynamic radius and molecular weight which has led to recent use in the characterisation of homopolymers, block copolymers[10] and mixtures of the two. This technique has proved particularly useful in determining whether the sample contains one copolymer species, multiple homopolymer species or detecting the presence of contaminants e.g. homopolymers where ^{1}H NMR and GPC data are inconclusive.

DOSY NMR was conducted upon a sample (run 5, Table A.1) to observe how many species were present in the precipitated sample. As can be seen from the spectrum presented below, (Figure A.3) a minimum of two distinct species with different diffusion coefficients can be seen. These have been shown by the horizontal lines added to the spectrum.

The diffusion coefficient peaks line up with the proton resonances of the product shown in the ^{1}H NMR. This enables identification of the environments present within the two different species. It is clear that one of these species is polyethylene, potentially with a single end chain AMS unit as a distinct and separate diffusion coefficient for the PE backbone (1.3 ppm) is observed. The other diffusion coefficient correlations belong to peaks which indicate that a second species present, and that this may be poly(α-methylstyrene), (PAMS). The diffusion coefficient occurring at 5.95 ppm is that of the NMR solvent, d^2-tetrachloroethane.

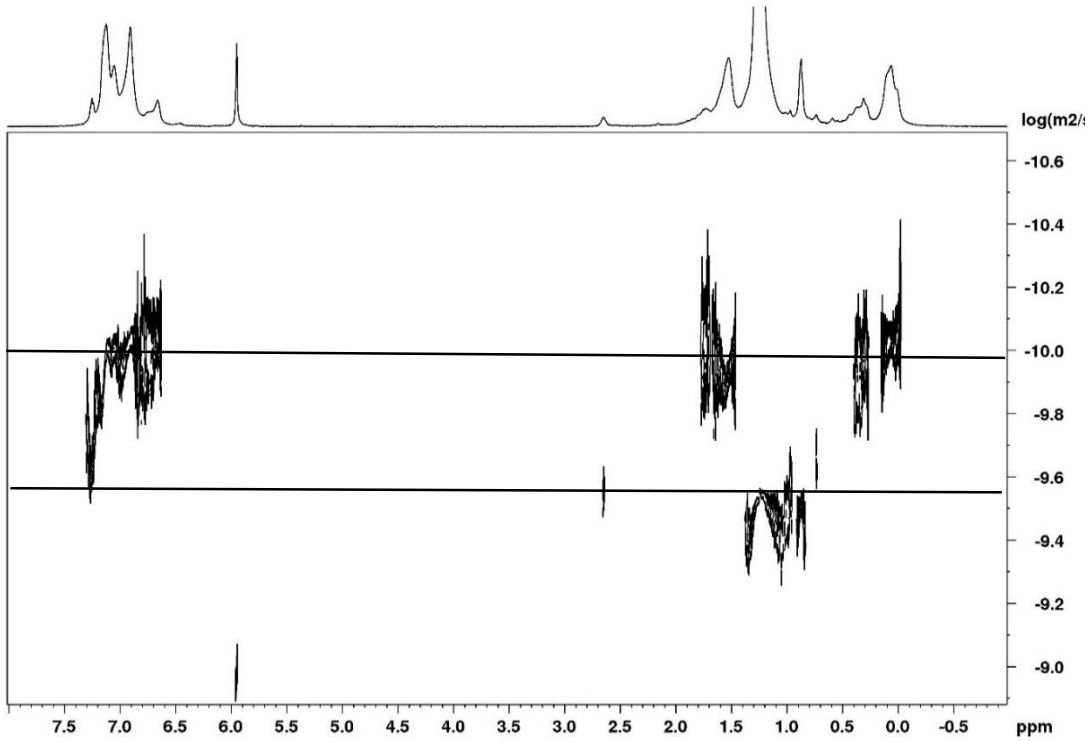

Figure A.3: DOSY ^{1}H NMR of PE/PAMS in d^2-TCE at 25°C (500 MHz).

A.4 2-dimentionsl NMR analysis

The structure of these materials was further examined using the 2-dimensional ^{1}H-^{13}C correlation spectra. The HMQC spectrum (Figure A.4) shows a number of correlations indicative of PAMS.

The backbone methylene protons appearing at 1.6 ppm in the ^{1}H NMR show a correlation with the attached carbon environment in the ^{13}C NMR. The methyl group environments at 0.42 and 0.2 ppm, show two separate correlations with methyl region carbon environments. They appear as two separate peaks due to the tacticity of the PAMS.[11, 12] Finally, a correlation is observed between the benzylic carbon and proton at the end chain unit.

The HMBC (Figure A.5) shows a number of expected correlations within PAMS homopolymer.[11,13] As HMBC is able to show correlations between environments several bonds away we are able to identify correlations which are indicative of the presence of PAMS.

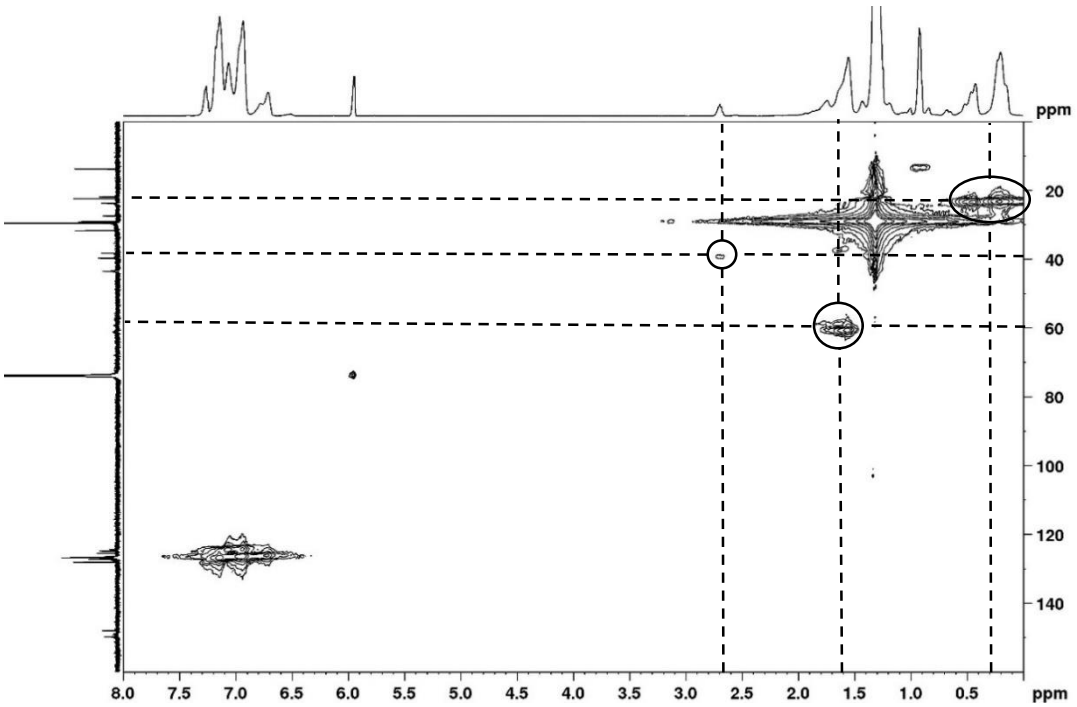

Figure A.4: ^{1}H-^{13}C HMQC NMR spectrum of PE/PAMS from run 5 in d^2-TCE at 100°C (500 MHz

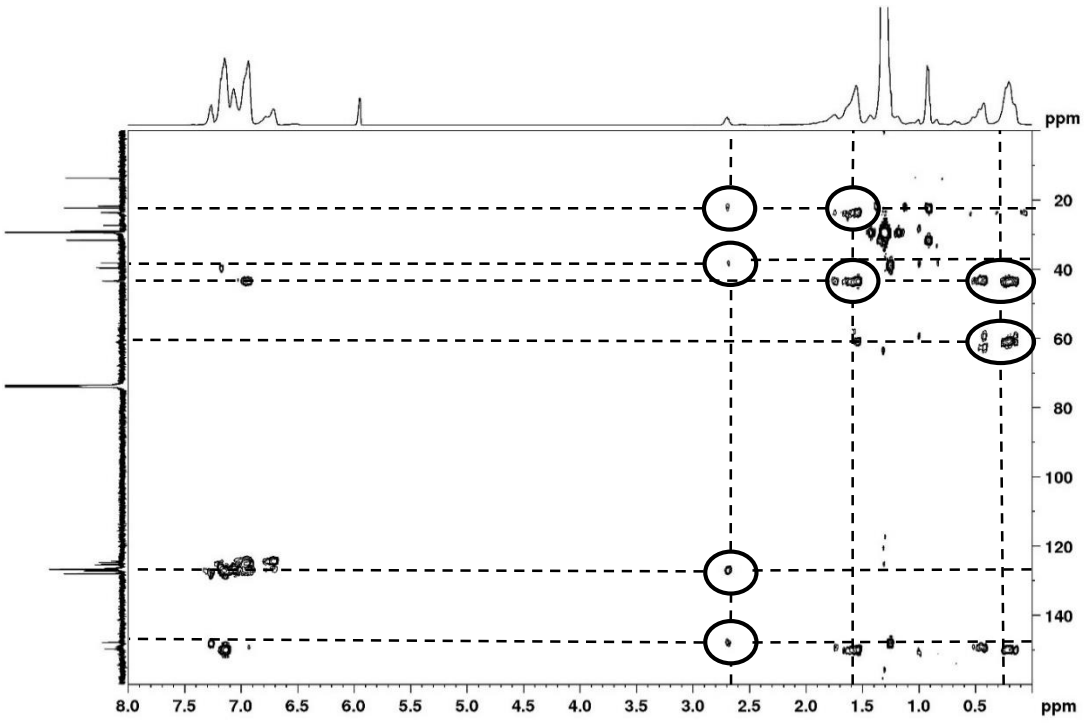

Figure A.5: ^{1}H-^{13}C HMBC NMR spectrum of PE/PAMS from run 5 in d^2-TCE at 100°C (500 MHz)

A.5 MALDI analysis of PE/PAMS

By examination of the MALDI spectrum of the copolymerisation products (runs 4-5, Table A.1), it is seen that the acquired spectra show two polymer distributions, albeit one with much higher intensity than the other. The primary distribution visible is that of PE-*i*-AMS with a separation between two adjacent peaks of 28 DA, indicative of an ethylene repeat unit. The second distribution is depicted in the two inserts (a) & (b) shown in Figure A.8, these show the repeat unit of PAMS and are spaced at 118 Da. This distribution is visible throughout the PE distribution.

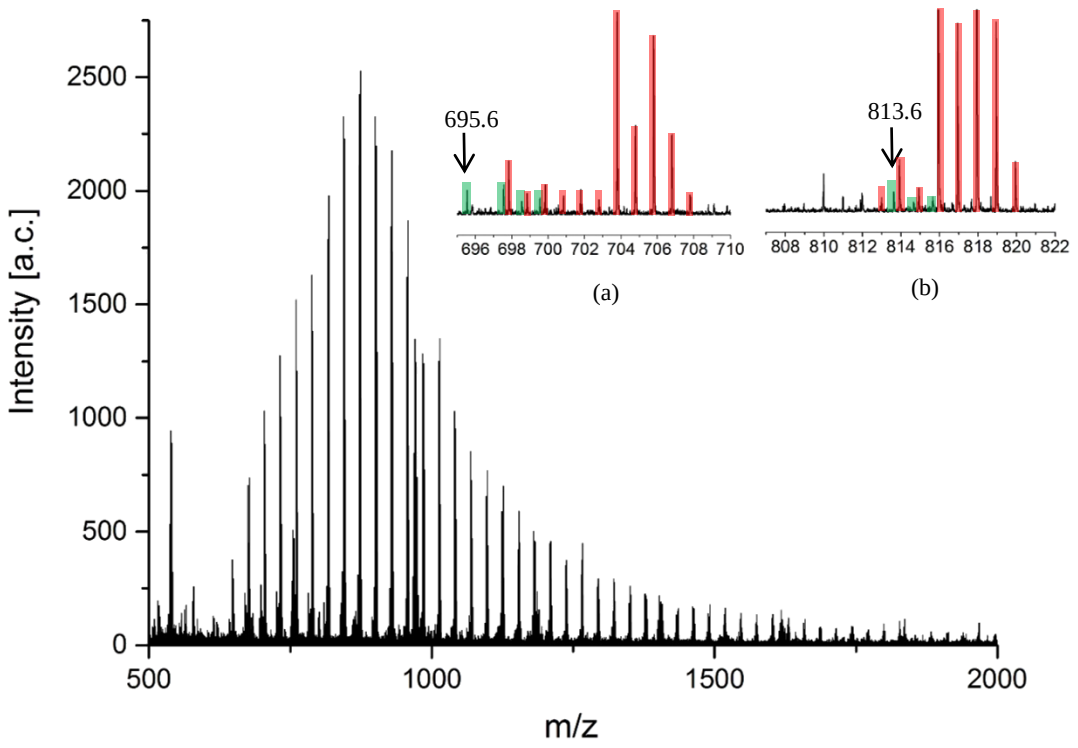

Figure A.6: MALDI spectrum of CB163 PE/AMS copolymerisation

The insert of Figure A.6 shows the isotope distribution pattern of a PAMS oligomer attached to a silver ion; this pattern matches with theory. All mass peaks in this distribution correspond with $[PAMS + AG]^+$. The number of monomer units in each oligomer can be calculated by subtracting the mass of a silver ion and then dividing by the molecular weight of an AMS unit, this gives the DP of the chain, and in the instance of insert (b) for instance the DP is shown to be 6 units. The combined results of the performed analysis indicates that the material is indeed a mixture of PE and PAMS.

A.6 PAMS Mechanism

Methylaluminoxane (MAO) is often found as a key component in many catalytic systems in a multitude of polymerisations including ethylene, styrene and polar

monomers. Over its history, MAO has been studied extensively, however to this day the structure of MAO is still unclear and its role in the mechanism of these polymerisations has not been fully explained.[14] Typically MAO is used to activate the transition metal catalysts in order to form the alkylated metal cation which forms the active species responsible for the polymerisation. However it is also possible for MAO to polymerise monomers itself. In most of these cases it is generally accepted that the reaction mechanism and structure of the active species are not known, and in fact can be interpreted in a number of ways. Examples of this include a study by Saegusa[15] who reported the use of $AlEt_3$/water/alkyl halide systems that produced aluminoxane species, to polymerise AMS, styrene and other vinyl monomers. Within this work it was proposed that ethylauminoxante ($AlEt_3$), acting as a Lewis acid, initiates polymerisation by forming a carbonium complex with the alkyl halide. However, in contrast to this it has been proposed the MAO/$AlMe_3$ may act via a radical mechanism to initiate the photopolymerisation of MMA[16], wherein a complex forms between the MMA monomer and the $AlMe_3$.

A.7 Conclusion

In conclusion, the polymerisations of ethylene and AMS (and it derivatives) in the presence of hydrogen by hafnocene catalysts was shown to produce a mixture of end functionalise PE-*i*-AMS and poly(α-methylstyrene). These materials were recovered in small quantities. The production of PAMS was determined to be a by-product of some Lewis acid catalysed process involving MAO but the mechanism by which this occurs was not elucidated. The produced materials were of little practical use and the productivity of the reaction was so low as to not be suitable for purpose and so polymerisations with hexene were not conducted.

A.8 References

1. T. Diesner, C. Troll and B. Rieger, *Top Organomet Chem*, 2009, 26, 47-63.
2. P. A. Deck, C. L. Beswick and T. J. Marks, *J. Am. Chem. Soc.*, 1998, 120, 1772-1784.
3. E. Y.-X. Chen and T. J. Marks, *Chem. Rev.*, 2000, 100, 1391-1434.
4. K. P. Bryliakov, E. P. Talsi, A. Z. Voskoboynikov, S. J. Lancaster and M. Bochmann, *Organometallics*, 2008, 27, 6333-6342.
5. W. A. King, S. Di Bella, A. Gulino, G. Lanza, I. L. Fragalà, C. L. Stern and T. J. Marks, *J. Am. Chem. Soc.*, 1999, 121, 355-366.
6. V. Busico, R. Cipullo, R. Pellecchia, G. Talarico and A. Razavi, *Macromolecules*, 2009, 42, 1789-1791.
7. H. G. Alt and A. Köppl, *Chem. Rev.*, 2000, 100, 1205-1222.
8. K. F. Morris and C. S. Johnson, *J. Am. Chem. Soc.*, 1992, 114, 3139-3141.
9. C. S. Johnson, *Prog. Nucl. Magn. Reson. Spectrosc.*, 1999, 34, 203-256.
10. F. Coumes, A. Malfait, M. Bria, J. Lyskawa, P. Woisel and D. Fournier, *Polym. Chem.*, 2016, 7, 4682-4692.
11. R. F. Nogueira and M. I. B. Tavares, *Polym. Test.*, 2001, 20, 379-382.
12. P. A. Berger, J. J. Kotyk and E. E. Remsen, *Macromolecules*, 1992, 25, 7227-7233.
13. M. Osa, M. Sumida, T. Yoshizaki, H. Yamakawa, K. Ute, T. Kitayama and K. Hatada, *Polym J*, 2000, 32, 361-369.
14. R. Po, L. Fiocca, N. Cardi, F. Simone, M. A. Cardaci, S. Spera and M. Salvalaggio, *Polym. Bull.*, 2006, 56, 101-109.
15. T. Saegusa, H. Imai and J. Furukawa, *Makromol. Chem.*, 1964, 79, 207-220.
16. S. S. Reddy and S. Sivaram, *J. Polym. Sci., Part A: Polym. Chem.*, 1996, 34, 3427-3430.

Appendix B: Dynamic light scattering (DLS) correlograms

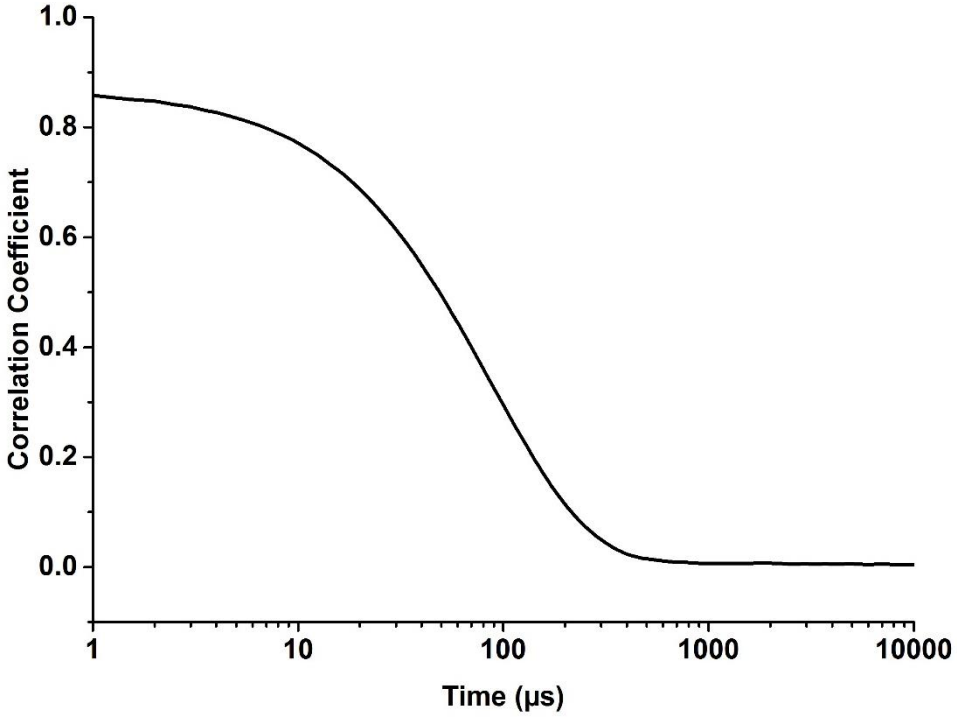

Figure B.1: DLS correlogram of the product of EH-*b*-P(*n*-BA) (run 1-128, Table 3.1) in THF (1 mg/mL) (average of three measurements)

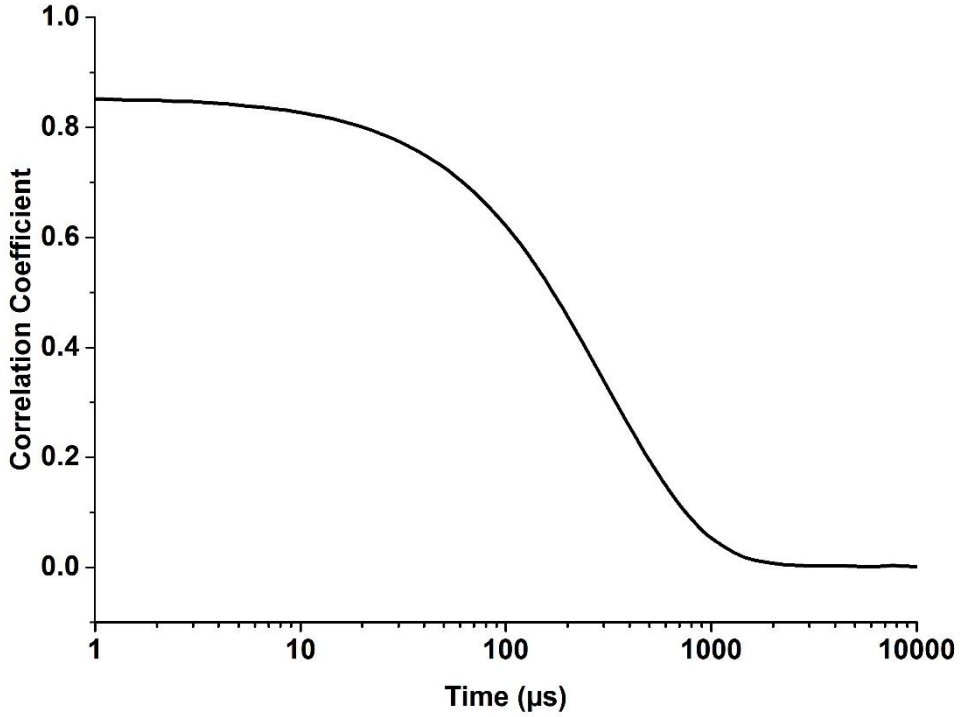

Figure B.2: DLS correlogram of the product of EH-b-P(VAc) (run 1, Table 3.4) in THF (1 mg/mL) (average of three measurements)

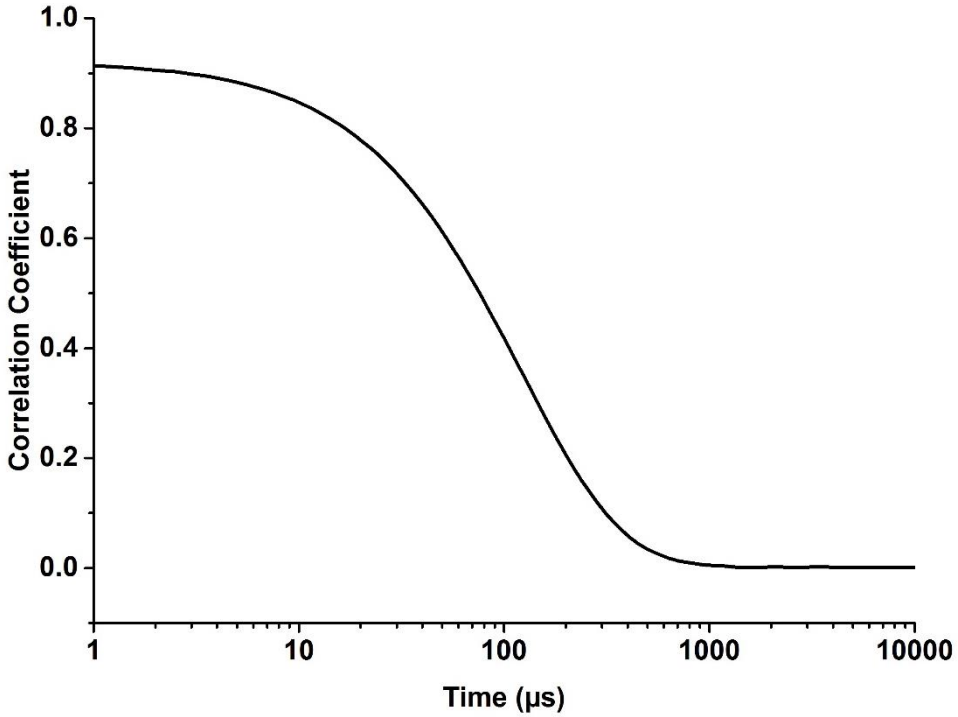

Figure B.3: DLS correlogram of the product of EH-*b*-P(V2EH) (run 1-128, Table 3.8) in THF (1 mg/mL) (average of three measurements)

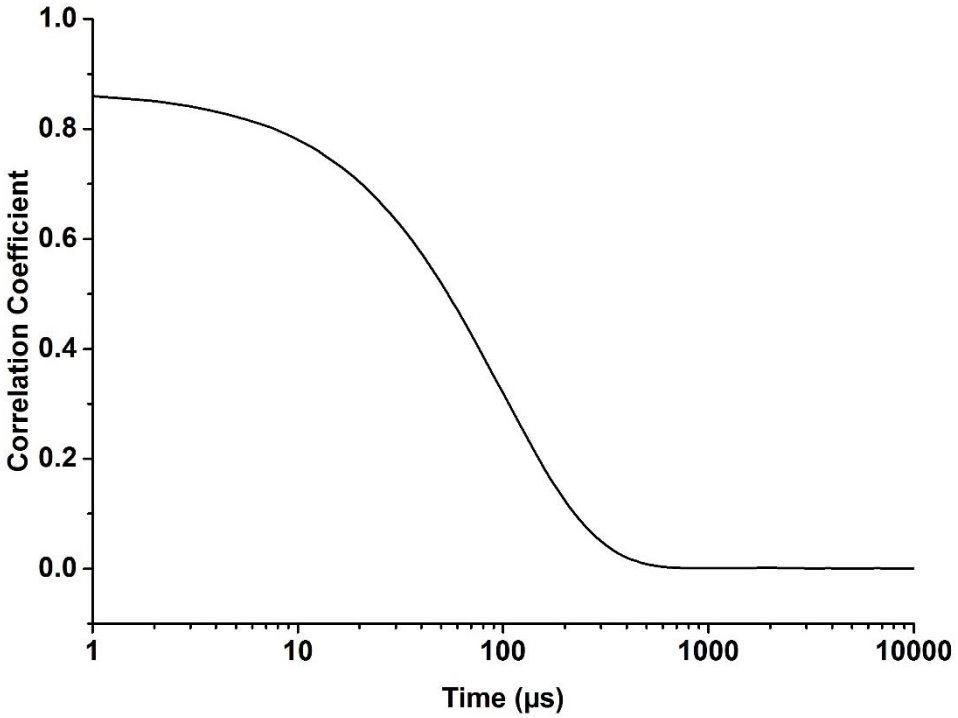

Figure B.4: DLS correlogram of the product of EH-b-P(C_{14}MA) (run 1-128, Table 3.9) in THF (1 mg/mL) (average of three measurements).

Appendix C: Design of the gas burette system used

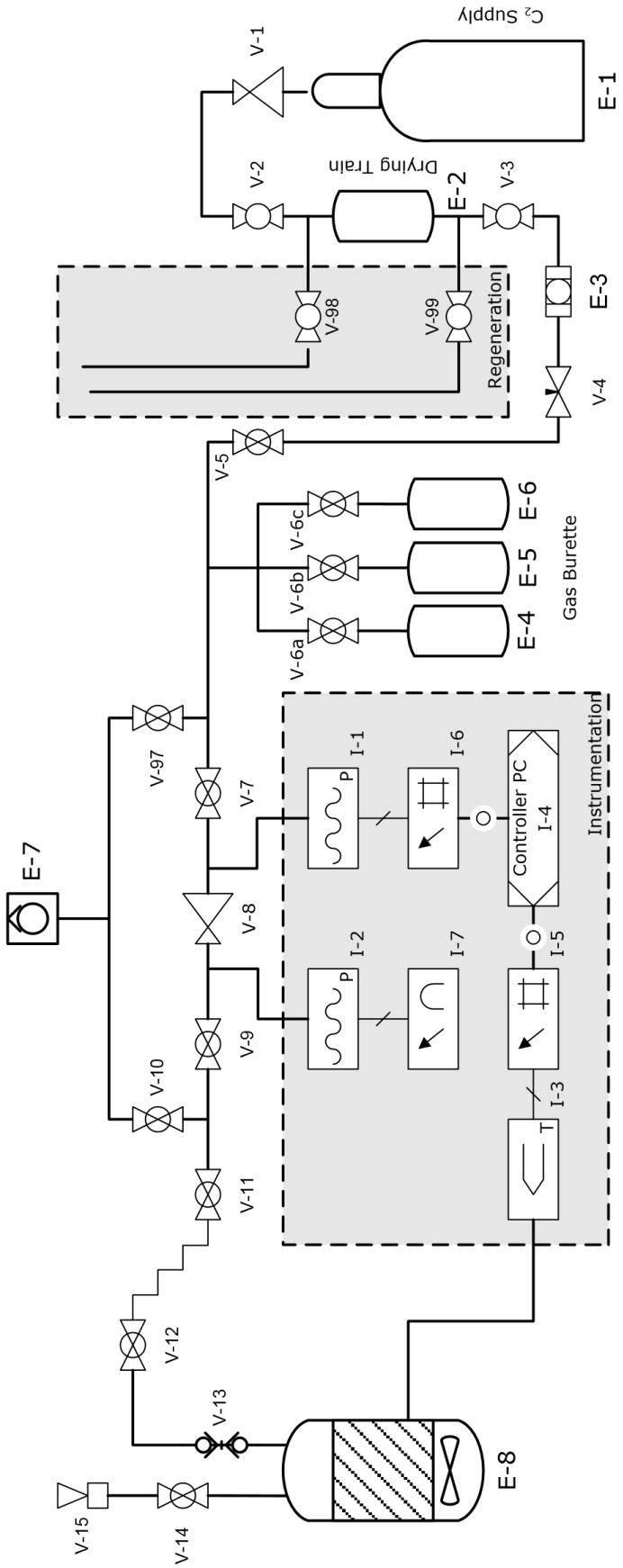

Table 1 Gas burette components[1]

Component	Description	Manufacturer	Model
E-1	Ethylene supply cylinder		
E-2	R3-11G/3A molecular sieves drying train	Swagelok	304L-HDF4-300
E-3	2 micron filter	Swagelok	SS-4FW-2
E-4	300CC sample cylinder	Swagelok	304L-HDF4-300
E-5	1000CC sample cylinder	Swagelok	304L-HDF4-1000
E-6	2250CC sample cylinder	Swagelok	304L-HDF4-2250
E-7	Connection to Schlenk line		
E-8	Reaction Vessel		
I-1	Input Gauge	Druck	PDCR 4010 (20 bar)
I-2	Output gauge	Tescom	4802-V200N
I-3	Thermocouple in reaction media		
I-4	Control		
I-5	Meter with RS232 interface	Druck	DPI282 with RS232 interface
I-6	ADC with RS232 Interface	Druck	DPI280 with RS232 interface
I-7	Pressure Dial	Tescom	4802-V200N
V-1	20 bar cylinder regulator	BOC	HP1502B-GL-BS4
V-2	C2 Isolation	Swagelok	SS-4P4T-BK
V-3	Rig isolation	Swagelok	SS-4P4T-BK
V-4	Meter Valve	Swagelok	SS-4L2
V-5, V-6, V-7		Swagelok	SS-42S4
V-8	Reactor Regulator	Tescom	44-2262-241
V-9, V-10, V-11, V-12		Swagelok	SS-42S4
V-13	Quick Connect	Swagelok	SS-QC4-D-400/SS-QC4B-400
V-14	Catalyst Injection Valve	Swagelok	SS-43S4
V-15	Catalyst Injection Port	Swagelok	
V-97	Commissioning purge	Swagelok	SS-42S4
V-98	Regeneration Gas Connection	Swagelok	SS-4P4T-RD
V-99	Regeneration Purge Connection	Swagelok	SS-4P4T-RD
Catalyst injector	25CC Sample cylinder + Male quick connect	Swagelok	SS-4CS-TW-25/SS-QC6D-600

References

1. M. L. Hammond, PhD Thesis, University of Warwick, 2006.